5-4-2018

Microwave Plasma assisted Ignition and Combustion Diagnostics

Che Amungwa Fuh

Microwave plasma assisted ignition and combustion diagnostics

By

Che Amungwa Fuh

A Dissertation
Submitted to the Faculty of
Mississippi State University
in Partial Fulfillment of the Requirements
for the Degree of Doctor of Philosophy
in Applied Physics
in the Bagley College of Engineering

Mississippi State, Mississippi

May 2018

Microwave plasma assisted ignition and combustion diagnostics

By

Che Amungwa Fuh

Approved:

Chuji Wang
(Major Professor)

Donna M. Pierce
(Committee Member)

Kalyan K. Srinivasan
(Committee Member)

Sundar R. Krishnan
(Committee Member)

Hendrik F. Arnoldus
(Committee Member/Graduate Coordinator)

Jason M. Keith
Dean
Bagley College of Engineering

Name: Che Amungwa Fuh

Date of Degree: May 4, 2018

Institution: Mississippi State University

Major Field: Applied Physics

Major Professor: Chuji Wang

Title of Study: Microwave plasma assisted ignition and combustion diagnostics

Pages in Study 148

Candidate for Degree of Doctor of Philosophy

Plasmas, when coupled to the oxidation process of various fuels, have been shown to influence the process positively by improving upon flameholding, reduction in ignition delay time, reduced pollutant emission, etc. Despite all these positive effects being known to the science community, the mechanisms through which the plasmas effects all these enhancements are poorly understood. This is often due to the absence of accurate experimental data to validate theoretical mechanisms and the availability of a myriad sources of plasmas having different chemistries.

The goal of this thesis is to further narrow the knowledge gap in the understanding of plasma assisted combustion by using a nonthermal microwave plasma to investigate the mechanism through which it enhances the oxidation of several fuel/oxidant combinations. The enhancement metrics used in these studies are minimum ignition energy, flameholding, and rotational temperature. A suite of noninvasive optical diagnostics techniques (camera for visual imaging, optical emission spectroscopy and cavity ringdown spectroscopy) are employed to probe the plasma assisted combustion flame and identify the species, obtain rotational temperatures, and identify pathways through which the microwave plasma enhances the combustion process. Initially, the

effect of a microwave plasma on the ignition and flameholding of an ethylene/air mixture was investigated. Then, based on observations from that study and previous studies, a novel plasma assisted combustion platform was designed, capable of discriminating between the various pathways through which the plasma enhances the combustion of a fuel/air mixture. Using the designed platform, a comparative study was carried out on the roles played by the plasma activated fuel vs. plasma activated oxidizer stream. The roles played by the plasma activated fuel or air molecules in the ignition of the fuel/air mixture were investigated. Data from this study led to the suggestion that there exists a minimum required plasma generated radical pool for ignition to occur, with reactive oxygen and nitrogen playing a more important role in the ignition and flameholding effects. Ground state OH(X) number densities were also measured for the first time in the hybrid ignition zone of a plasma assisted combustion reactor using cavity ringdown spectroscopy.

DEDICATION

To my parents,

Akombo Michael Fuh and *Fuh Rosaline Sirri*

Whose blessings and encouragements have strengthened me every step of my life

To my wife

Mary Sambou Che

For all her love, care and support

ACKNOWLEDGEMENTS

I wish to express my sincere gratitude to my advisor, Dr. Chuji Wang for his invaluable guidance and support throughout my Ph.D. study. The knowledge, skills and way of thinking imparted on me during Dr. Wang's mentorship will always be an asset not only in my career as a scientist but my life in general. I would also like to thank Dr. Donna Pierce, Dr. Henk Arnoldus, Dr. Kalyan Srinivasan and Dr. Krishnan Sundar for serving on my committee and raising questions to strengthen this study.

I would also like to express my sincere gratitude to the faculty at the Department of Physics and Astronomy at Mississippi State University whose academic and personal guidance was invaluable, always going above and beyond to address any problems I had academic or otherwise throughout my study.

I would also like to thank Dr. Wei Wu with whom I had so many fruitful discussions and who introduced me to the experimental systems of plasma assisted combustion. I will also like to express gratitude for my group mates past and current, Dr. Zhennan Wang, Dr. Burak M. Kaya, Dr. Peeyush Sahay, Haifa Alali, Mahesh Ghimire, Shane Clark, Zhiyong Gong, Rongrong Wu, Jeff Headley and Pubuduni Ekanayaka whose discussions and general friendship made the late nights and long weekends enjoyable and fun.

I would not be the person I am today or where I am today without my family and I would like to thank my parents, my brothers, and sister for their encouragement

throughout my studies. I want to specially thank my uncle Vitalis S. Amungwa who was instrumental in setting me on the path I am today and enabled me to pursue my passion studying Applied Physics at the graduate level. I also want to thank my external family for their love and support during my entire studies. I wish to express my gratitude to my friends both in the United States, Cameroon and around the world whose encouragement and companionship kept me contented when the going got tough. I am immensely grateful to my wife Mary Sambou for all her love, sacrifice and support throughout this process.

TABLE OF CONTENTS

LIST OF TABLES

LIST OF FIGURES

CHAPTER I

INTRODUCTION

1.1 Research motivation

Eighty five percent of the world's energy supply is obtained by combustion from fossil fuels [1], [2]. This is due to the high energy density of fossil fuels, and the ability to quickly refuel a device running on fossil fuel, as opposed to other renewable energy sources. However, the efficiency of our current combustion engines is quite low, resulting in the fast depletion of our natural energy reserves, a lot of emissions causing environmental pollution, and exacerbating the effects of climate change. Facing the ever rising energy requirements of our modern economies and the tough regulations put in place by our governments in order to protect our environment and communities, the scientific community is therefore faced with the need to redevelop current combustion systems.

Plasma assisted combustion is proving to be an effective tool in the quest to improve on conventional combustion systems. Plasma assisted combustion refers to the coupling of a plasma to the oxidation process of a fuel. The coupling of plasmas to the oxidation process of a fuel/air mixture has been shown by researchers in previous years to bring out enhancements such as improved flameholding, increased efficiency etc. For example, Stockman *et al.* [3] reported on the improvement of flame speeds by upto 20% due to microwave irradiation of the flat flame front of a premixed methane/air wall

stagnation flat flame. Fei *et al*. [4] employed a transient plasma consisting mainly of streamers to study the effect of plasmas on the ignition of quiescent and flowing fuel/air mixtures. They reported a reduction in ignition delay time by a factor of three in quiescent mixtures and more than a factor of four in a flowing pulse detonator engine. Kim *et al*. [5] reported on the improved stabilization of ultra-lean premixed methane/air flames by a pulsed discharge plasma. The improvement in stabilization was attributed to the production of stable intermediates species including hydrogen and carbon mono oxide. They also observed a 10 % increase in the blowout limit. Salvelkin *et al.* [6] demonstrated the improvement in combustion and flameholding in a supersonic flow over a wide range of fuel injection mass flow rates in the plasma assisted combustion of an ethylene/air mixtures. Ombrello *et al.* [7] showed that a 220% increase in the extinction strain rate was possible for low plasma inputs in a piecewise non-equilibrium gliding arc plasma discharge integrated with a counterflow flame burner. Leonov *et al*. [8], using a transversal electrical discharge at relatively low powers to generate a plasma in the fuel flow, reported on the reduction in ignition delay time and improved stabilization in the combustion of hydrogen and ethylene in a supersonic flow. They suggested that the stabilization effect of the plasma on the supersonic flow is multistage in nature. Hammack *et al.* [9] employed a tunable waveguide to initiate and enhance the combustion of a premixed methane/air flame. Hwang *et al.* [10] demonstrated the reduction in carbon monoxide and reduction in unburnt hydrocarbons during the microwave plasma assisted ignition and combustion in a single cylinder direct injection gasoline engine. They observed that irradiation by microwaves resulted in an improvement of the lean limit and a 6% increase in fuel efficiency. Bang *et al.* [11]

produced and showcased a microwave plasma burner capable of producing large volume flames by injecting methane into the microwave plasma torch generated in air. They reported a 98% combustion efficiency from gas chromatography studies and showed a significant temperature increase compared to non-plasma assisted flames. Hu *et al.* [12] reported a significant increase in the plasma propagation speeds, combustion intensity, and lean blow-off limits when a dielectric barrier discharge was used in the enhancement of a low heating value fuel (mixture of CO, H_2 and N_2). Based on numerical simulations, the enhancement was attributed to the creation of OH radicals by the DBD discharge which enhanced the combustion process. Kopecek *et al.* [13] reported an improvement in the lean burn limit during the ignition of a premixed methane/air in a high pressure chamber using a plasma generated by a 1064 nm Nd:YAG laser. Kim *et al.* [14], in another study investigated the effect of three different plasma discharges in enhancing flame stability. They observed a 20% higher coflow speed with a single electrode corona discharge between a platinum electrode and the flame base. They observed an improvement of up to 50% in the coflow speeds when an asymmetric barrier discharge was used and a tenfold increase in the stability limit when an ultrashort repetitively pulsed discharge was employed.

1.2 Research objective

Despite all these positive enhancements being reported, the exact mechanism through which these enhancement effects are brought about is still not clearly understood. This is due to the large variation in plasma properties available for use in combustion studies, and the complicated interactions between plasma chemistry, combustion chemistry, and transport process resulting in the inability to exactly pinpoint which

mechanisms are responsible for the enhancement effects [2]. Also, the lack of accurate experimental data to complement kinetic studies is another factor widening the knowledge gaps in our understanding of plasma assisted combustion. Hence, facing all these challenges, a number of experiments were designed and performed in a bid to narrow the current knowledge gap in our understanding of the phenomenon that is plasma assisted combustion. Initially, the effect of a microwave argon plasma on the ignition and flameholding in ethylene/air mixtures was investigated. This was done to study the relationship between minimum ignition plasma power and the fuel equivalence ratio as well as to investigate the mechanism of plasma assisted flameholding in ethylene/air mixtures. Building from the results from the first study and from published literature, it was observed that plasma assisted combustion is brought about through complex interacting pathways, with isolating and studying them independently being the key to understanding how a plasma assists the combustion process. Hence, a novel experimental platform was designed, aimed at discriminating between the various experimental pathways through which the plasma enhances the combustion process. Using the newly-minted PAC platform, we performed a comparative study on the plasma activated fuel vs. the plasma activated methane in the plasma assisted combustion of a nonpremixed methane/air mixture. Finally in a bid to curb the lack of accurate experimental data available on various important species for kinetic applications, cavity ringdown spectroscopy was employed to measure the ground state OH number density for the first time in the hybrid zone of a modified plasma assisted combustion reactor.

1.3 References

1. Y. Ju and W. Sun, 2015 “Plasma assisted combustion: Dynamics and chemistry,” *Prog. Energy Combust. Sci*., **48**, 21–83

2. A. Starikovskiy and N. Aleksandrov, 2013 “Plasma-assisted ignition and combustion,” *Prog. Energy Combust. Sci.*, **39**, 61–110

3. C. D. Carter, E. S. Stockman, S. H. Zaidi, R. B. Miles, and M. D. Ryan, 2009 “Measurements of combustion properties in a microwave enhanced flame,” *Combust. Flame,* **156**, 1453–1461

4. F. Wang, J. B. Liu, J. Sinibaldi, C. Brophy, A. Kuthi, C. Jiang, P. Ronney, and M. A. Gundersen, 2005 “Transient plasma ignition of quiescent and flowing air/fuel mixtures,” *IEEE Trans. Plasma Sci*., **33**, 844–849

5. W. Kim, M. G. Mungal, and M. Cappelli, 2010 “The role of in situ reforming in plasma enhanced ultra lean premixed methane/air flames,” *Combust. Flame*, **157**, 374–383

6. K. V Savelkin, D. A. Yarantsev, I. V Adamovich, and S. B. Leonov, 2015 “Ignition and flameholding in a supersonic combustor by an electrical discharge combined with a fuel injector,” *Combust. Flame*, **162**, 825–835

7. T. Ombrello, X. Qin, Y. Ju, A. Gutsol, A. Fridman, and C. Carter, 2006 “Combustion Enhancement via Stabilized Piecewise Nonequilibrium Gliding Arc Plasma Discharge,” *AIAA* J., **44**, 142–150

8. S. B. Leonov, I. V. Kochetov, A. P. Napartovich, V. A. Sabel’Nikov, and D. A. Yarantsev, 2011 “Plasma-induced ethylene ignition and flameholding in confined supersonic air flow at low temperatures,” *IEEE Trans. Plasma Sci*., **39**, 781–787

9. S. Hammack, S. Member, X. Rao, T. Lee, and C. Carter, 2011 “Direct-Coupled Plasma-Assisted Combustion Using a Microwave Waveguide Torch,” **39**, 3300–3306

10. J. Hwang, W. Kim, C. Bae, W. Choe, J. Cha, and S. Woo, 2017 “Application of a novel microwave-assisted plasma ignition system in a direct injection gasoline engine,” *Appl. Energy*, **205**, 562–576

11. C. Bang and Y. Hong, 2006 “Methane-augmented microwave plasma burner,” *IEEE Trans. plasma Sci*., **34**, 1751–1756

12. H. Hu, Q. Song, Y. Xu, G. Li, and C. Nie, 2013 “Non-equilibrium plasma assisted combustion of low heating value fuels,” *J. Therm. Sci.,* **22**, 275–281

13. H. Kopecek, S. Charareh, M. Lackner, C. Forsich, F. Winter, J. Klausner, G. Herdin, M. Weinrotter, and E. Wintner, 2005 “Laser Ignition of Methane-Air Mixtures at High Pressures and Diagnostics,” *J. Eng. Gas Turbines Power*, **127**, 213

14. W. Kim, H. Do, M. G. Mungal, and M. A. Cappelli, 2006 “Flame Stabilization Enhancement and NO_x Production using Ultra Short Repetitively Pulsed Plasma Discharges,” *44th AIAA Aerospace Sciences Meetings and Exibit*, 1–13,.

CHAPTER II

MICROWAVE PLASMA-ASSISTED IGNITION AND FLAMEHOLDING IN PREMIXED ETHYLENE/AIR MIXTURES

2.1 Introduction

The roles of nonthermal plasmas on combustion dynamics and kinetics have been investigated by the scientific community over the recent decades for their great potential to enhance flame stability, reduce pollutant emissions, extend flammability limits, improve on flameholding, reduce ignition delay time, etc., with recent reviews found in [1,2]. Enhancement by the nonthermal plasma is attributed to a cocktail of reactive chemical species, high energy electrons, and little-to-no thermal energy injected into the reaction zone [3]. Even though plasmas have been observed to have a significant effect on the combustion process, the detailed mechanism through which the plasma influences the process is still not well understood, with quantitative kinetic modeling remaining difficult, even in one dimension. There are still a host of challenges baffling the scientific community, such as which kinetic pathways are the most important in a particular plasma-assisted combustion case, which radicals and excited neutral species are the most important in plasma-assisted combustion, or the relative importance of the roles of plasma heating as compared to roles of plasma radicals [4].

The ability of nonthermal plasmas to improve on flameholding is one of the effects of plasmas on the combustion process that has recently been widely investigated. K. Savelkin *et al.* [5] demonstrated a novel scheme of plasma-assisted ignition and flameholding, which combined a wall fuel injector and high voltage electric discharge into a single module for supersonic combustors. The scope of the experiment included the characterization of the discharge interacting with the main flow and fuel injection jet, parametric study of ignition, and flame front dynamics. They demonstrated the significant potential of the new scheme for high-speed combustion applications, including cold start/restart of scramjet engines and the support of the transition regime in dual-mode on and off design operation. Similarly, A. Dutta *et al.* (6) investigated the plasma-assisted ignition and flameholding of premixed and nonpremixed ethylene/air and hydrogen/air flows using a repetitive pulsed nanosecond plasma at low pressures and high flow velocities up to 100 m/s. They observed that ignition of ethylene/air mixtures occurred via the formation of multiple arc filaments in the fuel/air plasma, although the air plasma at the same conditions remained diffuse until fuel was added. They determined that the slow rate of mixing, combustion instabilities caused by the feedback between fluctuations of the test section pressure and the flow rate, and the thermal choking of the flow in the extension channel downstream of the test section, to be the determinants which adversely affected flameholding. J. K. Lefkowitz *et al.* [7] carried out *in situ* species diagnostics and kinetic study of plasma activated ethylene dissociation and oxidation in a low temperature flow reactor. For the plasma activated dissociation experiment, it was observed that direct electron impact dissociation, and dissociation by excited and ionized argon collision reactions, were the major fuel consumption pathways.

For the plasma-assisted oxidation experiment, three different fuel consumption paths were identified: a plasma activated low temperature fuel oxidation pathway via O_2 addition reactions, a direct fragmentation pathway via collisional dissociation electrons, ions and electronically excited molecules, and a direct oxidation pathway by plasma generated radicals. Based on the observed experimental results, a new kinetic model for low temperature plasma activated fuel oxidation and dissociation was assembled. E. Mintusov *et al.* [8] carried out a study on the mechanism of plasma-assisted oxidation and ignition of ethylene air flows by a repetitively pulsed nanosecond plasma discharge where they identified two different operation regimes, an oxidization regime and an ignition regime. I. N. Kosarev *et al.* [9] using computer modeling, studied the kinetics in the afterglow of a pulsed nanosecond high voltage discharge for plasma-assisted combustion (PAC) in elevated temperatures. They calculated and analyzed the kinetic curves for electrons, OH, and O radicals. They also measured temporal dynamics of electron density, OH radicals, and discharge/combustion emission spectra for plasma-assisted combustion. M.S. Bak *et al.*[10] studied the stabilization of premixed and jet diffusion flames of methane, ethane, and propane using a nanosecond repetitively pulsed plasma discharge. Using laser induced breakdown spectroscopy and gas chromatography, they observed that for premixed flames, plasma-assisted flameholding takes place under fuel lean conditions, propagation of combustion occurs at or above the known lean flammability limit. They also observed that for diffusion jet flames, flame anchoring occurs best when the discharge is placed where the local fuel/air equivalence ratio is in a limited flammable regime even when the jet speeds were much higher than the normal blow off speeds.

Another important aspect of PAC is the investigation of the minimum plasma power or energy required to ignite a combustible mixture under different circumstances and great strides in this aspect have been made by investigators such as R. Ono *et al.*[11] who studied the electrostatic ignition of hydrogen/air mixtures. They measured the minimum ignition energy using a capacitance spark discharge and a U-shaped curve was obtained for the plot between minimum ignition energy and hydrogen concentration. They observed that the minimum ignition energy is relatively constant when they varied the relative humidity from 0% to 90% at room temperature and that the observed minimum ignition energy was constant when the spark duration was varied from 5 ns to 1 ms. J. Han *et al.* [12] carried out a numerical study on the spark ignition characteristics of a quiescent methane-air mixture using detailed chemical kinetics. They observed that for both computational and experimental results, the size of the electrodes significantly affected the value of the minimum ignition energy within the quenching distance but did not affect it above the quenching distance. A plot of the minimum ignition energy against the equivalence ratio revealed a U-shaped dependence with the minimum occurring at a fuel equivalence ratio of 0.9. It was also noted that for a short spark duration, the vortex gas motion and the temperature gradient around the flame kernel dramatically influenced the flame formation and the minimum ignition energy. W. Wu *et al.* [13] investigated the ignition characteristics in the plasma-assisted ignition of premixed and nonpremixed methane/air mixtures over a wide range of fuel equivalence ratios. They observed a U-shaped ignition curve of plasma power versus fuel equivalence ratio for the premixed methane/air combustion whereas for the nonpremixed case, a linearly-increasing curve was observed. It was concluded that for the premixed case, the lean fuel equivalence

ratios were more susceptible to heat loss to the external flow, and the rich fuel equivalence ratios were more susceptible to plasma quenching by the rich fuel/air mixture. For the nonpremixed case, the elevated local fuel equivalence ratio due to the inadequate mixing between the methane and air flows resulted in plasma quenching as observed for rich fuel equivalence ratios in the premixed case.

Even though there are several different sources of nonthermal plasmas used in plasma-assisted combustion research, such as silent discharge [14], radio frequency discharge (RFD) [15], microwave plasma torch (MPT) [16], fast ionization wave [17], nanosecond pulsed discharge [18–22], corona discharge [23,24], dielectric barrier discharge (DBD) [25], dc glow discharge (dcGD) [26,27] etc, nonthermal microwave plasma sources are favored for their high power coupling efficiency, excellent flexibility for PAC system configurations, abundant free radicals and other reactive species and long-time operational stability [28–33]. Investigators employing microwave plasma sources such as J. B. Michael *et al.* [34] achieved ignition in methane/air mixtures using low energy seed laser pulses and an overlapping subcritical microwave pulse. Experiments showed that the extremely weak ionization of the laser localizes the microwave energy deposition leading to rapid heating, high temperatures, and ignition. Interaction of the seed laser pulse and microwave heating pulse were observed using schlieren and shadowgraphs to record the intensity of heating, the scale of the interaction, and for confirmation of ignition. A model to estimate gas and vibrational heating was developed through coupling of gas dynamic equations and plasma kinetics. Strong temperature gradients observed by schlieren and shadowgraph and the temperature rise predicted by the model indicated heating by the combination of seed ionization laser and

subcritical microwave pulse in excess of 1000 K. They observed that for a methane/air mixture at equivalence ratio of 0.7, the energy deposited by the subcritical microwave pulse responsible for the observed increase in temperature and heating volume was greater than the minimum ignition energy for the mixture, indicative of a thermally dominated ignition process. A. I. Babaritskii *et al.* [35] reported results of a study on the microwave discharge plasma-induced processes of partial oxidation of kerosene and methane with air and oxygen. It was found that energy input in the form of plasma is 1.3 – 1.6 times as effective in the enhancement of kerosene conversion as thermal energy input. Wolk *et al.* [36] investigated the enhancement of flame development by microwave-assisted spark ignition in a constant volume combustion chamber and observed an extension in the lean and rich ignition limits. They also observed a reduction in the flame development time (time for 0 - 10% of total net heat released) and an increase in flame kernel size for all equivalence ratios tested. They proposed in the study that the flame enhancement was as a result of a nonthermal chemical kinetic enhancement from energy deposition to free electrons in the flame front and the induced flame wrinkling from excitation of flame (plasma) instability.

In our previous studies, we investigated the effect of a microwave argon plasma on the plasma-assisted combustion of methane, a single carbon hydrocarbon, at various fuel equivalence ratios, different plasma powers, different mixing schemes, total flow rates etc. [13,37,42,45]. In this study, we investigate the plasma assisted ignition and flameholding of ethylene, a two carbon hydrocarbon which has a higher energy density compared to methane. This study is aimed at paving a path to better understanding the effect of nonthermal microwave argon plasmas in the plasma-assisted combustion

dynamics of hydrocarbons. Here, a nonthermal microwave argon plasma is employed to study the role of the plasma in enhancing flame ignition and flameholding in the plasma-assisted combustion of a premixed ethylene/air mixture. The experimental setup is described below in section 2.2. The minimum plasma power required for ignition over a range of equivalence ratios and flame structure is discussed in section 2.3.1 and 2.3.2 respectively. Emission spectra characterizing the excited state species along with rotational temperature profiles are reported in sections 2.3.3 and 2.3.4. The electronic ground state OH number densities in the flame are measured by cavity ringdown spectroscopy and are discussed in section 2.3.5. Finally, a summary is presented in section 2.4.

2.2 Experimental setup

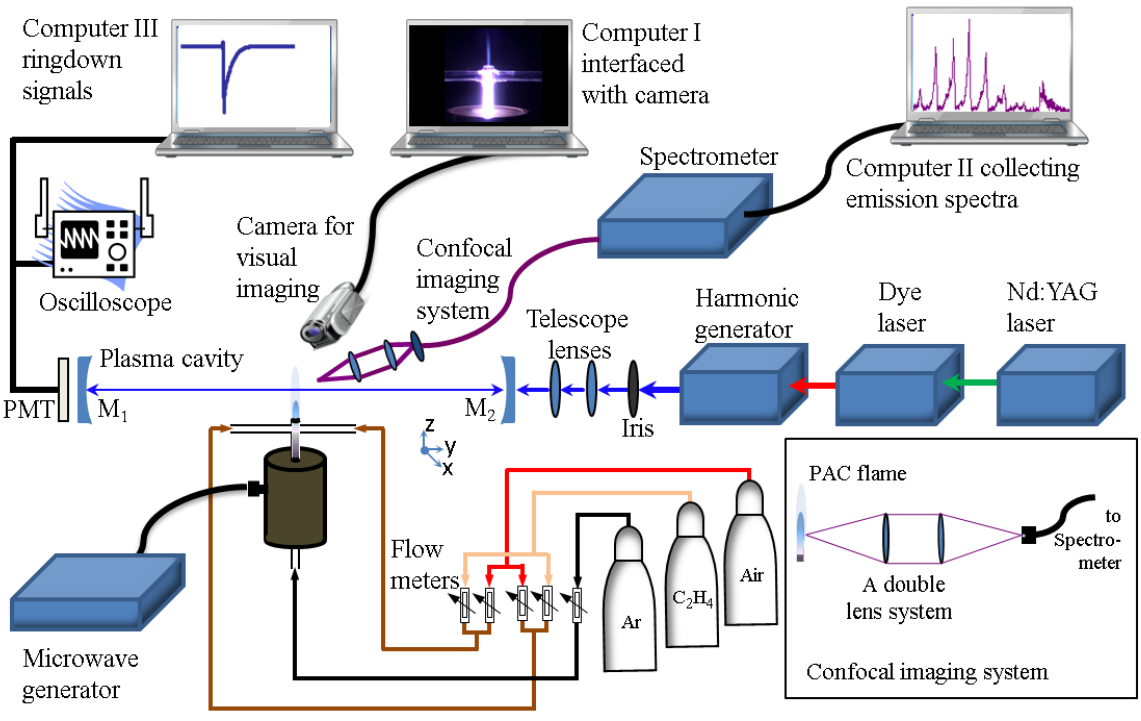

Figure 2.1 Schematic of the experimental setup

A schematic of the experimental setup is shown in figure 2.1. A detailed description of the experimental setup can be found in [37]. Briefly, the experimental setup consists of three main components, a plasma-assisted combustion reactor, a gas flow control manifold, and an optical diagnostic system. Each of the components is described subsequently.

2.2.2 Microwave plasma-assisted combustion reactor

The microwave plasma-assisted combustion reactor consists of a microwave plasma cavity (surfatron) and a cross shaped quartz tube of inner diameter 2 mm and outer diameter 6 mm. The surfatron was powered via a 0.6 m low-loss coaxial cable (LMR-400, Times Microwave Systems) by a 2.45 GHz microwave source (AJA International). The forward and reflected microwave powers were provided as readouts from the microwave source. In this study, the forward microwave power was in the range of 60 - 140 W, the reflected power was typically between 1 ~ 4 W. It should be noted that even though the forward and reflected powers were known, the microwave coupling efficiency into the plasma was not measured. Hence in this study, the forward power of the plasma source is referred to as the microwave plasma power. One arm of the quartz tube was inserted vertically into the surfatron and was used to confine and conduct the diffused argon plasma generated by the surfatron. The parameters of the microwave argon plasma jet used in this study including plume shapes, emission spectra, plasma temperatures, plasma power effects, plasma gases, etc, have been previously investigated and can be seen in [38–41]. The typical electron number density in this argon plasma is on the order of 10^{14} cm^{-3} with the electronic excitation temperature of 8000 – 9000 K. [41]. The two horizontal arms of the cross tube were used to symmetrically introduce the

premixed ethylene/air mixture into the system. The premixed ethylene/air mixture in the horizontal arms met with the argon plasma in the vertical arms at the joint part of the cross shaped tube and a jet-shaped flame was observed emerging from the forth arm. A more detailed description of this reactor facility can be found in [41].

2.2.3 Gas flow control manifold

The gas flow control manifold was made up of five flow meters and was connected to the microwave plasma-assisted reactor as shown in figure 1. An identical pair of flow meters was used for the regulation of the air flow with a range of 0 – 1.38 standard liter per minute (slm). The second pair of flow meters was used for ethylene flow rate control with a range from 0 to 434 standard cubic centimeter per minute (sccm, 1 slm = 1000 sccm).The last flow meter was used to regulate the flow rate of the argon plasma gas in the rate of 0 – 1.78 slm. The purities of argon, ethylene and air used in this study were 99.99% (Airgas), 99.99% (Airgas) and 99.99% (Airgas) respectively. The argon plasma feed gas flow rate was fixed at 0.663 slm throughout the entire study.

2.2.4 The optical diagnostic system

The optical diagnostic system consists of three subsystems: a digital imaging system, a pulsed cavity ringdown spectroscopy (CRDS) system, and a fiber-guided optical emission spectroscopy (OES) system. The digital imaging system was used to record plasma and flame structures. Visual documentation of the plasma and combustion flame was done using a digital camera (Sony, FCB-EX78BB) which has a time resolution of 100 μs – 1 s. At this range, the resolution of the camera is capable of resolving plasma filaments along with fine plasma and flame structures as used in a previous study [41].

The shutter speed was adjusted to optimize the visual effect of the plasma jet and combustion flame behavior. The operation of the imaging system was controlled by computer II.

The fiber-guided OES system was employed for characterizing emissions from the plasma-assisted combustion reactor at different locations along the z-axis of the combustor. Optical emissions were collected perpendicularly to the jet axis using a confocal microscope lens system as shown in the inset in figure 2.1. The confocal microscope lens system consists of two identical focal length lenses (f = 5.0 cm), with emissions transmitted to a dual channel spectrometer (Avantes) via a section of optical fiber of aperture size 400 μm. The dual channel spectrometer housed two gratings of 600 grooves mm^{-1} and 1200 grooves mm^{-1} which was used to cover a spectral range of 200 – 600 nm. The spectrometer resolution was 0.07 nm at 350 nm. The plasma-assisted combustion reactor was mounted on a 2-axis high precision translation stage (0.01 mm resolution in both the z and x axis) which enabled 1-D spectra acquisition along the z-axis. Given the confocal lens setup, the small aperture size of the optical fiber of cross sectional area 0.5 mm^2 and the high precision of 0.01 mm of the translation stage used, a spatial resolution of 0.5 mm was achieved without the need for spatial filtering. Emission spectra were obtained perpendicularly to the jet axis with 10 spectra acquired and their average obtained at each fixed spatial location in order to have a better signal to noise ratio. For this study, the integration time of the spectrometer was adjusted based on the emission intensity ranging from 20 ms to 2 s. The optical emission spectroscopy system was operated by Computer III as shown in figure 2.1.

The CRDS system was used to measure absolute number density of the ground state OH radicals. The ringdown cavity was constructed using a pair of highly reflective (R = 99.9% at 308 nm) plano-concave mirrors with a cavity length of 61 cm. The plasma-assisted combustion flame was placed at the center of the ringdown cavity. The optical axis (y-axis) of the ringdown cavity was perpendicular to the flame axis as shown in figure 2.1. The UV laser beam was obtained by frequency doubling (Inrad Autotracker III) the output of a tunable narrow line width, dual grating dye laser (Narrowscan, Radiant), which was pumped by a 20 Hz Nd:YAG laser (Powerlite 8020, Continuum). The minimum scanning step for the dye laser was 0.0005 nm with a single pulse energy of a few μJ. The cross-section of the laser beam in the flame was ~ 0.5 mm^2. The laser beam path lengths inside the flame were estimated from the geometries of the flame images. A detailed description of the cavity ringdown system can be seen elsewhere [43]. The ringdown signal was detected using a photomultiplier tube (PMT, R928, Hamamatsu) with 10 nm band pass interference filter mounted in front and was monitored by an oscilloscope (TDS 410A, Tektronix) interfaced with computer III running a home-developed ringdown software. The ringdown baseline noise averaged over 100 ringdown events was typically 0.5% without plasma-assisted combustion running and 0.8% with the plasma-assisted combustion flame on.

2.3 Results and discussion

2.3.1 Plasma-assisted ignition: A modified U-shaped dependence of ignition power on fuel equivalence ratio

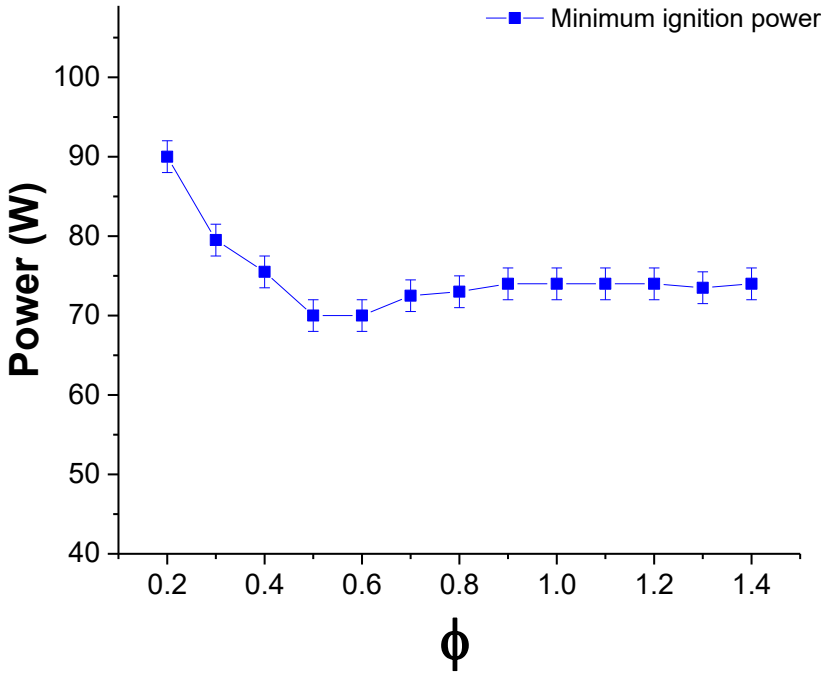

Figure 2.2 The modified U-shaped curve of plasma power vs. fuel equivalence ratio

The modified U-shaped curve of plasma power vs. fuel equivalence ratio (ϕ) showing the minimum plasma power required to ignite a premixed ethylene/air mixture. The curve was obtained by slowly increasing the plasma power from its minimum sustainable power of 5 W until a flame was observed outside the combustor for a fixed fuel equivalence ratio. The argon plasma flow rate and total flow rate of the ethylene/air mixture were fixed at 0.66 slm and 1.0 slm respectively.

The role of the plasma power on the ignition of ethylene/air mixtures at various equivalence ratios was investigated. Figure 2.2 shows the dependence of the minimum plasma power required to ignite and maintain a flame outside the combustor on fuel equivalence ratio at a fixed plasma gas flow rate. Figure 2.2 was obtained by increasing the argon plasma power for a fixed fuel equivalence ratio, from the minimum plasma

power where a stable plasma could be sustained by the surfatron of 5 W until when a flame was observed outside the combustor. The profile of the plot of the minimum power required for ignition vs. the fuel equivalence ratio obtained in this study displays similarities to the U-shaped plot of the minimum ignition power vs. fuel equivalence ratio which was previously reported for microwave plasma-assisted premixed methane/air combustion using a similar setup [37,44,45]. Despite the similarities with the U-shaped plot of plasma power required for ignition vs. fuel equivalence ratio reported in the literature, there exists the distinct independence of the ignition power at high fuel equivalence ratios forming a relatively flat part of the curve on the right side. Compared to the previously observed U-shaped curves [11], [12], [37,44,45], this new feature allows us to refer to the curve in figure 2.1 as the modified U-shaped curve. The similarities arise from the observation that, in both cases, a higher argon plasma power, which decreases with increase in fuel equivalence ratio, is required to ignite the premixed fuel/air mixture for ultra lean fuel equivalence ratios, in this case, fuel equivalence ratios in the range 0.2 – 0.6. The difference in both cases is observed for richer fuel equivalence ratios where it is seen that for a premixed methane/air mixture, the plasma power required for ignition increases with an increase in fuel equivalence ratio whereas in the case of ethylene/air mixture, the power required for ignition is independent of the fuel equivalence ratios.

In this study, it was observed that the degree of mixing of the plasma and fuel/air mixture due to the combustor geometry coupled with the energy density of ethylene influenced the plasma power required for ignition at different fuel equivalence ratios. The effect of combustor geometry which affects the mixing scheme in plasma-assisted

combustion was investigated by Hammack *et al.* [33], where they studied different combustor geometries to determine which offered the most efficient coupling of plasma energy for the enhancement of thermal oxidation of a methane/air mixture. Even though a similar fuel/air mixture was used in either case, the enhancement effects observed were varied for each of the combustor geometries. In this study, it was noticed that, the effect of the mixing scheme (due to the combustor geometry) and energy density of the fuel was however weak at ultra-lean fuel equivalence ratios and strong at stoichiometric to rich fuel equivalence ratios.

In a previous numerical study by J. Han *et al.* [46], on the spark ignition characteristics of a premixed methane/air mixture, it was shown that leaner mixtures were more sensitive to heat loss to the surrounding environment. Hence, the decrease in power required for ignition with increase in fuel equivalence ratio for ultra-lean fuel equivalence ratios in the range 0.2 – 0.6, is explained by the hypothesis that, even though the radical pool supplied by the plasma is sufficient to initiate ignition, the thermal energy released is not enough to offset the heat loss to the surrounding flow through diffusion, convection, and radiation. Therefore, a higher plasma power is required to provide more thermal energy to sustain the combustion process. This power was observed to reduce as the fuel equivalence ratio was increased from 0.2 – 0.6, because the thermal energy released by the premixed fuel/air mixture became higher and consequently a lower plasma power was required to offset the loss to the environment upon ignition.

The decrease in plasma power required for ignition with increase in fuel equivalence ratio for ultra-lean fuel equivalence ratios was also observed in a previous study using the same setup with methane as fuel which has a lower energy density

compared to ethylene [13]. A similar trend was also observed in the plasma-assisted combustion of ethylene using a different combustor geometry [47], thereby showing that at ultra-lean fuel equivalence ratios, the mixing schemes of the plasma and fuel/air mixture and the energy density of the fuel used have little influence on the ignition process which is more dependent on heat loss to the environment.

However, for fuel equivalence ratios in the range 0.7 – 1.4, the non-dependence of ignition plasma power on fuel equivalence ratios can be attributed to the high energy density of ethylene and the symmetric introduction of the plasma into the reaction zone allowed for by the geometry of the combustor used. When the plasma power was increased from 5 W until ignition was achieved for fuel equivalence ratios in the range 0.7 – 1.4, the energy released due to the high energy density of ethylene was enough to counter the thermal energy loss to the surrounding coflow. The high energy density of ethylene is partly credited for the non-dependence of the ignition plasma power on fuel equivalence ratios in the range 0.7 – 1.4 because different results were obtained from another study with a less energy dense fuel (methane) using a similar experimental setup [13, 44, 45]. The observance of different ignition phenomena for stoichiometric to rich fuel equivalence ratios of ethylene and the previously reported methane which have different energy densities is further supported by I. N. Kosarev *et al.* [48] who experimentally and numerically analyzed the ignition dynamics for various C_2 hydrocarbons and concluded that the efficiency of nonequilibrium excitation for ignition and combustion control is strongly dependent on the type of fuel used. The non-dependence of ignition power for higher fuel equivalence ratios ($\phi > 0.7$) is also partly attributed to the symmetrical introduction of the plasma into the combustion zone which

improves mixing of the plasma and fuel, allowing for the efficient coupling of the argon plasma into the combustion zone. This is supported by the fact that, a similar study using a premixed ethylene/air mixture carried out using a gamma (Γ) shaped combustor (47) did not yield the same results.

For all equivalence ratios investigated in this study, (0.2 ~ 1.4) flameholding could not be achieved when the fuel mixture was ignited using an external ignition source without the presence of plasma. Therefore, the observed modified U-shaped plot of the minimum required plasma power required for ignition vs. fuel equivalence ratio is a manifestation of the enhancement effect of the nonthermal microwave argon plasma on the premixed ethylene/air ignition.

2.3.2 Effect of plasma power on flame structure.

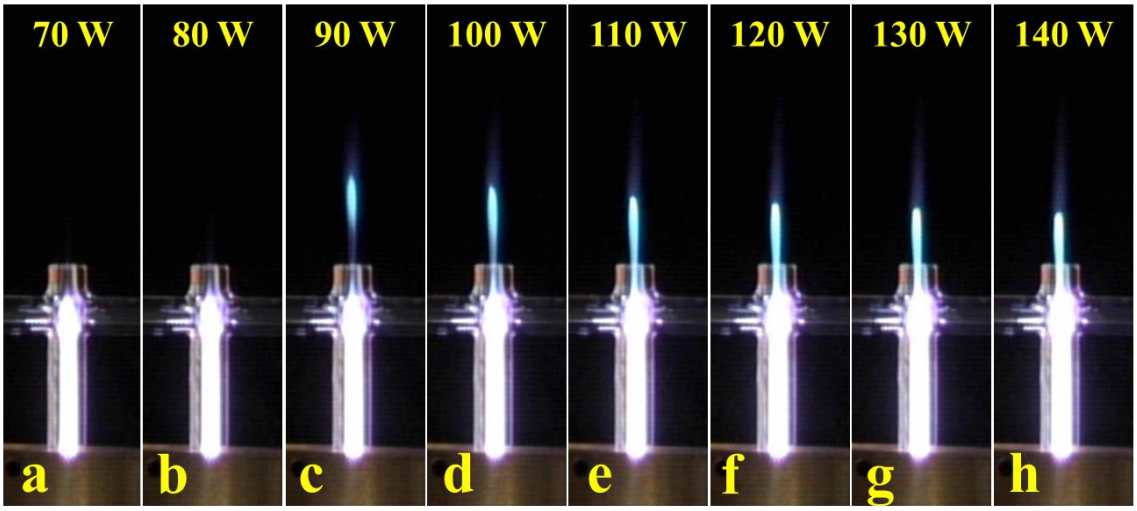

Figure 2.3 Effects of plasma power on flame structure

Effects of plasma power on flame structure in the microwave argon plasma-assisted ignition and combustion of a premixed ethylene/air mixture. The fuel equivalence ratio was fixed at 1.0 and the total flow rate of the fuel/air mixture was fixed at 1.0 slm while the argon plasma flow rate was fixed at 0.66 slm. Camera exposure was set at 1/60 s.

Figure 2.3 shows how the plasma power influences changes in flame structure, depicting the effect of plasma power on the flameholding of premixed ethylene/air mixtures. The plasma power was gradually increased from zero at 10 W intervals and images were taken after letting the setup run for 300 s to ensure that transient effects were excluded. No flame was observed for plasma powers less than 70 W but as the plasma power was increased above 70 W, a blue flame was seen extruding out of the combustor's orifice, as seen in figure 2.3b. Upon continuous increase in the plasma power, a lifted flame was observed at 90 W, figure 2.3c, with subsequent tethering of the lifted flame as shown in figure 2.3e. Further increase in the plasma power beyond 130 W (figures 2.3g and 2.3h) did not result in any significant observable change in the geometry of the flame. The observed structure of the flame was made up of an inner most layer surrounded by an outermost layer. The inner most layer referred to henceforth as the flame core was white in color and was observed to recede upstream of the flow and became anchored to the plasma column with increase in the plasma power. The outermost layer of the flame henceforth referred to as the outer flame layer had a blue hue and was observed to increase in length with flame power as shown in figure 2.3.

The tethering of the lifted flame with increase in plasma power demonstrates the ability of the plasma to improve on the flameholding. We propose that flameholding by the plasma is achieved by expediting the onset of fuel ignition and oxidation due to the influx of active radicals and thermal energy into the ethylene/air mixture. The infusion of the radicals and the thermal energy results in the creation of the innermost bright layer, the flame core, which is a product of the onset of fuel ignition and oxidation. The outermost blue flame layer develops because of the ignition of unburnt fuel/air mixture

and continuous combustion of the plasma activated fuel/air mixture with the surrounding air. Increasing plasma power increases the number density of radicals supplied by the plasma along with the thermal energy supplied to the flame core, which improves the flame speed upstream of the flow. Improving the flame speed enhances the tethering process which results in the observed increase in degree of flameholding (tethering of the flame to the combustor orifice) as seen in figure 2.3 with increase in plasma power. Saturation of the radical number density supplied by the plasma is attained at a plasma power of 130 W where it is observed that further increase in plasma power has no influence on the flame geometry. This is because at this plasma power, all the species present in the plasma gas are fully ionized and an increase in plasma power does not increase the number density of the radicals supplied by the plasma. This argument is buttressed by the study carried out by W. Wu et al. [44] who observed that in the plasma zone, the relative emission intensity of the excited state OH radical remained constant when the plasma power was increase to 100 W and higher. This occurred because saturation had been achieved at 100 W and further increase in plasma power did not yield production of more OH radicals. The color of the inner and outer flame is as a result of emission from the dominant radicals involved in the continuous oxidation of the ethylene/air mixture in each respective layer. More observations buttressing this speculation are presented in sections 2.3.3 and 2.3.4. In a similar study, W. Kim et al. [20] employed an ultra-short nanosecond repetitively discharge operated at 50 kHz and 6 kV to stabilize a premixed methane/air flame where they observed a dual layered flame with a white inner flame and a blue main flame. From observations made, they suggested

that ignition of the outer flame may be due to the inner flame OH rather than resulting directly from the discharge.

2.3.3 PAC flame structures via emission spectra

Emission spectra were obtained vertically along the axis of the plasma-assisted combustion flame and three distinct zones were identified, the plasma zone, the hybrid plasma-flame zone (hybrid zone), and the flame zone, as defined in our previous publications using this combustion facility [37, 49]. However the flame zone in this study is split into two distinct layers, a flame core and an outermost flame layer, which are distinguished by their characteristic emission spectra. It should be noted that the sizes of the three zones vary, depending on the PAC parameters such as fuel equivalence ratio, plasma power, argon plasma gas feed flow rate, and total fuel/air mixture flow rate; and the boundaries are just approximate with the zones clearly defined by their characteristic emission fingerprints. The following description of the locations of the zones is given based on the inset in figure 2.4, with combustor parameters fixed at a fuel equivalence ratio of 1.0, plasma power of 90 W, an argon plasma gas feed flow rate of 0.66 slm, and total fuel/air mixture flow rate of 1.0 slm. The plasma zone refers to the region from the combustor orifice to z = -10 mm as shown in the inset in figure 2.4 and is characterized by emissions from the electronic systems of the $OH(A^2\Sigma^+–X^2\Pi_{3/2})(0–0)$, $NH(A^3\Pi–X^3\Sigma^-)(0–0)$, and atomic lines from H_α, H_β, and Ar. Emissions observed from the plasma zone are characteristic of a typical atmospheric argon microwave plasma as observed in our previous publication [50]. The OH radicals in the plasma zone were formed mainly through electron impact dissociation of water coming from the impurities in the argon plasma feed gas [51].

The hybrid zone begins from the point where the microwave argon plasma meets with the premixed fuel/air mixture which occurs at z = - 10 mm. The hybrid zone is characterized by emissions from the electronic systems of the NO($A^2\Sigma^+$-$X^2\Pi$)(0–1)(0–2)(0–3), OH($A^2\Sigma^+$–$X^2\Pi_{3/2}$)(0–0), NH($A^3\Pi$-$X^3\Sigma^-$)(0–0), N_2($C^3\Pi_u$-$B^3\Pi_g$)(0–1), CN($B^2\Sigma^+$-$X^2\Sigma^+$)(0–0), CH($A^2\Delta$-$X^2\Pi$)(0–0), and C_2($d^3\Pi_g$-$a^3\Pi_u$)(0–0) (52). The hybrid zone extend downstream to ~ z = - 3 mm, the point at which the relative concentration of the excited state plasma generated radicals become negligible and goes below the detection threshold. The radicals observed are a manifestation of the radical pool created by the plasma upon interactions with the fuel/air mixture. These are formed as a result of the thermal dissociation, electron bombardment, and excited neutrals supplied by the argon microwave plasma, facilitating the breakdown of the fuel/air mixture and bringing about the chain initiation and chain branching reactions responsible for the ignition of the mixture [2].

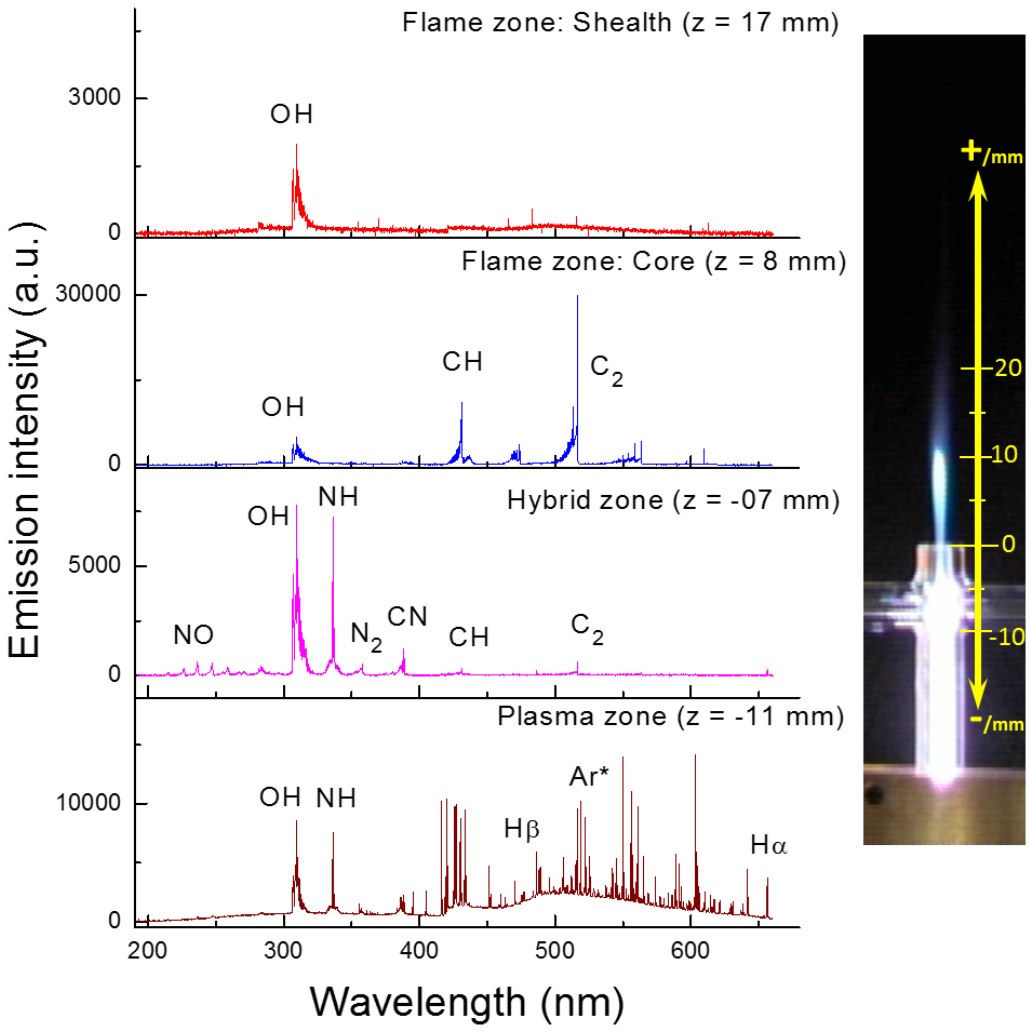

Figure 2.4 Optical emission spectra obtained at different spatial locations

Optical emission spectra obtained for the fixed, plasma power and flow rate of 90 W and 0.66 slm respectively, fuel equivalence ratio (ϕ) of 1.0, and total flow rate of the premixed ethylene/air mixture of 1.0 slm. The spectra show the three different zones: the plasma zone at z = - 11 mm inside the combustor, the hybrid plasma-flame zone at z = - 07 mm still inside the combustor, and the flame zone in both the flame core at z = 8 mm and the outer flame layer at z = 17 mm both outside the combustor. The spectra show the different species present in the different zones by their emission fingerprints.

The flame zone is split into two separate layers in this study, the flame core and the outer flame layer. The flame core refers to the zone z = - 3 mm to z = 11 mm and is

characterized by emissions from the OH($A^2\Sigma^+$–$X^2\Pi_{3/2}$)(0–0), CH($A^2\Delta$-$X^2\Pi$)(0–0), and C_2($d^3\Pi_g$-$a^3\Pi_u$)(0–0). This is due to chemiluminescence reactions initiated in the hybrid zone as well as chain initiation reactions from the re-ignition of the surrounding fuel/air coflow. The spectra from the outer flame layer are characterized by emission from the OH($A^2\Sigma^+$–$X^2\Pi_{3/2}$)(0–0) because of chain termination reactions occurring in this region.

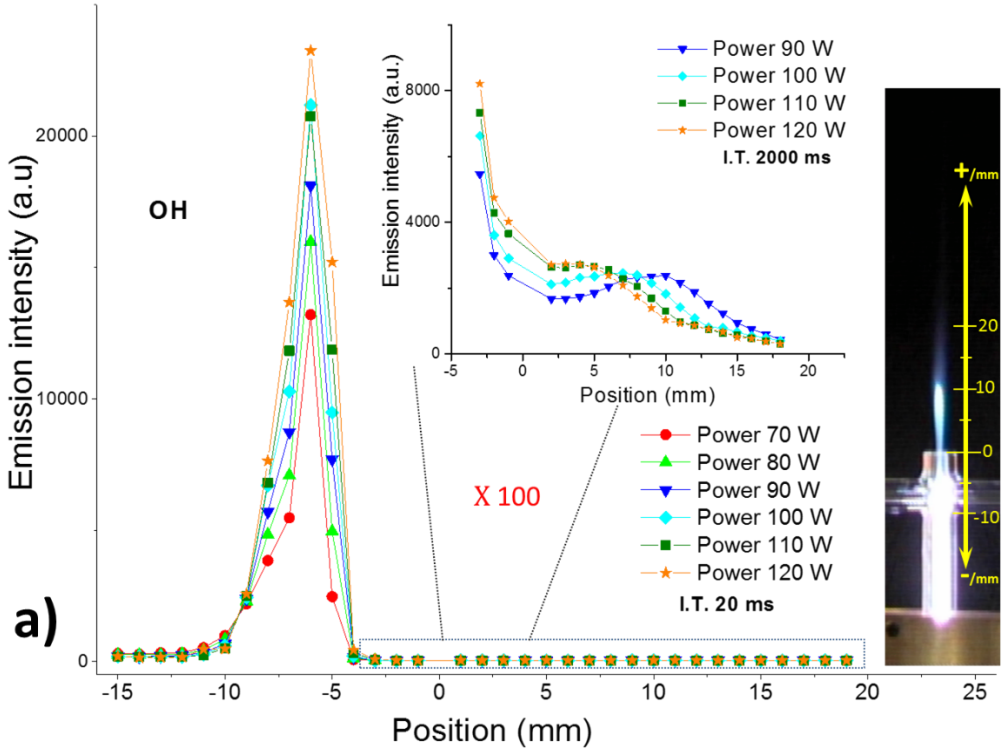

Figure 2.5 Plot of (a) OH(A), (b) CH(A), (c) C_2(d) emission intensity profiles

Plot of (a) OH(A) emission intensity profiles for the fixed fuel equivalence ratio (ϕ) of 1.0, fixed argon plasma flow rate of 0.66 slm, and fixed total flow rate of a premixed mixture of ethylene/air at 1.0 slm. The picture inserts were taken at plasma power 90 W, ϕ of 1.0, total flow rate 1.0 slm, and camera exposure time of 1/30 s

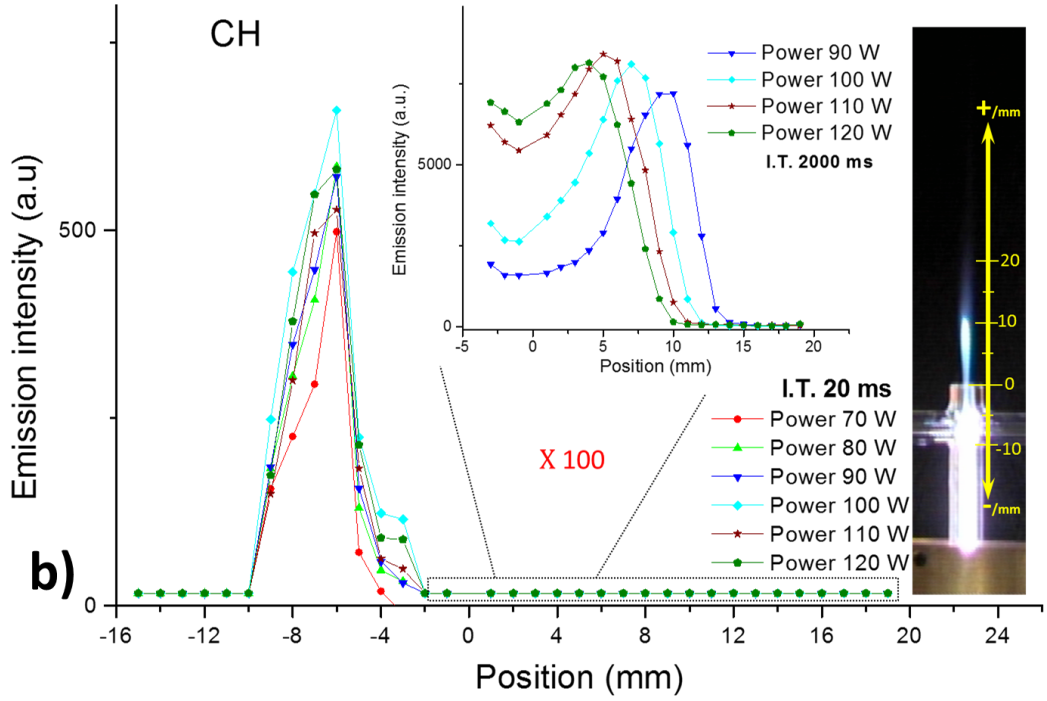

Figure 2.5 (continued)

Plot of (b) CH(A) emission intensity profiles for the fixed fuel equivalence ratio (ϕ) of 1.0, fixed argon plasma flow rate of 0.66 slm, and fixed total flow rate of a premixed mixture of ethylene/air at 1.0 slm. The picture inserts were taken at plasma power 90 W, ϕ of 1.0, total flow rate 1.0 slm, and camera exposure time of 1/30 s.

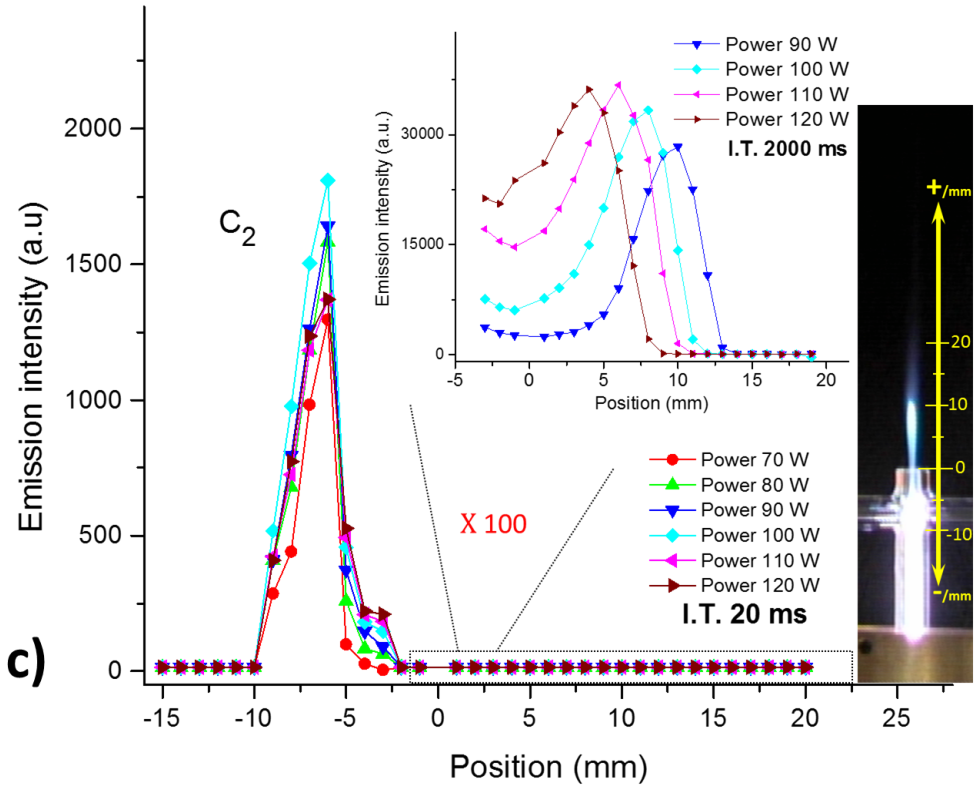

Figure 2.5 (continued)

Plot of (c) C_2(d) emission intensity profiles for the fixed fuel equivalence ratio (ϕ) of 1.0, fixed argon plasma flow rate of 0.66 slm, and fixed total flow rate of a premixed mixture of ethylene/air at 1.0 slm. The picture inserts were taken at plasma power 90 W, ϕ of 1.0, total flow rate 1.0 slm, and camera exposure time of 1/30 s.

Current understanding of the mechanism for the lifted flame implies that the flame stabilization occurs when the flame base is anchored instantaneously on a triple point of three branches where competition occurs between the flame propagating speed and the local flow velocity (53–55). In a recent study on the mechanisms of stabilization and blow off of a premixed flame downstream of a conducting plate, K. Kedia et al. [56] observed that the base of the flame was stabilized at the stagnation point, where the flame displacement speed was equal to the flow speed. The fact that in the current study, the flame could not be ignited or sustained without the presence of the plasma, shows that the

microwave plasma assists in the ignition and flameholding of ethylene/air mixtures; and it is speculated that ignition and flameholding occur in two stages. The first stage is the ignition of a flame core by the microwave plasma which acts as the radical pool required in the second stage. The second stage refers to the ignition and stabilization of the surrounding coflow due to the radicals and thermal energy supplied by the flame core.

This speculation is supported by the presence of the two peaks in the plot of the emission intensity profiles of the OH(A-X), CH(A-X), and C_2(d) systems along the flame propagation axis as shown in figure 2.5. It should be noted that in all three plots, the initial surge of OH(A), CH(A), and C_2(d) is very strong and prominent, easily observable at an integration time of the spectrometer of only 20 ms for all powers studied. The second peak is however, much weaker requiring an increase in the integration time by a factor of 100 to be observed and could not be observed at 70 W and 80 W. The surge in OH(A) radicals in the hybrid zone was used as an indicant of ignition [57]. The rapid drop in the emission intensity is due to OH(A) being used up in chain branching and chain propagating reactions. It is proposed that the initial surge in emission intensities of OH(A), CH(A) and C_2(d) radicals in the hybrid zone is a consequence of ethylene ignition by the nonthermal microwave plasma. The dominant mechanism for OH(A) formation is from the contribution of ongoing plasma processes such as electron impact dissociation of water and from chain initiation and chain propagation mechanisms during the break down of ethylene by plasma generated radicals. CH(A) and C_2(d) radicals are mainly produced from the chain propagation reactions $C_2H + O \rightarrow CH(A) + CO$, $C_2H + O_2 \rightarrow CH(A) + CO_2$, (58), and $CH_2 + C \rightarrow C_2(d) + H_2$ [59,60]. The subsequent drop in emission intensities of OH(A), CH(A) and C_2(d) is as a result of the radicals being

consumed in chain propagation and termination reactions. Even though an initial surge in OH(A) is observed for all the powers investigated, the relative intensities are different, with higher peak OH(A) emission intensities recorded for higher powers as seen in figure 2.5.

As reported in a previous study using a similar setup, N. Srivastava et al. [40] investigated OH radicals in an atmospheric pressure helium microwave plasma jet and concluded that OH radicals increase with increase in plasma power. Therefore, an increase in plasma power results in more reactive species being created by the plasma and combined with the observation that an increase in plasma power results in the increase in the relative emission intensities of the OH(A-X), CH(A-X) and C_2(d) species, we confirmed that an increase in plasma power increases the size of the radical pool generated by the plasma. Hence, the relative emission intensity of OH(A) can be used as an indicator of the size of the radical pool created by the plasma prior to the ignition. For plasma powers 80 W and below, no secondary peak was observed because the size of radical pool generated at these plasma powers is small as inferred from the relatively low emission intensity of the peak of the OH(A) radical profile in figure 2.5. The small size of the radical pool generated results in the inadequate supply of radicals to help ignite and stabilize the surrounding coflow. An increase in the plasma power from 90 W to higher results in the occurrence of a secondary peak in the emission intensity that is observed to increase with an increase in plasma power. The formation of the secondary peak is due to chemiluminescence reactions from the ongoing ignition of the surrounding coflow via a series of reactions detailed by T. Kathrotia et al. [61],

$$CH + O_2 \rightarrow OH^* + CO \qquad (2.1)$$

$$HCO + O \rightarrow OH^* + CO \quad (2.2)$$

$$H + O + M \rightarrow OH^* + M \quad (2.3)$$

$$C_2H + O \rightarrow CH^* + CO \quad (2.4)$$

$$C_2H + O_2 \rightarrow CH^* + CO_2 \quad (2.5)$$

$$C_2 + OH \rightarrow CH^* + CO \quad (2.6)$$

$$CH_2 + C \rightarrow C_2^* + H_2 \quad (2.7)$$

$$C_3 + O \rightarrow C_2^* + CO \quad (2.8)$$

The presence of the secondary peak for powers 90 W and above suggests that the size of the radical pool is large enough to sustain ignition of the surrounding coflow. It should however be noted that for powers 90 W and above, the position of the secondary peak is observed to recede toward the hybrid zone with increase in plasma power. The receding of the secondary peak position can be accounted for by the fact that an increase in plasma power results in an increase in the size of the radical pool formed prior to the ignition. This increase in the size of the radical pool results in more of the fuel being consumed as seen by the increase in the CH(A) and C_2(d) emission intensities with increase in power. More fuel being oxidized in the flame core results in a higher temperature as discussed subsequently facilitating a faster ignition of the surrounding coflow. This fast ignition of the surrounding coflow coupled with a rich radical pool and thermal energy supplied by the flame core results in an enhancement in the flame propagation speeds upstream of the flow which counters the mixture flow speed thereby resulting in the observed receding in the position of the peak of the secondary peak in the emission profiles of the OH(A-X), CH(A-X) and C_2(d) as seen in figure 2.5. Therefore, an increased flame propagation speed dominating the mixture flow speed results in a

more tethered flame. Hence, the observed improvement in flameholding with increase in plasma power.

2.3.4 Rotational temperature

Figure 2.6 shows the rotational temperatures simulated using the relative emission intensities of the R and P branches of the OH(A-X)(0-0) band using Specair [62]. The rotational temperature was obtained by fitting the simulated spectra to the experimental spectra acquired by taking the average of ten emission spectra at each fixed spatial location. The rotational temperature obtained is the average rotational temperature along the line of the sight of the spectrometer. There was a ±50 K error margin obtained when simulating the best fit curve. From figure 2.6, it is observed that the rotational temperature drops at z = - 9 mm due to dilution of the plasma gas with the incoming room temperature fuel/air mixture. Upon dilution, the temperature is observed to surge at z = - 5 mm. This increase in temperature is attributed to the onset of ignition of the ethylene/air mixture due to fuel breakdown and oxidation reactions. A similar phenomenon was also reported in a related study on the ignition of ethylene/air flows by a nanosecond repetitively pulsed discharge plasma conducted by A. Bao *et al.* [63] where they recorded an increase in temperature of about 230 − 350 ºC upon addition of fuel to the air flow and only 50 ºC when adding fuel to nitrogen flow under the same flow and discharge conditions. They concluded that the rise in temperature was a consequence of plasma chemical fuel oxidation reactions initiated by radicals generated in the plasma.

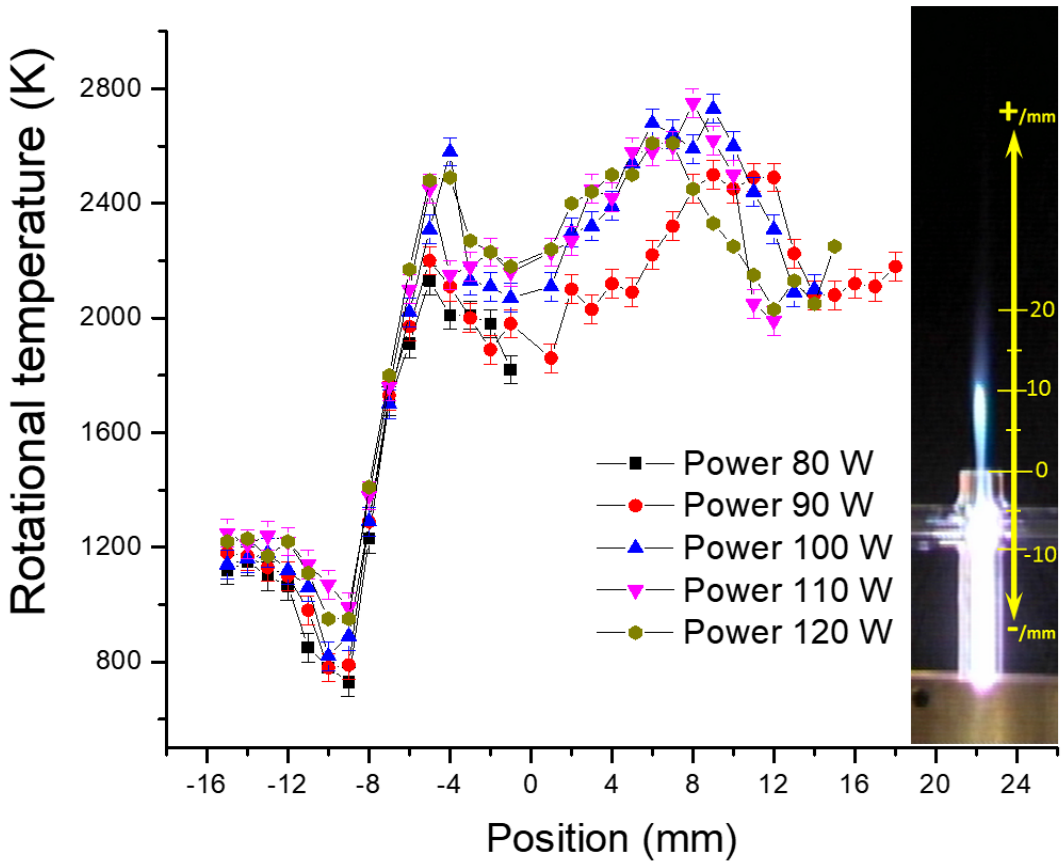

Figure 2.6 Rotational temperature profile variation with power

Temperature profiles for fixed fuel equivalence ratio (ϕ) of 1.0, fixed argon plasma flow rate of 0.66 slm, and fixed total flow rate of a premixed mixture of ethylene/air at 1.0 slm. The picture insert was taken for plasma power 90 W, ϕ of 1.0, total flow rate 1.0 slm, and camera exposure time of 1/30 s.

Using the surge in temperature to define the position at which ignition occurs, the same convention used by S. Nagaraja et al. [57] who numerically investigated the ignition of a preheated hydrogen/air mixture excited by a pulsed nanosecond dielectric barrier discharge. It was observed that the rotational temperature at the location where ignition occurs, increases with an increase in plasma power.

We propose that the observed increase in temperature at the position at which ignition occurs with increase in plasma power is due to the ignition of a larger percentage

of fuel with increase in plasma power. An increase in plasma power results in an increase in the radical number density being supplied by the plasma to the hybrid zone. This point is supported by the study done by C. Wang *et al.* [64] on the OH number densities and plasma jet behavior in the atmospheric microwave plasma jets operating with different gasses. In that study, they observed an increase in OH number densities with increase in plasma power for all the different plasma gasses used. Thus the increased influx of radicals due to the increase in plasma power in turn facilitates the ignition of a larger percentage of the incoming fuel/air mixture and consequently, the observed increase in temperature at the position at which ignition occurs. This argument is supported by a related study by S. Nagaraja et al. [65] who investigated the ignition of hydrogen/air mixtures using a nanosecond dielectric barrier plasma discharge in plane to plane geometry. They showed that number of radicals and excited species (size of the radical pool) increased with increase in the number of pulses in each discharge burst. They observed that ignition delay exhibited a threshold like dependence on input plasma energy and increased steeply as the number of pulses in the burst was reduced. It can therefore be inferred that an increase in the number of pulses in each burst results in the increase in the size of the radical pool generated which in turn reduces the ignition delay time of the fuel flow. The increase in the size of the radical pool as evidenced by a reduced ignition delay time results in the ignition of a larger volume of the fuel/air mixture, thus giving rise to a higher temperature.

The drop in temperature observed after the initial peak for all powers investigated is due to thermal losses to the surrounding coflow. This preheating of the surrounding coflow coupled with the radical pool generated by the plasma, facilitates the ignition of

the coflow. The ignition of the coflow and exothermic chain termination reactions from the flame core results in a secondary peak at a much higher temperature occurring downstream of the flame. The temperature profiles are observed to taper off downstream of the flow as a result of thermal losses to the surrounding atmosphere.

2.3.5 Cavity ringdown measurements of the number densities of the OH(X) radicals

The OH(X) number density profiles obtained by scanning along the z direction at the center of the flame axis with a spatial resolution of 1 mm are shown in the inset in figure 2.7. A section of the rotationally-resolved CRDS of the OH(A-X)(0-0) band near 308 nm was initially scanned with a low spectral resolution of 0.005 nm. All the OH A-X (0-0) rotational lines in the spectral scan were clearly resolved and assigned by comparing with simulated spectra from LIFBASE (66). The $R_2(1)$ line was selected for OH(X) number density measurements because it has no spectral overlap with other rotational lines.

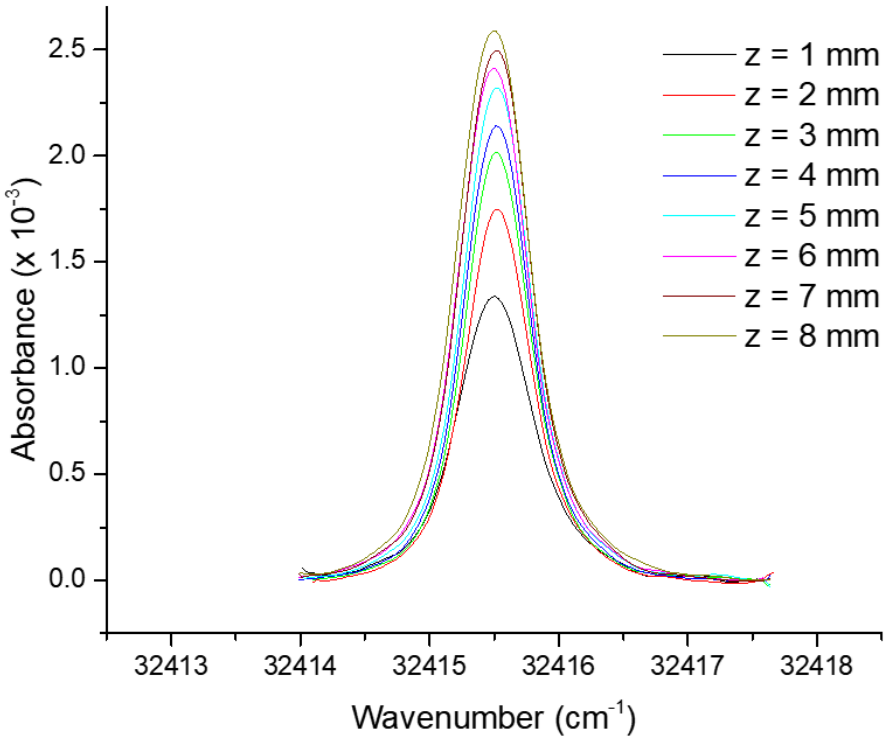

Figure 2.7 The measured $R_2(1)$ line shapes at different locations outside the combustor orifice. A ten-point adjacent-average was taken to smooth each of the line shape scans.

Shown in figure 2.6 are plots of the absorbance vs. wavenumber (cm^{-1}) obtained by high resolution scans of the OH $R_2(1)$ line shape at different locations in the flame outside the combustor orifice. Due to the impedance of the laser beam by the quartz combustor, cavity ringdown spectra could not be acquired in the hybrid zone inside the combustor. The integrated absorbance was used to determine the OH number density. The absolute number densities of the electronic ground state OH radicals in the lower rotational energy level of the $R_2(1)$ transition were derived from the ringdown measurements using the formula,

$$\text{Integrated absorbance} = \int_{\nu} \frac{L}{c}\left(\frac{1}{\tau^{f}(\nu)} - \frac{1}{\tau_0^{f}}\right) d\nu = S(T)nl \qquad (2.9)$$

where n is the total OH number density; and are the ringdown times obtained in the plasma-assisted combustion flames when the laser wavelength is tuned on and off the absorption peak, respectively; c is the speed of light; L and l are the ringdown cavity length and the laser beam path-length respectively. S(T) is the temperature-dependent line intensity and can be calculated using Equation (2.2) [67]

$$S(T) = 3.721963\times10^{-20}\frac{T(K)}{273.16}\frac{1}{8\pi c\nu^2}\left(\frac{N}{P}\right)\left(\frac{e^{-1.4388E''/T}}{Q_{VR}}\right)A^{v'J'}_{v''J''}(2J'+1)\left(1-e^{\frac{-1.4388\nu}{T}}\right)$$

(2.10)

where T is the temperature in Kelvin, ν is the transition frequency of the OH $R_2(1)$ line of 32415.452 cm^{-1}, N is the total number density (molecule cm^{-3}) at pressure P (atm) and temperature T, is the Einstein coefficient in s^{-1}, E″ is the lower state energy, i.e. 126.449 cm^{-1}, and Q_{VR} is the vibrational rotational partition function with V and J vibrational and rotational quantum numbers, respectively. In this study, the temperatures used to calculate the temperature-dependent line intensities S(T) were determined by the spectra simulations using Specair as discussed in Section 3.4

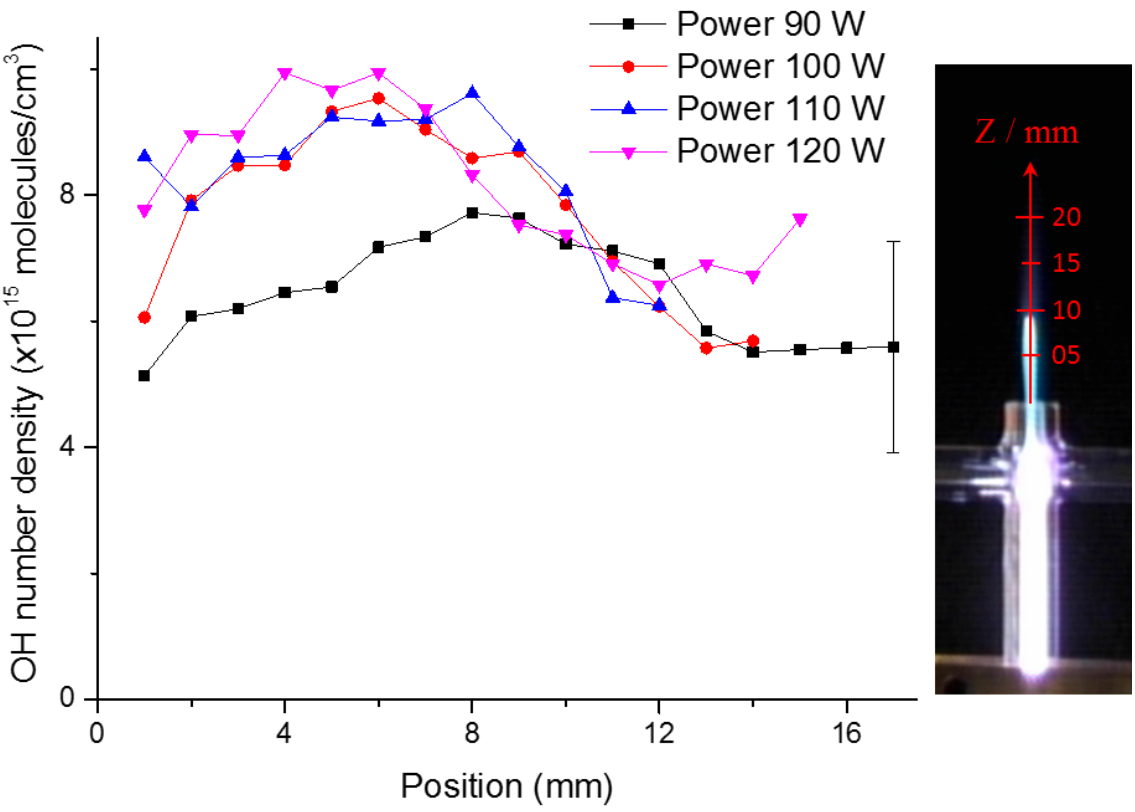

Figure 2.8 OH(X) number density profiles in the flame zone at different plasma powers.

The measured OH(X) number densities in the plasma-assisted combustion of premixed ethylene/air flames. The error bars indicate the maximum measurement uncertainty of ±30%. The picture insert was taken for plasma power 90 W, ϕ of 1.0, total flow rate 1.0 slm, and camera exposure time of 1/30 s.

Figure 2.8 shows the measurement results of the absolute OH(X) number density in the flame region at different plasma powers with the measurement uncertainty of OH(X) number densities being estimated by the measurement errors in the gas temperature and in the laser beam path-length. The temperature sensitivity of the line intensity of the OH A-X (0-0) $R_2(1)$ line was approximately 5% per 100 K at 2000 K. The error in determining path-lengths from the images is in the scale of up to 0.5 mm,

which accounts for 25% of a typical path-length near 2 mm. Therefore, the overall maximum uncertainty of the measured OH(X) number densities was ±30%.

OH(X) number density was observed to increase to a maximum before dropping off downstream of the flame for all powers investigated. For power 90 W, the OH(X) number density was observed to increase from 5.1×10^{15} molecules cm^{-3} outside the combustor orifice to a maximum of 7.7×10^{15} molecules cm^{-3} at z = 08 mm before dropping to 5.6×10^{15} molecules cm^{-3} downstream of the flame. The OH(X) number density was of the same order of magnitude, 10^{16} molecules cm^{-3}, as measured in a previous study using the same combustor facility [12] as well as in another study using a similar PAC system employing the plane-LIF technique [33]. The initial increase in OH(X) indicates that the mechanism of OH(X) production, $O(^3P) + H_2O \rightarrow OH + OH$ (25) and $O(^1D)+H_2O\rightarrow 2OH(X)$ (41)(31), supersede the mechanism of OH(X) consumption by chain termination reactions which can only happen if the flame core is igniting the surrounding fuel/air mixture. It should be noted that the OH(X) number density profiles simultaneously increased or decreased with the OH(A) emission intensity profiles. Hence, the increase in OH(A) previously discussed in Section 2.3 is not a consequence of excitation of the ground state OH(X) to the excited state OH(A) but is a result of chain initiating and chain propagation reactions described above.

From the measured OH(X) number densities, it was concluded that the electronic ground state OH(X) and the excited state OH(A) varied similarly along the axis of the combustor for all powers measured. This implied that the increase in number densities of OH(X) was not solely because of relaxation of the excited state OH(A) but due to continuous formation of the radicals; so is the increase in the OH(A) intensity profile not

solely a consequence of excitation of the OH(X) to the excited state, because they both increased and decreased simultaneously. Hence, taking into consideration the simultaneous rise and fall in the emission intensity of OH(A) and the number density profiles of OH(X), it can be concluded that the total concentration of OH (A, X) radicals in the combustion system exhibits a dual peak phenomenon. The first peak occurs in the hybrid zone indicating the ignition of the flame core which establishes the radical pool that facilitates the ignition of the surrounding coflow. The ignition of the secondary coflow results in the observed second peak. The existence of the dual peaks in the total OH radical number densities thereby buttresses the hypothesis that the flameholding occurs in two stages with the inner radically rich core driving the ignition of the surrounding coflow.

2.4 Summary

The effect of a nonthermal microwave argon plasma on the plasma-assisted combustion of a premixed ethylene/air mixture has been studied. A modified U-shaped minimum ignition plasma power curve vs. fuel equivalence ratio in the plasma-assisted ignition of an ethylene/air mixture was reported in this study. The modified U-shaped curve is similar yet significantly different from the U-shaped minimum ignition power vs. fuel equivalence ratio reported in previous methane/air studies in that, even though it displays the similar trend of decrease in minimum ignition plasma power with increase in fuel equivalence ratio for ultra-lean fuel equivalence ratios (0.2 – 0.6), the trend is different for lean to rich fuel equivalence ratios. For lean to rich fuel equivalence ratios in ethylene/air ignition (0.7 ─ 1.4), the minimum ignition plasma power remained fairly constant throughout, whereas an increase in the minimum ignition plasma power was

observed with increase in fuel equivalence ratio for the methane/air ignition. The results obtained suggest that the PAC at leaner fuel equivalence ratios is more susceptible to heat losses to the environment but less sensitive to the mixing scheme between the plasma and fuel/air mixture, whereas the PAC at richer fuel equivalence ratios is less susceptible to heat losses but more sensitive to the mixing scheme. Images of the PAC flames revealed the existence of a dual layered flame with an inner white flame core and an outer blue flame layer due to emissions from the dominant species present in either layer. Emission spectra obtained along the burner axis reinforced the dual layered nature of the PAC flame with clearly distinct emission spectra from the flame core and the outer flame layer. Using the emission intensity of the OH(A-X) transitions as an indicator of the size of the radical pool created, it was observed that a larger radical pool resulted in improved flameholding, more fuel consumed as evidenced by the corresponding increase in the emission intensities of C_2 and CH radicals and subsequently a higher flame rotational temperature. Measured OH(X) number density profiles outside the combustor using CRDS provided evidence supporting the ignition of the surrounding coflow. It was observed that both OH(X) number density profiles and OH(A) emission intensity profiles peaked simultaneously at the same location for all powers investigated. This result shows that the total OH(A,X) radicals in the system experienced a secondary peak downstream of the hybrid zone indicating ignition of the coflow. From the above observations, we propose that the mechanism of the plasma-assisted flameholding in the ethylene/air flame studied in this work is dominantly radical driven and occurs in two steps with the formation of an inner radically rich flame core which ignites and stabilizes the surrounding coflow.

2.5 References

1. Starikovskii A Y, Anikin N B, Kosarev I N, Mintoussov E I, Starikovskaia S M and Zhukov V P 2006 Plasma-assisted combustion. *Pure Appl Chem* **78** 1265 – 98

2. Sun W and J Y Nonequilibrium Plasma-Assisted Combustion: A Review of Recent Progress *Plasma Fusion Res*. 2013 **89** 208–19

3. Starikovskiy A 2015 Physics and chemistry of plasma-assisted combustion *Philos Trans R Soc London A Math Phys Eng Sci* **373** 20150074

4. Ju Y and Sun W 2015 Plasma assisted combustion: Dynamics and chemistry. *Prog Energy Combust Sci* **48** 21–83

5. Savelkin K V, Yarantsev D A, Adamovich I V and Leonov S B 2015 Ignition and flameholding in a supersonic combustor by an electrical discharge combined with a fuel injector *Combustion and Flame* **162** 825 – 35

6. Dutta A, Yin Z and Adamovich I V 2011 Cavity ignition and flameholding of ethylene–air and hydrogen–air flows by a repetitively pulsed nanosecond discharge *Combustion and Flame* **158**1564 – 76

7. Lefkowitz, J K, Uddi M, Windom B C, Lou G and Ju Y 2015 In situ species diagnostics and kinetic study of plasma activated ethylene pyrolysis and oxidation in a low temperature flow reactor *Proceedings of the Combustion Institute* **35** 3505 – 12

8. Mintusov E, Serdyuchenko A, Choi I, Lempert W R and Adamovich I V 2009 Mechanism of plasma assisted oxidation and ignition of ethylene–air flows by a repetitively pulsed nanosecond discharge *Proceedings of the Combustion Institute* **32**3181 – 8

9. Kosarev I N, Ivanov G V, Kindysheva S V, Sagulenko P V, Aleksandrov N L, Starikovskaia S M and Starikovskii A Y 2008 Measurement of intermediates in the process of plasma assisted ignition *International conference on Gas Discharges and their Applications* **14** 621 – 4;

10. Bak M S, Im S, Mungal M G and Cappelli M A 2013 Studies on the stability limit extension of premixed and jet diffusion flames of methane, ethane, and propane using nanosecond repetitive pulsed discharge plasmas *Combustion and Flame* **160** 2396 ─ 2403

11. Ono R and Oda T Spark ignition of hydrogen-air mixture 2008 *J Phys Conf Ser* **142** 012003.

12. Han J, Yamashita H and Hayashi N 2010 Numerical study on the spark ignition characteristics of a methane–air mixture using detailed chemical kinetics *Combustion and Flame* **157** 1414 – 21

13. Wu W, Fuh C A and Wang C Comparative study on microwave plasma-assisted combustion of premixed and nonpremixed methane/air mixtures *Combustion Science and Technology* **187** 999 – 1020

14. Inomata T, Okazaki S, Moriwaki T, and Suzuki M 1983 The application of silent electric discharges to propagating flames *Combust Flame* **50** 361–3

15. Chintala N, Bao A, Lou G, and Adamovich I V 2006 Measurements of combustion efficiency in nonequilibrium RF plasma-ignited flows *Combust Flame* **144** 744–56.

16. Hemawan K W, Wichman I S, Lee T, Grotjohn T A, and Asmussen J 2009 Compact microwave re-entrant cavity applicator for plasma-assisted combustion *Rev Sci Instrum* **80** 053507

17. Udagawa K, Gorbatov S, Pliavaka F, Nishihara M, and Adamovich V 2008 Experimental study of a fast Ionization wave discharge at high pulse repetition rates *AIAA Aerospace Sciences Meetings and Exhibit* **46** 1104

18. Pancheshnyi S V, Lacoste D A, Bourdon A and Laux C O 2006 Ignition of propane-air mixtures by a repetitively pulsed nanosecond discharge *IEEE Trans Plasma Sci* **34** 2478 – 87

19. Starikovskaia S M, Kosarev I N, Krasnochub A V, Mintoussov E I and Starikovskii A Y. 2005 Control of combustion and ignition of hydrocarbon-containing mixtures by nanosecond discharges *AIAA Aerospace Sciences Meeting and Exhibit* **43** 1195

20. Kim W, Do H, Mungal M G and Cappelli M A 2006 Flame stabilization enhancement and nox production using ultra short repetitively pulsed plasma discharges *AIAA Aerospace Sciences Meeting and Exhibit* **44** 560

21. Lou G, Bao A, Nishihara M, Keshav S, Utkin Y G, Rich J W, Lempert W R and Adamovich I V 2007 Ignition of premixed hydrocarbon–air flows by repetitively pulsed, nanosecond pulse duration plasma *Proceedings of the Combustion Institute* **31** 3327 – 34

22. Adamovich I V, Lempert W R, Nishihara M, Rich J W and Utkin Y G 2008 Repetitively pulsed nonequilibrium plasmas for magnetohydrodynamic flow control and plasma-assisted combustion *Journal of Propulsion and Power* **24** 1198–215

23. Wang F, Liu J B, Sinibaldi J, Brophy C, Kuthi A, Jiang C, Ronney P and Gundersen M A 2005 Transient plasma ignition of quiescent and flowing air/fuel mixtures *IEEE Trans Plasma Sci* **33** 844 – 9.

24. Liu J, Wang F, Li G, Kuthi A, Gutmark E J, Ronney P D and Gundersen M A 2005 Transient plasma ignition *IEEE Trans Plasma Sci* **33** 326–7

25. Tang J, Zhao W, Duan Y. 2011 Some observations on plasma-assisted combustion enhancement using dielectric barrier discharges *Plasma Sources Sci Technol* **20** 045009.

26. Korolev Y D, Frants O B, Landl N V, Geyman V G, Shemyakin I A, Enenko A A, and Matveev I B. 2009 Plasma-assisted combustion system based on nonsteady-state gas-discharge plasma torch. *IEEE Trans Plasma Sci* **37** 2314–20

27. Korolev Y D, Frants O B, Landl N V, Geyman V G and Kasyanov V S 2014 Methane oxidation in a low-current nonsteady-state plasmatron *IEEE Trans Plasma Sci* **42** 1615–22

28. Rao X, Hammack S and Carter C 2011 Microwave Plasma Coupled Re-Ignition of Methane and Oxygen Mixture Under Auto-Ignition Temperature *IEEE Trans Plasma Sci* **39** 3307 – 13

29. Shibkov V M, Shibkova L V, Gromov V G, Karachev A A and Konstantinovskii R S 2011 Influence of surface microwave discharge on ignition of high-speed propane-air flows **49** 155 – 67

30. Rao X, Hemawan K, Wichman I, Carter C, Grotjohn T, Asmussen J and Lee T 2011 Combustion dynamics for energetically enhanced flames using direct microwave energy coupling *Proc Combust Inst* **33** 3233 – 40

31. Rao X, Hammack S, Lee T, Carter C and Matveev I B 2010 Combustion Dynamics of Plasma-Enhanced Premixed and Nonpremixed Flames *IEEE Trans Plasma Sci* **38** 3265–71

32. Kopyl P V, Surkont O S, Shibkov V M and Shibkova L V 2012 Stabilization of liquid hydrocarbon fuel combustion by using a programmable microwave discharge in a subsonic airflow *Plasma Phys Reports* **38** 503 – 12

33. Hammack S, Lee T and Carter C 2012 Microwave plasma enhancement of various flame geometries at atmospheric pressure *IEEE Trans plasma Sci* **40** 3139–46

34. Michael J B, Dogariu A, Shneider M N and Miles R B 2010 Subcritical microwave coupling to femtosecond and picosecond laser ionization for localized, multipoint ignition of methane/air mixtures *J Appl Phys* **108** 093308.

35. Babaritskii A I, Baranov I E, Bibikov M B, Demkin S A, Zhivotov V K, Konovalov G M, Lysov G V, Moskovskii A S, Rusanov V D, Smirnov R V and Cheban'kov F N 2004 Partial hydrocarbon oxidation processes induced by atmospheric pressure microwave discharge plasma *High Energy Chemistry* **38** 407–11

36. Wolk B, DeFilippo A, Chen J-Y, Dibble R, Nishiyama A and Ikeda Y 2013 Enhancement of flame development by microwave-assisted spark ignition in constant volume combustion chamber. *Combustion and Flame* **160** 1225 – 34

37. Wang C and Wu W 2013 Simultaneous measurements of OH(A) and OH(X) radicals in microwave plasma jet-assisted combustion of methane/air mixtures around the lean-burn limit using optical emission spectroscopy and cavity ringdown spectroscopy. *J Phys D Appl Phys* **46** 464008

38. Srivastava N and Wang C 2011 Effects of water addition on OH radical generation and plasma properties in an atmospheric argon microwave plasma jet *J Appl Phys* **110** 053304

39. Wang C, Srivastava N and Dibble T S 2009 Observation and quantification of OH radicals in the far downstream part of an atmospheric microwave plasma jet using cavity ringdown spectroscopy *Appl Phys Lett* **95** 051501.

40. Srivastava N and Wang C. 2011 Determination of OH radicals in an atmospheric pressure helium microwave plasma jet *IEEE Trans Plasma Sci* **39** 918 – 24

41. 41. Wang C, Srivastava N, Scherrer S, Jang P R, Dibble T S and Duan Y 2009 Optical diagnostics of a low power – low gas flow rates atmospheric-pressure argon plasma created by a microwave plasma torch *Plasma Sources Sci Technol* **18** 025030

42. Wang C and Wu W. 2014 Roles of the state-resolved OH(A) and OH(X) radicals in microwave plasma assisted combustion of premixed methane/air: An exploratory study *Combustion and Flame* **161** 2073–84.

43. Wang C 2007 Plasma-cavity ringdown spectroscopy (P-CRDS) for elemental and isotopic measurements *J Anal At Spectrom* **22** 1347 – 63.

44. Wang C and Wu W 2014 Roles of the state-resolved OH(A) and OH(X) radicals in microwave plasma assisted combustion of premixed methane/air: An exploratory study *Combustion and Flame* **161** 2073–84

45. Fuh C A, Wu W and Wang C. 2014 Effects of a microwave induced argon plasma jet on premixed and nonpremixed methane/air mixtures *AIAA Plasma dynamics and Laser conference* **45** 2240

46. Han J, Yamashita H and Yamamoto K 2009 Numerical study on spark ignition characteristics of a methane-air mixture using detailed chemical kinetics *J Therm Sci Technol* **4** 305–13

47. Wu W, Fuh C A and Wang C A parametric study of the microwave plasma-assisted combustion of premixed ethylene/air mixtures: OH, CH, and C_2 radicals, To be submitted.

48. Kosarev I N, Kindysheva S V, Momot R M, Plastinin E A, Aleksandrov N L and Starikovskiy A Y 2016 Comparative study of nonequilibrium plasma generation and plasma assisted ignition for C_2 hydrocarbons *Combustion and Flame* doi:10.1016/j.combustflame.2015.12.011

49. Wang C and Wu W 2014 Roles of the state-resolved OH (A) and OH (X) radicals in microwave plasma assisted combustion of premixed methane/air: An exploratory study *Combustion and Flame* **161** 2073-2084

50. Wang C and Srivastava N 2010 OH number densities and plasma jet behavior in atmospheric microwave plasma jets operating with different plasma gases (Ar, Ar/N_2, and Ar/O_2). *Eur Phys J D* **60** 465–77

51. Bruggeman P and Schram D C. 2010 On OH production in water containing atmospheric pressure plasmas. *Plasma Sources Sci Technol* **19** 045025

52. Herzberg G and Huber K P 1979 *Molecular Spectra and Molecular Structure* (New York, NY: Van Nostrand Reinhold)

53. Joedicke A, Peters N and Mansour M, 2005 The stabilization mechanism and structure of turbulent hydrocarbon lifted flames *Proc Combust Inst* **30** 901–9

54. Ko Y S, Chung S H, Kim G S and Kim SW 2000 Stoichiometry at the leading edge of a tribrachial flame in laminar jets from Raman scattering technique *Combustion and Flame*. **123** 430–3

55. Kim W, Do H, Mungal M G and Cappelli M A 2007 Investigation of NO production and flame structure in plasma enhanced premixed combustion *Proc Combust Inst* **31** 3319 – 26

56. Kedia K S and Ghoniem A F 2012 Mechanisms of stabilization and blowoff of a premixed flame downstream of a heat-conducting perforated plate. *Combustion and Flame* **159** 1055 – 69

57. Nagaraja S, Yang V, Yin Z and Adamovich I 2014 Ignition of hydrogen-air mixtures using pulsed nanosecond dielectric barrier plasma discharges in plane-to-plane geometry *Combustion and Flame* **161** 1026 – 37

58. Glassman Iand Yetter R A 2008 *Combustion*, (New York, NY :Academic Press)

59. Grebe J and Homann K H 1982 Blue-green Chemiluminescence in the System C_2H_2/O/H. Formation of the Emitters CH($A^2\Delta$), $C_2(d^3\Pi g)$ and C_2H^*. *Berichte der Bunsengesellschaft für Phys Chemie* **86** 587–97

60. Smith G P, Park C, Schneiderman J and Luque J 2005 C_2 Swan band laser-induced fluorescence and chemiluminescence in low-pressure hydrocarbon flames *Combustion and Flame.* **141** 66 – 77

61. Kathrotia T, Riedel U and Warnatz J 2009 A numerical study on the relation of OH*, CH*, and C2* chemiluminescence and heat release in premixed methane flames *Proc Eur Combust Meet* **4** 2–6

62. Laux C O, Spence T GKruger C H and Zare R N 2003 Optical diagnostics of atmospheric pressure air plasmas *Plasma Sources Sci Technol* **12** 125 – 138

63. Bao A, Utkin Y G, Keshav S, Lou G and Adamovich I V 2007 Ignition of ethylene-air and methane-air flows by low-temperature repetitively pulsed nanosecond discharge plasma *IEEE Trans Plasma Sci* **35** 1628–38

64. Wang C and Srivastava N 2010 OH number densities and plasma jet behavior in atmospheric microwave plasma jets operating with different plasma gases (Ar, Ar/N2, and Ar/O2). *Eur Phys J D* **60** 465–77

65. Nagaraja S, Yang V, Yin Z and Adamovich I 2014 Ignition of hydrogen-air mixtures using pulsed nanosecond dielectric barrier plasma discharges in plane-to-plane geometry *Combustion and Flame* **161** 1026–37

66. Luque J and Crosley D R 1999 “LIFBASE: Database and spectral simulation (version 1.5)”, SRI International Report MP 99-009

67. Goldman A and Gillis JR. 1981 Spectral line parameters for the $A^2\Sigma$-$X^2\Pi(0,0)$ band of OH for atmospheric and high temperatures. *Journal Quant Spectrosc Radiat Transf* **25** 111– 35

CHAPTER III

A NOVEL COMBUSTION PLATFORM FOR MICROWAVE PLASMA-ASSISTED COMBUSTION STUDIES

3.1 Introduction

Plasma assisted combustion (PAC) refers to the enhancement of the combustion process through the addition of a plasma to a combustion system. Despite several enhancement effects being reported, such as reduced ignition delay time [1]–[3], improved combustion efficiency [4][5], improved flame holding [6]–[8], the mechanisms through which these enhancements are brought about are not completely understood. Plasmas employed in plasma assisted combustion studies can be thermal or non-thermal with non-thermal plasma sources highly desired due to low energy cost, availability of highly reactive species etc. Non-thermal plasma enhancement is effected by the interaction of several complex processes (thermal, physical, and kinetic processes arising from the coupling of the excited species, radicals, ions etc. generated by the plasma to the fuel/oxidant mixture) and unraveling these processes is the key to understanding the mechanism through which PAC is achieved [9]. Several studies have been performed aimed at providing further insight into the mechanisms of PAC. Chintala *et al.* [5] studied the range of flow parameters at which non-thermal plasma ignition enhancement was most effective in premixed hydrocarbon/air and CO/air mixtures excited by a low temperature transverse RF discharge. They concluded that the non-thermal species

generated by the plasma contribute to fuel oxidation which results in flow heating and subsequent thermal ignition and combustion. Hammack *et al.* [10] employed a tunable microwave waveguide in the PAC of premixed and non-premixed methane-air mixtures to study the enhancement effects achieved while using various nozzle geometries. They also varied other experimental parameters such as flow rates, plasma power and fuel equivalence ratios, where they concluded that non-premixed configurations were ill suited for plasma enhancements. Other works detailing the recent efforts expended by the scientific community in understanding the complicated processes involved in PAC can be found in the reviews [9], [11], and [12].

Unraveling the interwoven, complex processes responsible for the plasma enhancements observed in PAC is important in furthering our understanding of how these enhancements are effected. In a bid to understand the process of PAC, many studies have been performed using several plasma sources such as nanosecond repetitively pulsed discharges [13]–[15], microwave waveguides [16]–[18], in which the plasma employed is generated at the ignition/reaction site. Although this approach has the advantage of delivering intermediate reactive species to the reaction sites, it however does very little to simplify the issue of decoupling the several complex processes involved in PAC.

In an effort to separate the plasma gas kinetics from the combustion reaction kinetics, we – in our previous studies – developed a PAC platform whereby a microwave surfatron is used to separately generate an argon plasma which is then transported and coupled to a fuel/air mixture. By separating the plasma and the fuel/air interaction, we are able to track the evolution of the plasma species using a suite of optical techniques from generation in the plasma to consumption in the combustion process. Using that platform,

we explored the effect of a microwave generated plasma on the ignition and combustion of various fuel and oxidant combinations and different mixing schemes [8], [19]–[22]. However, in all these studies, the plasma interacted simultaneously with both the fuel and the oxidant. The coupling of the plasma simultaneously to both the fuel and oxidant as in our previous studies does little to discriminate between the various pathways through which the plasma enhances the combustion process such as enhancement through the creation of excited intermediates, the creation of radicals and ions or the dissociation of fuel to smaller molecules by plasma, etc. Hence, in this study, we go a step further by developing a novel plasma assisted combustion system with the ability to discriminate between the various pathways through which the plasma assists the combustion process. The separation of the individual reaction pathways is achieved by initially separating the plasma, the fuel and the oxidizer streams and then systematically coupling them to each other in various orders. The coupling of the plasma stream to the oxidizer stream allows for the investigation of the enhancement effects of plasma generated reactive oxygen and nitrogen species on the combustion mechanisms. Whereas coupling the plasma to the fuel stream allows for the investigation of the enhancement effects of the plasma due to the plasma assisted dissociation of the larger fuel molecules into smaller fragments. Hence, we present this novel PAC platform which allows for the separation and systematic coupling of the plasma, the fuel and the oxidant. Plasma assisted combustion is brought about by several interwoven complex processes going on simultaneously. Even though the separation of the plasma, oxidant and fuel does not allow for the study of the enhancement of the combustion process by very short-lived intermediate species, the combustor is still capable of highlighting and discriminating between other enhancement

pathways through which the plasma enhances the combustion process. A study is thus conducted with the novel PAC platform operating in three different schemes under the same experimental condition to demonstrate the ability of the PAC platform to discriminate between the different reaction pathways. The ability to differentiate and highlight the different reaction pathways makes the developed platform an invaluable tool in the continuous quest for understanding the underlying mechanisms of plasma assisted ignition and combustion. Methane and air are used as the fuel and oxidizer in this study. The PAC platform is described in detail in section 3.2 while results obtained from the plasma assisted oxidation of methane by air and summary are presented in sections 3.3 and 3.4, respectively.

3.2 Experimental setup

Figure 3.1 shows the schematic for the experimental setup used in this study. The experimental setup consists of a plasma assisted combustion platform, a gas supply and control manifold, and an optical diagnostics system. Each individual component is discussed subsequently.

3.2.1 The plasma assisted combustion platform

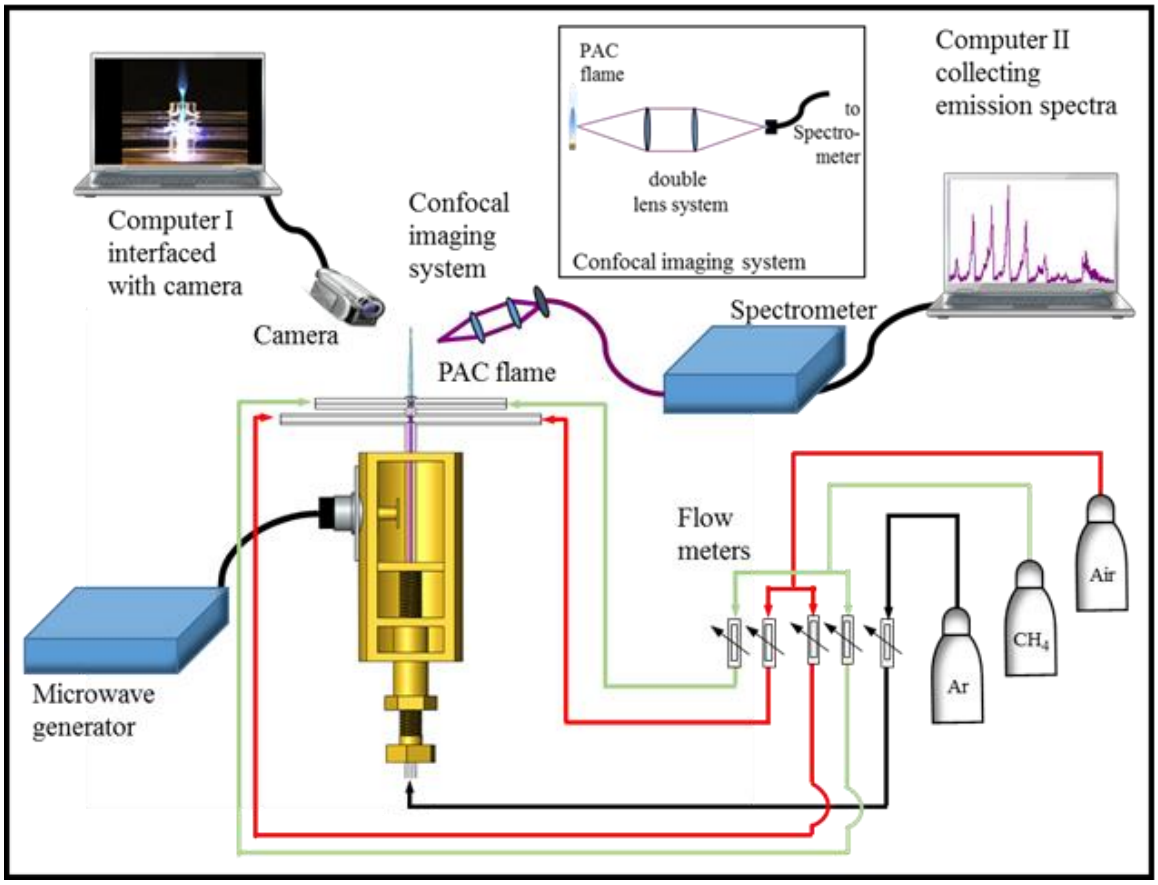

Figure 3.1 Schematic of experimental setup

The plasma assisted combustion (PAC) platform is made up of a PAC reactor powered by a 2.45 GHz microwave power source. The PAC reactor is composed of a double-cross shaped quartz combustor inserted into a microwave plasma cavity as shown in figure 3.2a. The 2.45 GHz microwave plasma source (AJA International) is used to power the microwave plasma cavity via a 0.6 m low loss coaxial cable (LMR-400, Times Microwave Systems). The attenuation rate of the coaxial cable was 0.144 dBm^{-1} at 2.45 GHz (equivalent to a 2% transmission loss in the cable). The microwave cavity was tuned for a reflected power of 0 – 6 W when the forward power was between 0 – 160 W. The

forward and reflected microwave powers were given as readouts from the microwave plasma source. The maximum of 4% loss in reflected power combined with the 2% loss in transmission resulted in a maximum total loss of 6% in microwave power. No exact radiation losses in the coupling of the plasma to the air, fuel or premixed mixture was measured in this experiment and, due to the low percentage power loss, the forward power is henceforth referred to as the plasma power. Figure 3.2b shows the geometry of the double-cross shaped quartz combustor.

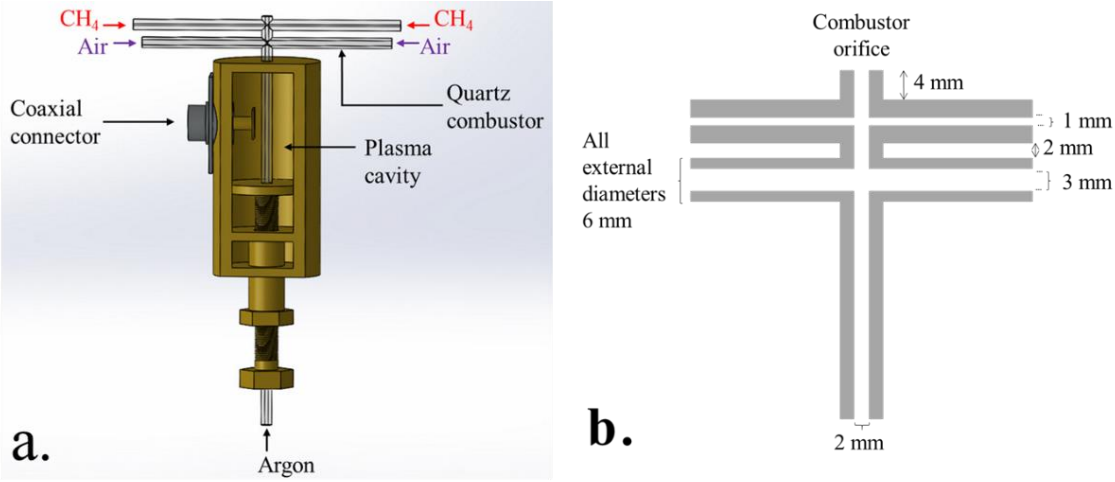

Figure 3.2 a) A schematic of the plasma assisted combustion reactor operating in Scheme II. b) A quartz combustor showing the dimensions of the combustor arms.

The double-cross shaped combustor is comprised of quartz tubes with varying inner diameters and a constant external diameter of 6 mm. The outer diameters of the plasma reactor tubes were constrained by the surfatron resonator cavity. The inner diameter of the vertical arm is 2 mm to ensure the generation of a stable and uniform argon plasma plume. The inner diameters of the lower and upper horizontal arm are 3 mm and 1 mm, respectively. These dimensions were chosen so as to ensure forward flow

with no backward diffusion when either the fuel or the oxidizer streams are coupled into the activation and ignition zones in Schemes II and III. The lower and upper horizontal arms are vertically separated by 2 mm. The separation was kept at 2 mm so as to optimize the tradeoff between allowing short lived intermediate species into the ignition site and decoupling the reaction mechanisms while taking into consideration the physical limits placed on the combustor during the construction process.

The vertical arm of the combustor, which is used to convey the argon plasma feed gas, is inserted into the plasma cavity. The PAC platform was operated in three different operation schemes, the premixed scheme (Scheme I), the air activated scheme (Scheme II), and the fuel activated scheme (Scheme III). In all the schemes, the argon plasma is always generated in the vertical arm of the double-cross shaped quartz combustor inserted into the plasma cavity. When the system is being operated in Scheme I or the premixed scheme, the upper horizontal arms are closed off and a premixed methane/air mixture flowing through the lower horizontal arms is coupled to the argon plasma flowing in the vertical arm. With the system operating in Scheme II or the air activated scheme, the microwave argon plasma, generated when the plasma feed gas was introduced into the cavity via the vertical arm, was initially mixed with the oxidizer stream, air, in the lower horizontal arms before the resulting mixture was coupled to the fuel flow in the upper horizontal arms. Whereas in Scheme III or the fuel activated scheme, the argon plasma, generated in the vertical arm of the combustor first interacts with the methane in the lower horizontal arm before the resulting mixture is coupled with the air flowing in the upper horizontal arms. Figure 3.2a depicts the plasma assisted combustion system operating in Scheme II.

3.2.2 Gas supply and control manifold

Argon (99.99% purity, Airgas), methane (99.99 % purity, Airgas), and air (Ultra zero grade, Airgas) were used in this study. The flow control manifold utilized in this study consisted of five rotameters which were used to vary the flow rates of the argon, methane, and air, to the PAC reactor. A pair of identical rotameters, with a range of 0 to 1.38 standard liters per minute (slm), was used to vary the air flow rate and each was connected to the lower horizontal arms or the top horizontal arms when the system was operated in Scheme II or Scheme III respectively. Another identical pair of rotameters, with a range of 0 to 434 standard cubic centimeters per minute (sccm, 1 slm = 1000 sccm), was used to vary the methane flow rates. These rotameters were connected to the lower horizontal arms of the double-cross shaped quartz combustor or the upper horizontal arms when the system was operated in Scheme III or Scheme II respectively. The last rotameter, with a range of 0 to 1.78 slm, was connected to the vertical arm of the quartz combustor as shown in figure 3.1 and was used to vary the flow rate of the argon plasma feed gas. The total flow rate of the fuel and air flows was fixed at 0.6 slm during this study since higher total flow rates for the fuel and air resulted in carbon deposition on the combustor walls when the platform was operated in Scheme III. The argon plasma feed gas flow rate was set constant at 0.84 slm during the entirety of this study to ensure the creation of a stable uniform plasma.

3.2.3 The optical diagnostic system

The optical diagnostics system was made up of a digital imaging subsystem and an optical emission spectroscopy subsystem. The digital imaging subsystem consists of a camera (Sony, FCB-EX78BB) for visual documentation of the plasma and flame

structures and shapes. This camera has a resolution between 100 µs – 1 s and was used in previous studies to resolve the plasma filaments and fine structures in a plasma plume [23]. This imaging subsystem was operated by computer I as shown in figure 3.1a.

The optical emission subsystem was run by computer II and utilizes a dual grating spectrometer (Avantes) attached to a confocal lens setup. The confocal lens setup was used to collect emissions from the plasma assisted combustion reactor via an optical fiber with an aperture size of 400 µm. The confocal microscope lens setup is comprised of two identical bi convex lenses (f = 15 cm) as shown in the inset in figure 3.1. The dual grating spectrometer housed two gratings (600 grooves mm^{-1} and 1200 grooves mm^{-1}) which were used to cover a spectral range of 200 to 600 nm with a resolution of 0.07 nm at 350 nm. Due to the fact that the plasma assisted combustion reactor was mounted on a high precision 3D translation stage (0.01 mm resolution in all axis), the small aperture size of the fiber, and the confocal microscope lens setup, 1D spectrum acquisition was achieved with a spatial resolution of 0.5 mm without the need for spatial filtering. The integration time was adjusted based on the emission intensity and ranged from 20 ms to 80 s.

3.3 Results and discussion

3.3.1 Operation schemes and corresponding flame structures.

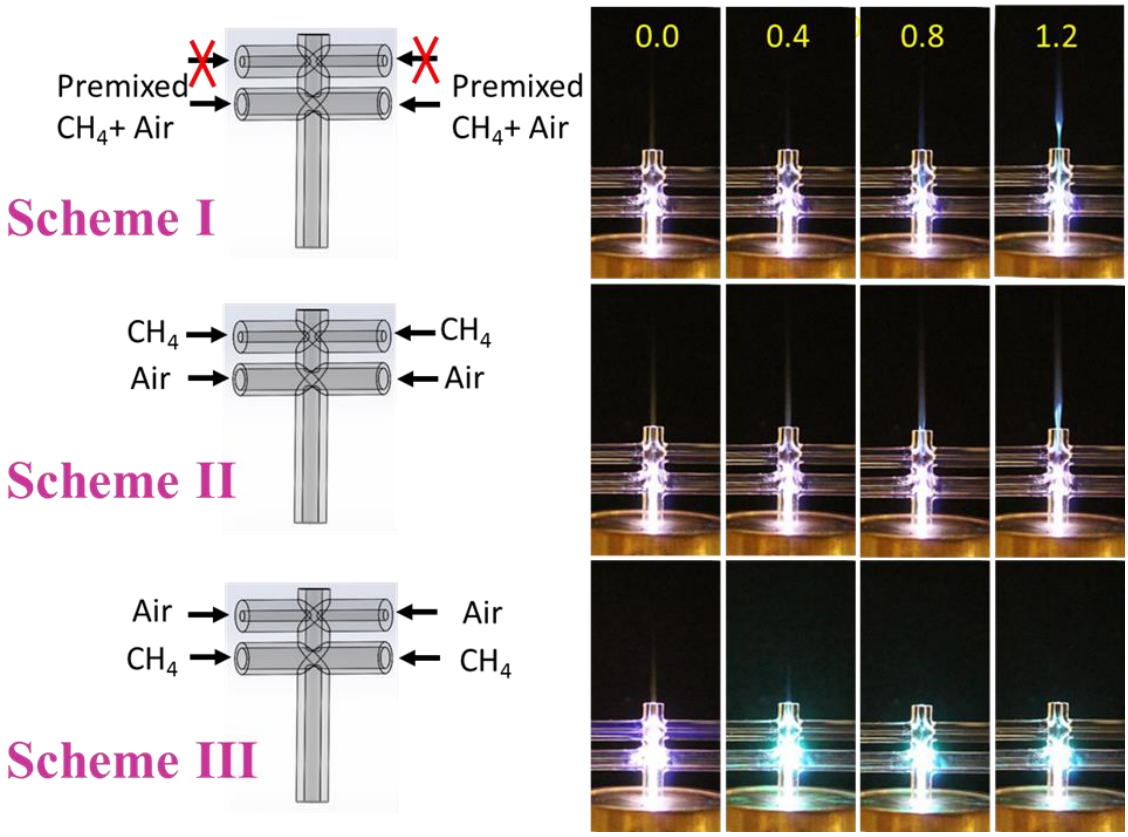

Figure 3.3 Images showing PAC flame structures in different operation schemes

Images showing flame structures obtained at different fuel equivalence ratios for three different operation schemes. The PAC platform parameters were kept constant for all three operation schemes at a plasma power of 140 W, plasma feed gas flow rate of 0.84 slm, and total fuel/air mixture flow rate of 0.6 slm

The ability of the plasma assisted ignition and combustion platform to highlight the various reaction pathways is investigated with the system operating under Schemes I, II and III. The plasma power was kept constant at 140 W while the fuel equivalence ratio was varied to study the change in the plasma assisted combustion flame structure when the combustor was operated in the three different operation schemes. Figure 3.3, shows

the flame structures corresponding to different fuel equivalence ratios of 0, 0.4, 0.8 and 1.2 while the combustion reactor was operated in Scheme I, Scheme II, and Scheme III. The plasma feed gas flow rate and the total air mixture flow rate were fixed at 0.84 slm and 0.6 slm, respectively. For all operation schemes investigated, at a fuel equivalence ratio of 0, a pink plasma plume was observed emanating from the combustor orifice. With the PAC platform operating in Scheme I, the upper horizontal arms were closed while a premix fuel/air mixture flowing in the lower horizontal arms was coupled to the argon plasma flowing in the vertical arm. This resulted in a blue flame observed outside the combustor. Increasing the fuel equivalence ratio at constant power resulted in an increase in flame volume and a dual layer flame structure for higher fuel equivalence ratios. In Scheme II, the oxidant, air, flowing in the lower horizontal arms was initially coupled to the argon plasma flowing in the vertical arm. Methane, flowing in the upper horizontal arms was then added to the plasma activated air mixture resulting in a blue flame emanating from the combustor orifice. Increasing the fuel equivalence ratio at constant plasma power, constant argon flow rate and constant total fuel/air mixture flow rate resulted in an increase in flame volume and luminosity as shown in figure 3.3. A dual layered flame – with a white inner core surrounded by a blue outer layer – was observed for near stoichiometric to rich fuel equivalence ratios. When operated in Scheme III, the lower horizontal arms conducted methane which was coupled to the argon plasma conveyed in the vertical arm. The resulting plasma activated methane stream was coupled to the air stream in the upper horizontal arms. At a constant plasma power of 140 W in Scheme III, a greenish flame was observed for a fuel equivalence ratio of 0.4 with no flame observed for higher fuel equivalence ratios. However, upon prolonged usage, soot

was deposited on the combustor's walls and the time it took for soot to form upon ignition decreased with an increase in fuel equivalence ratio. The dual-layered structured flame observed for Schemes I and II is similar to the previously reported dual flame structure observed in the study of the plasma assisted flameholding in a premixed ethylene/air mixture [8]. Curiously, the flame volume was thicker in Scheme II compared to the other two Schemes. We observed that for all three operation schemes and fuel equivalence ratios investigated, the fuel/air mixture could not be ignited with an external ignition source in the absence of the plasma. These differences in flame behavior for different operation schemes under the same experimental conditions provides evidence to suggest that the enhancement mechanisms are different. The different flame geometries obtained under the same experimental conditions for different operation schemes thus demonstrate the capability of the novel combustion platform to highlight the various reaction pathways which will contribute to further our understanding of the phenomenon of plasma assisted combustion.

3.3.2 Optical emission characteristics in the different operation schemes

Optical emission spectroscopy was employed to determine the spatial composition of the species present and how they evolved along the propagation axis of the combustor when the platform was operated in the different operation schemes. The emission spectra were collected perpendicularly to the direction of propagation with a spatial resolution of 1 mm. Ten spectra were collected and averaged at each spatial location to improve on the signal to noise ratio. The experimental parameters were fixed, with the plasma power at 140 W, the fuel equivalence ratio at 0.4, the argon plasma feed gas flow rate at 0.84 slm, and the total fuel/air mixture flow rate at 0.6 slm for all three

operation schemes investigated. For each scheme, four different reaction zones were identified and characterized based on their distinct emissions features. The zones are henceforth referred to as the plasma zone, the hybrid plasma flame or activation zone, the ignition zone, and the flame zone.

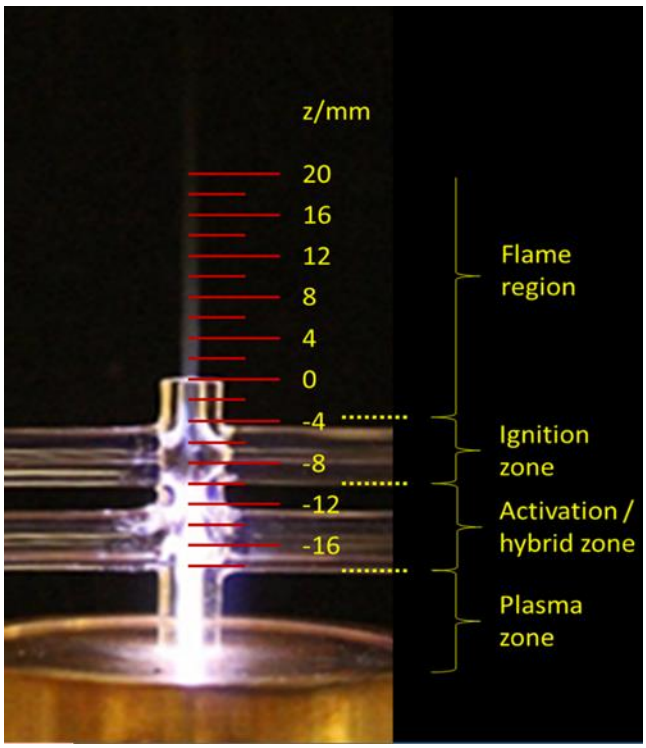

Figure 3.4 An image depicting the approximate spatial locations of the various reaction zones

An image of the plasma assisted combustion reactor, operating in Scheme II, depicting the approximate spatial locations of the various reaction zones, identified based on their distinct emission features. The plasma power was fixed at 140 W, the fuel equivalence ratio at 0.4, the feed gas flow rate at 0.84 slm, and the total fuel/air mixture flow rate at 0.6 slm

Figure 3.4 shows an image of the annotated combustion reactor operating in Scheme II which depicts the approximate spatial location of all four zones identified in this study. The plasma zone refers to the region z < - 18 mm before the plasma interacts

with the premixed methane/air mixture in Scheme I or either the air or fuel in Scheme II or Scheme III respectively. The hybrid zone applies only to Scheme I whereas the activation zone applies only to Scheme II and Scheme III. The hybrid, or activation, zone falls in the range $z > -18$ mm and $z < -10$ mm. In Scheme I, this region is referred to as the hybrid zone since the plasma is coupled to the premixed methane/air mixture in this region. With the platform operating in Scheme II or Scheme III, this region is referred to as the activation zone since the plasma is initially coupled to the air or fuel, respectively. The ignition zone refers to the region in which the activated air or fuel meets the incoming fuel or air, respectively. At this location, oxidation of the fuel is initiated. This region lies approximately between -10 mm $< z < -4$ mm. The flame zone refers to the region downstream of the hybrid zones for Scheme I and the ignition zones for Scheme II or Scheme III, respectively. It should be noted that there is no distinct boundary between the zones, with the boundary rather defined by the species present in these regions.

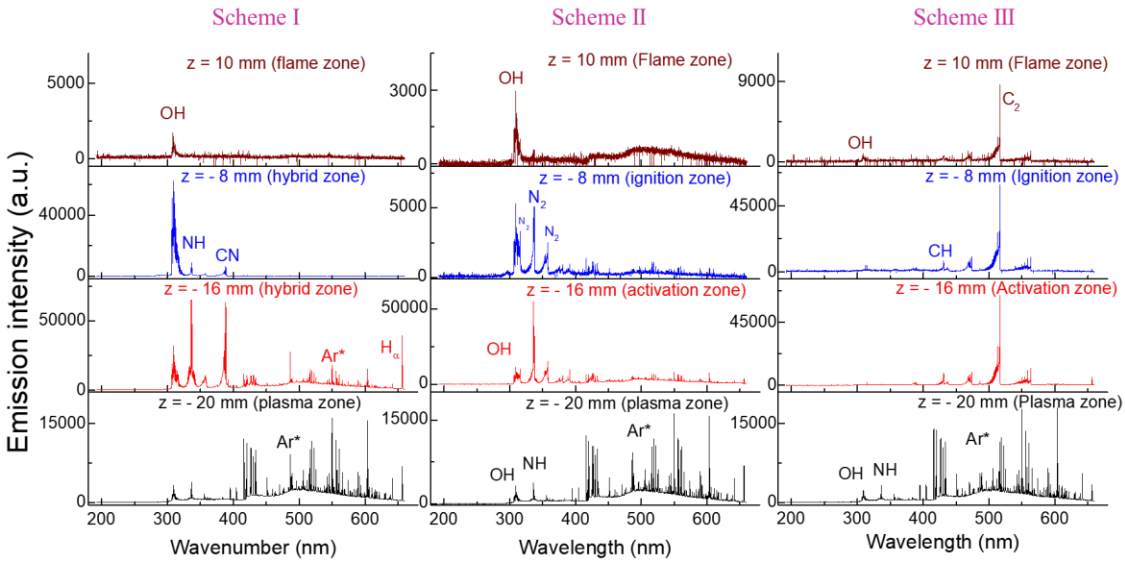

Figure 3.5 Emission spectra were obtained at the various reaction zones for the three operation schemes

Emission spectra were obtained at the various reaction zones for the three operation schemes. The plasma power was kept constant at 140 W, with the fuel equivalence ratio at 0.4, plasma feed gas flow rate at 0.84 slm, and total fuel/air mixture flow rate at 0.6 slm for all operation schemes investigated

Figure 3.5 shows the emission spectra obtained at the plasma zone, the hybrid plasma flame or activation zone, the ignition zone and the flame zone when the PAC platform was operated in the three schemes. The experimental parameters were kept constant for all the three operation schemes during this study. In the plasma zone, at z = -20 mm, the emission spectra obtained from all three operation schemes were dominated by emissions from the electronic systems of the OH($A^2\Sigma^+$–$X^2\Pi_{3/2}$)(0–0), NH($A^3\Pi$-$X^3\Sigma^-$)(0–0), and atomic lines from H_α, H_β, and Ar. It should be noted that the emissions from the plasma zone are the same for all three operation schemes since the plasma has not yet interacted with either the fuel, the air, or the premixed fuel/air mixture. In the plasma zone, the OH is mainly generated from the electron impact dissociation of water present as impurities in the argon gas and from the recombination reactions of O and H as shown

in reactions 3.1 – 3.3. NH, in the plasma zone is produced from the recombination reactions of H and N both generated from electron impact dissociation reactions [20], [24].

$$e + H2O \rightarrow H + OH(A,X) + e \quad (3.1)$$

$$e + O2 \rightarrow 2O + e \quad (3.2)$$

$$O + H2O \rightarrow OH + OH \quad (3.3)$$

$$N + H \rightarrow NH \quad (3.4)$$

When operating in Scheme I, the plasma interacts with the premixed methane/air mixture in the hybrid zone. The hybrid zone features emissions from the electronic systems of OH($A^2\Sigma^+$–$X^2\Pi_{3/2}$)(0–0), NH($A^3\Pi$-$X^3\Sigma^-$)(0–0), N_2($C^3\Pi_u$-$B^3\Pi_g$)(0–1), CN($B^2\Sigma^+$-$X^2\Sigma^+$)(0–0), and atomic lines from Ar* and H_α as shown in figure 3.5 at z = - 16 mm. Due to electron impact dissociation reactions, the methane present in the hybrid zone acts as a source of hydrogen which reacts with nitrogen to produce NH. A plausible route for CN production is from the hydrogen abstraction of HCN [25].

The emission spectra obtained from the activation zones when operated in Scheme II were similar yet different from those obtained for Scheme I and featured emissions from OH($A^2\Sigma^+$–$X^2\Pi_{3/2}$)(0–0), N_2($C^3\Pi_u$-$B^3\Pi_g$) (1–0) (0–0) (0–1) and atomic lines from Ar*. In Scheme II, the notable differences were the absence of NH($A^3\Pi$-$X^3\Sigma^-$)(0–0), CN($B^2\Sigma^+$-$X^2\Sigma^+$)(0–0), and H_α and the overall weaker relative emission intensities of all other observed species. The abundance of H_α and OH(A) in Scheme I was a result of the onset of the plasma assisted ignition of the fuel whereas in the Scheme II, due to the absence of methane as a source of hydrogen, the species are mainly from electron impact dissociation of water present as impurities in the oxidizer stream, thus the relative

lower emission intensities. Collisional quenching of the Ar* by nitrogen results in the population of several vibrational states as seen by emissions from $N_2(C^3\Pi_u\text{-}B^3\Pi_g)$ (1–0) (0–0) (0–1) transitions, etc. The activation zone with the platform operating in Scheme III features emissions mainly from $CH(A^2\Delta\text{-}X^2\Pi)$(0-0) and $C_2(d^3\Pi_g\text{-}a^3\Pi_u)$(0-0) systems respectively. The CH(A) and C_2(d) observed are primarily formed as products from electron impact dissociation of the fuel present and recombination reactions [26].

In the downstream of the hybrid zone with the platform operating in Scheme I, at z = - 8 mm, the spectra features emissions from $OH(A^2\Sigma^+\text{–}X^2\Pi_{3/2})$(0–0) with very little $NH(A^3\Pi\text{-}X^3\Sigma^-)$(0–0) and $CN(B^2\Sigma^+\text{-}X^2\Sigma^+)$(0–0) observed. However, when operating in Scheme II, the ignition zone featured emissions from $OH(A^2\Sigma^+\text{–}X^2\Pi_{3/2})$(0–0) and $N_2(C^3\Pi_u\text{-}B^3\Pi_g)$(1–0) (0–0) (0–1) only. Due to the lean nature of the mixture, CH(A) and C_2(d) are not observed during the ignition of the fuel in Scheme II. With the system operating in Scheme III, the emission spectra were marked by emissions from $CH(A^2\Delta\text{-}X^2\Pi)$(0–0), and $C_2(d^3\Pi_g\text{-}a^3\Pi_u)$(0–0).

The emission spectra from the flame zone when the system was operated in both Schemes I and Scheme II were characterized by emissions from OH(A) whereas, when the PAC platform was operated in Scheme III, the spectra were dominated by C_2(d) emissions and with very little from OH(A). Soot was deposited along the walls of the combustor upon prolonged operation in Scheme III. The existence of three distinct emission spectra showing different species when the combustion platform was operated under uniform experimental conditions for the three different operation schemes further showcased the ability of the current combustion platform to highlight the different PAC pathways.

The near absence of atomic lines from Ar in the ignition and flame zones is therefore proof that the radical contribution by the plasma ends upon activation of the air or fuel mixtures in Schemes II and III respectively. Thus the plasma has very little to no effect in the ignition zone. Hence the combustor allows for the investigation of the role of select radicals in the various enhancement pathways.

3.3.3 Rotational temperature profiles

The rotational temperature of the plasma assisted combustion flame was obtained for the three different operation schemes by simulation. The rotational temperatures were simulated by comparing the relative intensities of the P and R branches from a simulated spectrum with an experimentally obtained spectrum from each spatial location using Specair [27] with an uncertainty of ±50 K as shown in figure 3.6.

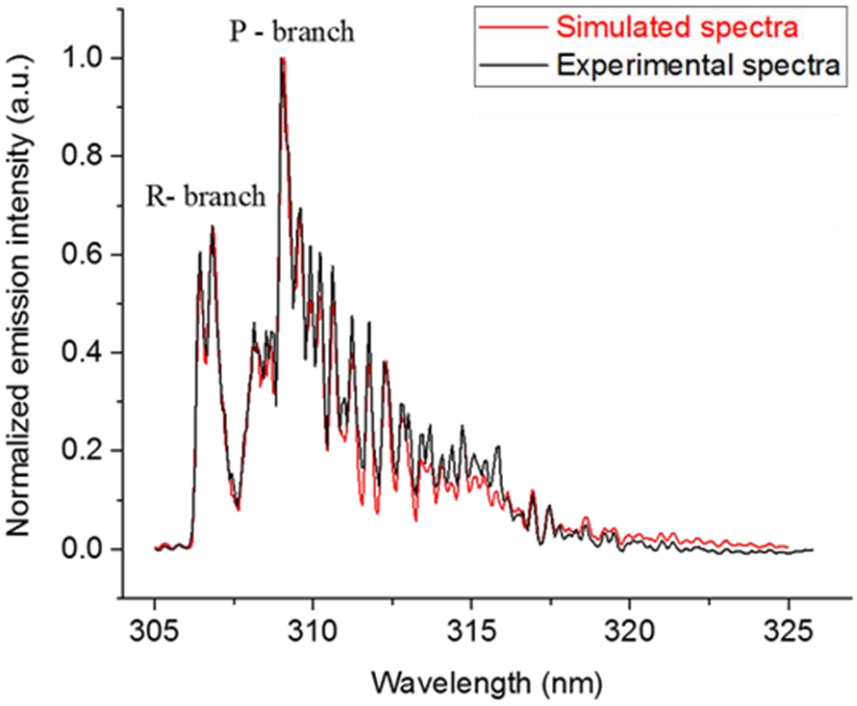

Figure 3.6 Comparison between the experimentally obtained spectra and simulated spectra of the OH($A^2\Sigma^+$–$X^2\Pi_{3/2}$)(0–0)

Comparison between the experimentally obtained spectra and simulated spectra of the OH($A^2\Sigma^+$–$X^2\Pi_{3/2}$)(0–0) from Specair at z = - 18 mm from which the rotational temperature was determined in Scheme I

Figure 3.7 shows the rotational temperature profile obtained spatially along the propagation axis of the plasma assisted combustion flame, for the three operation schemes investigated. The plasma power was kept constant at 140 W, the fuel equivalence ratio was also fixed at 0.4 while the argon plasma feed gas flow rate and total flow rates were fixed at 0.84 slm and 0.6 slm, respectively. Wu et al. [21] investigated the relationship between the plasma power required for ignition and the fuel equivalence ratio in the argon microwave plasma assisted ignition of premixed methane/air mixture. They concluded that lean fuel equivalence ratios were more susceptible to thermal energy losses to the environment compared to rich fuel equivalence ratios. Hence due to the lean

fuel equivalence ratios employed in this study, the plasma enhances the ignition and combustion process by supplying thermal energy to counteract the flame quenching effect while generating radicals which contribute to flame ignition and holding. Due to the fact that the plasma power was kept constant at 140 W for all three operating schemes, it is thus suggested that the differences in the combustion enhancements observed are due to the different reactive species generated as observed from the emission spectra in each reaction scheme by the plasma interaction. For all three operation schemes, the rotational temperature in the plasma zone, at fixed plasma power, was constant within experimental error. However, the rotational temperature was observed to vary significantly above the plasma zone for all three operation schemes. With the PAC platform operating in Scheme I, the rotational temperature was observed to increase dramatically from 650 K at z = 18 mm to 975 K at z = 16 mm before reaching a peak of 1570 K downstream at z = - 6 mm from whence the rotational temperature dropped downstream of the flow. The increase in rotational temperature when the plasma becomes coupled with the premixed methane/air mixture was due in part to plasma heating caused by the relaxation of energetic electrons and radicals during collisions with the methane/air mixture and also from the exothermic thermochemical reactions during the plasma assisted oxidation of the fuel. This increase in temperature upon coupling of plasma to the premixed mixture is buttressed by a similar observation by Bao et al. [28] in which the authors observed a 250 ºC – 350 ºC increase in temperature upon addition of fuel to an air plasma whereas only a 50 ºC increase in temperature was observed upon addition of fuel to a nitrogen plasma under the same experimental conditions. Bao et al. concluded from that study that the increase in temperature upon addition of the fuel to

nitrogen plasma was due to plasma heating while the 5 to 7 fold increase observed in the air plasma was due to both plasma heating and fuel oxidation. With the PAC platform operating in Schemes II and III, an increase in the rotational temperature was observed when the air and fuel streams were coupled to the plasma, respectively. The increase in temperature observed upon coupling the air and fuel streams to the plasma stream was mainly due to plasma heating with the observed temperature profile slightly dipping downstream of the activation zones. The dip observed in the rotational temperature profiles for both Schemes II and III in the activation zones prior to ignition zones was as a result of thermal losses to the environment.

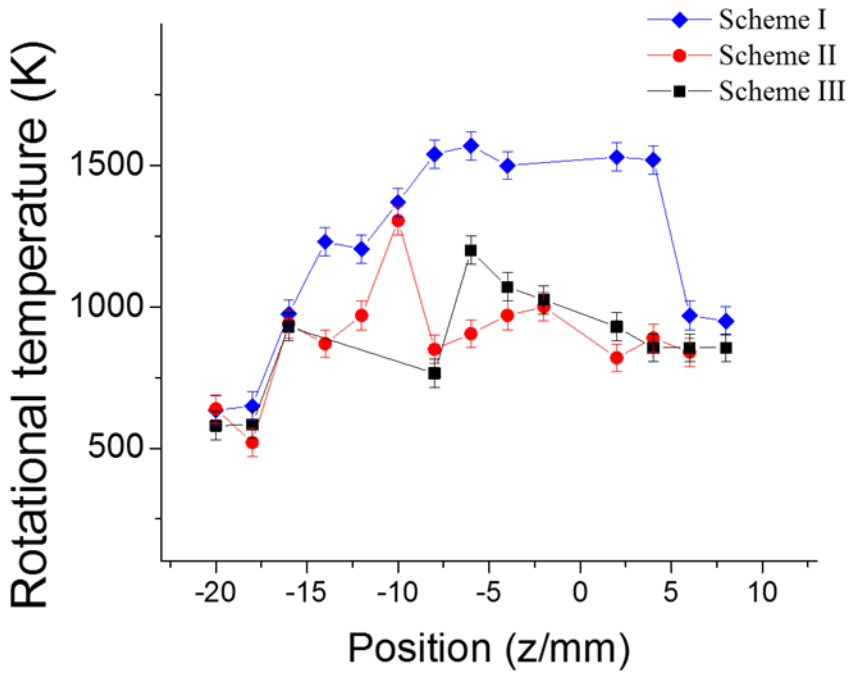

Figure 3.7 Rotational temperature profiles obtained for the three operation schemes

The PAC platform parameters were kept constant with the plasma power at 140 W, the fuel equivalence ratio at 0.4, the plasma feed gas flow rate at 0.84 slm, and the total fuel/air mixture flow rate at 0.6 slm for all operation schemes investigated

Ignition of the activated mixtures was achieved in the ignition zone. The rotational temperature profiles were observed to peak in both Schemes II and III with a higher peak temperature observed in Scheme II at 1305 K compared to 1200 K at Scheme III. In all three operation schemes, the rotational temperature profiles obtained exhibited a dual peak nature. In both Scheme II and Scheme III, the initial peak is attributed to heating by the plasma whereas the secondary peak is attributed to the onset of fuel oxidation. For Scheme I, both processes of plasma heating and fuel oxidation are occurring simultaneously, with plasma heating being initially prevalent during the pre-ignition stage and fuel oxidation taking over as the main source of thermal energy increase as discussed in our previous publication [19].

The highest peak rotational temperature was obtained in Scheme I while the lowest was obtained in Scheme III. Thus with the plasma assisted combustion platform operating under the same experimental conditions, three different temperature profiles were obtained for the three different operation schemes, indicative of the different reaction pathways through which the plasma influences the combustion process. This further demonstrates the capability of the new PAC platform in highlighting the different processes in the plasma assisted combustion.

3.4 Summary

Plasma assisted combustion is thought to be brought about by the interaction of several complex processes and the decoupling of these processes is the key to understanding the enhancement role played by the plasma in the combustion process. To this end, we have developed a novel plasma assisted combustion platform capable of highlighting the different reaction pathways in plasma assisted combustion. This is

achieved by initially separating and systematically coupling the plasma, oxidizer, and fuel streams while allowing for the varying of other combustion parameters for plasma assisted combustion studies. A study investigating the flame geometry and optical emission spectra with the system operating in three different operation schemes at constant experimental parameters was conducted. Although the PAC platform was operated under the same parameters, the different operation schemes yielded different flame geometries. It is thus inferred from the variance in the flame geometries that the plasma enhancement mechanisms were different in each case. Furthermore, the emission spectra obtained at different spatial locations along the propagation axis of the combustor for the three operation schemes depicted different distinct emission features. This observation provides further evidence supporting the hypothesis that the mechanism through which the plasma assists the combustion in each of this operation schemes is different. The observed difference in flame structures, emission spectra and temperature profiles for the three operation schemes thus highlight the capability of the novel PAC system presented in unraveling the various pathways through which plasma enhancement is achieved. The results obtained demonstrate the versatility of the novel PAC platform in decoupling the plasma interaction with the lean fuel/air mixture with the goal of demystifying the processes through which the observed plasma enhancements are effected.

3.5 References

1. S. Nagaraja, W. Sun, and V. Yang, 2014 “Effect of non-equilibrium plasma on two-stage ignition of n-heptane,” *Proc. Combust. Inst*., 35, 3497–3504

2. Z. Yin and I. Adamovich, 2011 “Ignition delay and time-resolved temperature measurements in nanosecond pulse hydrogen-air and ethylene-air plasmas at elevated initial temperatures,” *49th AIAA Aerosp. Sci. Meet. Incl.* New Horizons Forum Aerosp. Expo. Orlando, Fl, , USA, 1–24.

3. S. V. Pancheshnyi, D. A. Lacoste, A. Bourdon, and C. O. Laux, 2006 “Ignition of propane-air mixtures by a repetitively pulsed nanosecond discharge,” *IEEE Trans. Plasma Sci.*, **34**, 2478–2487

4. M. S. Bak, H. Do, M. G. Mungal, and M. A. Cappelli, 2012 “Plasma-assisted stabilization of laminar premixed methane/air flames around the lean flammability limit,” *Combust. Flame*, **159**, 3128–3137

5. N. Chintala, A. Bao, G. Lou, and I. V. Adamovich, 2006 “Measurements of combustion efficiency in nonequilibrium RF plasma-ignited flows,” *Combust. Flame*, **144**, 744–756

6. K. V Savelkin, D. A. Yarantsev, I. V Adamovich, and S. B. Leonov, 2015 “Ignition and flameholding in a supersonic combustor by an electrical discharge combined with a fuel injector,” *Combust. Flame*, 162, 825–835

7. S. B. Leonov, I. V. Kochetov, A. P. Napartovich, V. A. Sabel’Nikov, and D. A. Yarantsev, 2011 “Plasma-induced ethylene ignition and flameholding in confined supersonic air flow at low temperatures,” *IEEE Trans. Plasma Sci.,* **39**, 781–787

8. C. A. Fuh, W. Wu, and C. Wang, 2016 “Microwave plasma-assisted ignition and flameholding in premixed ethylene/air mixtures,” *J. Phys. D. Appl. Phys*., **49**, 285202

9. W. Sun and J. Yiguang, 2013 “Nonequilibrium plasma-assisted combustion: A review of recent progress,” *J. Plasma Fusion Res*, **89**, 208–219

10. S. Hammack, S. Member, T. Lee, and C. Carter, 2012 “Microwave plasma enhancement of various flame geometries at atmospheric pressure,” *IEEE Trans on Plasma Sci.*, **40**, 3139–3146

11. A. Y. Starikovskii, N. B. Anikin, I. N. Kosarev, E. I. Mintoussov, S. M. Starikovskaia, and V. P. Zhukov 2006 "Plasma-assisted combustion," *Pure Appl. Chem.,* **78**, 1265–1298

12. Y. Ju and W. Sun, 2015 "Plasma assisted combustion: Dynamics and chemistry," Progress in Energy and Combustion Science, **48**, 21–83

13. G. Lou, A. Bao, M. Nishihara. S. Keshav, Y. G. Utkin, J. W. Rich, W. R. Lempert, and I.V. Adamovich 2007 "Ignition of premixed hydrocarbon–air flows by repetitively pulsed, nanosecond pulse duration plasma," *Proc. Combust. Inst.*, **31**, 3327–3334

14. I. V Adamovich, I. Choi, N. Jiang, J. H. Kim, S. Keshav, W. R. Lempert, E. Mintusov, M. Nishihara, M. Samimy, and M. Uddi 2009 "Plasma assisted ignition and high-speed flow control: non-thermal and thermal effects," Plasma Sources Sci. Technol., **18**, 34018

15. G. Cui, W. Zeng, Z. Li, Y. Fu, H. Li, and J. Chen, 2016 "Experimental study of minimum ignition energy of methane / air mixtures at elevated temperatures and pressures," *Fuel*, **175**, 257–263

16. X. Rao, K. Hemawan, I. Wichman, C. Carter, T. Grotjohn, J. Asmussen, and T. Lee 2011 "Combustion dynamics for energetically enhanced flames using direct microwave energy coupling," *Proc. Combust. Inst*., **33**, 3233–3240

17. C. U. Bang, Y. C. Hong, S. C. Cho, H. S. Uhm, and W. J. Yi, 2006 "Methane-augmented microwave plasma burner," *IEEE Transactions on Plasma Science,* **34**, 1751–1756

18. E. S. Stockman, S. H. Zaidi, R. B. Miles, C. D. Carter, and M. D. Ryan, 2009 "Measurements of combustion properties in a microwave enhanced flame," *Combust. Flame*, **156**, 1453–1461

19. C. Wang and W. Wu, 2014 "Roles of the state-resolved OH (A) and OH (X) radicals in microwave plasma assisted combustion of premixed methane/air: An exploratory study," *Combust. Flame*, **161**, 2073–2084

20. C. Wang and W. Wu, 2013 "Simultaneous measurements of OH(A) and OH(X) radicals in microwave plasma jet-assisted combustion of methane/air mixtures around the lean-burn limit using optical emission spectroscopy and cavity ringdown spectroscopy," *J. Phys. D. Appl. Phys.*, **46**, 464008

21. W. Wu, C. A. Fuh, and C. Wang, 2014 "Comparative study on microwave plasma-assisted combustion of premixed and nonpremixed methane/air mixtures," *Combust. Sci. Technol*., **187**, 999–1020

22. W. Wu, C. A. Fuh, and C. Wang, 2015 “Plasma-enhanced ignition and flame stabilization in microwave plasma-assisted combustion of premixed methane / oxygen / argon mixtures,” *IEEE Trans. on Plasma Sci.*, **43**, 3986-3994

23. C. Wang, N. Srivastava, S. Scherrer, P. R. Jang, T. S. Dibble, and Y. Duan, 2009 “Optical diagnostics of a low power—low gas flow rates atmospheric-pressure argon plasma created by a microwave plasma torch,” *Plasma Sources Sci. Technol.,* **18**, 25030,.

24. C. Wang, N. Srivastava, and T. S. Dibble, 2009 “Observation and quantification of OH radicals in the far downstream part of an atmospheric microwave plasma jet using cavity ringdown spectroscopy,” *Appl. Phys. Lett.*, **95**, 51501

25. W. Juchmann, H. Latzel, D. I. Shin, G. Peiter, T. Dreier, H. R. Volpp, J. Wolfrum, R. P. Lindstedt, and K. M. Leung 1998 “Absolute radical concentration measurements and modeling of low-pressure CH_4 /O_2 /NO flames,” *Proc. Combust. Inst*., **27**, 469

26. D. A. Erwin and J. A. Kunc, 2005 “Electron impact dissociation of the methane molecule into neutral fragments,” *Physical Review A*, **72**, 052719

27. C. O. Laux, T. G. Spence, C. H. Kruger, and R. N. Zare, 2003 “Optical diagnostics of atmospheric pressure air plasmas,” *Plasma Sources Sci. Technol.*, **12**, 125-138

28. A. Bao, Y. G. Utkin, S. Keshav, G. Lou, and I. V. Adamovich, 2007 “Ignition of ethylene-air and methane-air flows by low-temperature repetitively pulsed nanosecond discharge plasma,” *IEEE Trans. Plasma Sci.*, **35**, 1628–1638,.

CHAPTER IV

COMPARATIVE STUDY OF THE PLASMA ACTIVATED METHANE AND PLASMA ACTIVATED AIR IN THE PLASMA ASSISTED COMBUSTION OF NON-PREMIXED METHANE/AIR MIXTURES

4.1 Introduction

The quest for low flammability limits, reduced ignition time, improved flame stabilization and flameholding, reduction in pollutant emission etc. have been the driving factors fueling research into the field of plasma assisted combustion. Plasma assisted combustion refers to the coupling of a plasma to a fuel/air mixture to enhance the combustion process. Plasmas have been shown to significantly improve upon the combustion process with researchers such as Yu *et al.* [1] reporting on the stabilization of a methane/air flame using a high repetition nanosecond laser induced plasma where they investigated the plasma coupling energy and the temporal evolution of the flame kernels generated. De Giorgi *et al.* [2] demonstrated a significant improvement in the stabilization of a methane/air flame by plasma generated by a nanosecond repetitively pulsed high voltage and a sinusoidal dielectric barrier high voltage discharge. Also, Stockman *et al.* [3] measured the combustion properties in a microwave-enhanced flame and demonstrated an increase in laminar flame speed of up to 20% and thermal enhancements of 100–200 K. Hammack *et al.* [4] coupled an atmospheric microwave plasma discharge to a premixed methane/air flame and reported an increase in

combustion temperature of up to 40%. Pancheshnyi *et al.* [5] while conducting a study to investigate the efficiency of the ignition of a propane air/mixture by a high voltage repetitively pulsed nanosecond discharge observed a reduction in ignition delay and an increase in overall combustion duration with aid of the plasma. Korolev *et al.* [6] while employing a plasma generated by a nonsteady state plasmatron were able to demonstrate an increase in efficient ignition and flame control of propane/air mixtures over a wide range of fuel equivalence ratios. Aleksandrov *et al.* [7] reported a decrease of more than an order of magnitude in the ignition delay times of stoichiometric premixed C_nH_{2n+2}:O_2:Ar mixtures for n = 1-5 when the combustible mixture was coupled with a plasma generated by a high voltage nanosecond discharge. Further reported enhancements of the combustion process by plasmas can be found in the review articles refs. [8], [9].

Nonthermal plasmas interact and enhance the combustion process through preheating of the fuel/air flows and chemically through radicals, excited neutrals and electrons supplied to the combustion process. However, many researchers have been able to show that the radicals supplied by the nonthermal plasmas play a vital role in the observed combustion enhancement in terms of reduced ignition limits, flame holding and stabilization, reducing ignition delay time etc. For example researchers such as Chintala *et al.* [10] attributed the improved ignition of hydrocarbon/air and CO/air flows when acted on by an RF discharge plasma to the radical species generated in the discharge. Li *et al.* [11] investigated the effects of a laser ablation plasma on the stabilization of a premixed methane/air mixture. They proposed that the radicals generated by the ablation plasma are responsible for the reported increase in the flame propagation velocity and

subsequent improvement in stabilization observed. In our previous study [12], we have investigated the effects of a microwave plasma on the flameholding of a premixed ethylene/air mixture where we showed that flameholding was achieved by the creation of a radically rich inner flame which ignited and stabilized the surrounding coflow. It is well known that the interaction of plasma and fuel/air mixtures result in the creation of a variety of radical species which then go on to enhance the combustion process. Identifying which radicals are vital to the enhancement effects is very important as it can help in fine-tuning the plasma generated to produce the desired radicals for optimum ignition and combustion enhancement. One method of achieving this feat of identifying important reactive species is through theoretical investigation by modeling the kinetics of the plasma assisted combustion process and comparing the theoretical results with experimentally obtained data. But this method is currently plagued by inaccurate or unknown reaction constants, instrument limitation on the sensitivity of the experimental data reported etc. [13]. Hence, in this study, by varying the scheme of the interaction of the plasma with the fuel and air, we are able to experimentally investigate which group of radicals and plasma processes are more vital in the plasma assisted ignition and combustion process. We also measure the absolute ground state concentrations of OH(X) radicals using cavity ringdown spectroscopy which is a very sensitive absorption technique requiring no calibration thus providing accurate experimental data for fine tuning current reaction schemes. The metrics used in this study to investigate the enhancement effects are the minimum ignition energy/plasma power and fuel efficiency. Three mixing schemes are explored in this study, whereby in the first scheme (Scheme I), the plasma is coupled to the premixed fuel/air mixture. This mixing scheme has been

previously investigated [14] and is used as a control or background from which the other two schemes are compared. The second mixing scheme (Scheme II) involves the plasma being coupled initially to the air and then subsequently mixed with the fuel. Lastly, in the third mixing scheme (Scheme III) the plasma is coupled to the fuel flow before mixing with the air downstream. The fuel and oxidizer employed in this study are methane and air respectively. The effects of the various radicals generated on ignition and flame holding are discussed. The experimental system used is described in section 4.2 while the results and a summary of the chapter are presented in sections 4.3 and 4.4 respectively.

4.2 Experimental setup

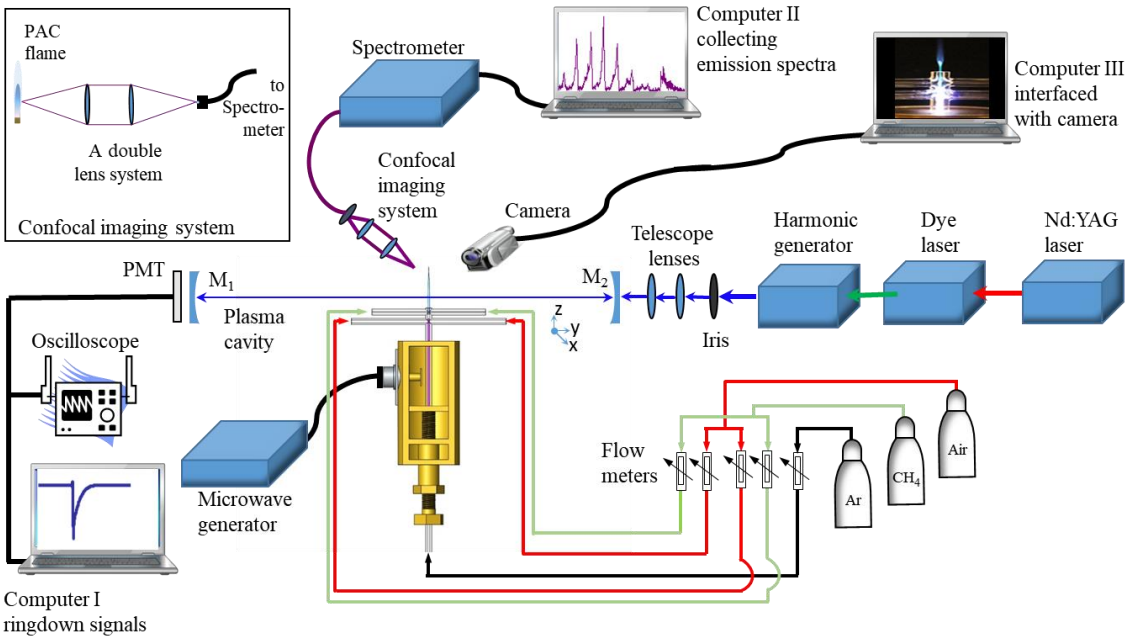

Figure 4.1 Schematic of the experimental setup

Figure 4.1 shows the experimental facility used in this study with a detailed description given in [15]. The experimental facility is made up of three components: a

plasma assisted combustion reactor, an optical diagnostic system and a gas flow control manifold. Each component is described in brief subsequently.

4.2.2 Microwave plasma-assisted combustion reactor

The plasma source used in this study was a microwave surfatron which was powered by 2.45 GHz microwave source (AJA International) via a 0.6 m low loss coaxial cable (LMR-400, Times Microwave Systems). At 2.45 GHz, the attenuation rate of the coaxial cable was 0.144 dBm^{-1} (equivalent to a 2% loss in transmission). The plasma generated by the surfatron was confined to a doubled- cross shaped quartz tube of outer diameter 6 mm and inner diameter of 2 mm which was inserted into the surfatron and conveyed the plasma feed gas. The 2 mm inner diameter was chosen so as to ensure the generation of a uniform plasma by the surfatron. The two top horizontal arms of the quartz tube had an inner diameter of 1 mm while the lower horizontal arms had an inner diameter of 3 mm. These dimensions were chosen so as to ensure forward flow only in the combustor when it was operated in Schemes II or III respectively. The external diameter of the combustor was constrained by the surfatron to 6 mm. Considering the physical limitations due to the manufacturing process of the combustor, the vertical separation between the upper and lower horizontal arms was fixed at 2 mm so as to optimize the tradeoff between allowing short lived plasma generated species to reach the ignition site while ensuring complete plasma activation of the fuel or oxidizer. The forward and reflected powers were obtained as readouts from the solid state microwave generator. The coupling efficiency of the microwaves generated by the surfatron into the plasma feed gas was not measured but for forward plasma powers in the range 60 - 160 W, the reflected power was typically between 1 ~ 4 W. The total accountable loss in the

microwave power was ~ 5% (2% in transmission and ~ 3% in the reflected power) and due to this low percentage, the forward power is henceforth referred to as the plasma power. The electron number density generated in this argon plasma is typically on the order of 10^{14} cm^{-3} with an electronic excitation temperature of 8000 – 9000 K [16]. Other plasma parameters such as emission spectra, plasma temperatures, plume shapes, plasma gases, plasma power effects, etc., can be seen in refs. [16]–[19]. In operational Scheme I, the top arms were closed off and a premixed methane/air mixture was introduced into the lower horizontal arms. The top and bottom horizontal arms conveyed methane and air respectively when the reactor was operated in Scheme II or air and methane when the reactor was being operated in Scheme III respectively. In either operation scheme, the air or fuel or premixed mixture in the lower arm, met with the argon plasma column coming up in the vertical tube and a flame was observed at the top of the combustion reactor

4.2.3 Gas flow control manifold

Five rotameters were used to control the gas flow rates to the plasma assisted combustion reactor making up the gas flow control manifold. Two identical pairs of rotameters were used to vary the air and methane flow rates. The first identical pair controlled the air flow rates which had a range of 0 - 1.38 standard liters per minute (slm) were connected individually to the bottom horizontal arms when operated in the Scheme II or to the top horizontal arms when operated in Scheme III. The second identical pair varied the methane flow rate with a range of 0 – 434 standard cubic centimeter per minute (sccm, 1 slm =1000 sccm) and were connected to the top horizontal arms in Scheme II or the bottom horizontal arms in Scheme III. The fifth rotameter was used to

vary the argon plasma feed gas flow rate and had a range from 0 - 1.78 slm. The purities of methane, air, and argon used in this study were 99.99% (Airgas), 99.99% (Airgas) and 99.99% (Airgas) respectively. The argon plasma feed gas flow rate was fixed at 0.84 slm throughout the entire study.

4.2.4 The optical diagnostic system

This system was made up of a digital imaging system, a fiber-guided optical emission spectroscopy (OES) system and a cavity ringdown spectroscopy (CRDS) system. The digital imaging system was used for visual documentation of the plasma and flame structures. Visual documentation was achieved using a digital camera (Sony, FCB-EX78BB) which has a resolution between 100 µs – 1 s. At this range, the resolution of the camera is capable of resolving plasma filaments along with fine flame structures as used in our previous study [20]. The digital imaging system was operated by computer III with the shutter speed adjusted to optimize the visual effect of the plasma jet and combustion flame behavior.

Emissions from the plasma-assisted combustion reactor at different locations along the z-axis of the combustor were obtained by the fiber-guided OES system. The optical emission spectroscopy system consisted of a confocal microscope lens system made up of two identical focal length lenses (f = 15 cm) (see inset in figure 4.1) used to collect the emissions which was transmitted via an optical fiber of aperture size 400 µm to a dual channel spectrometer (Avantes). The dual channel spectrometer housed two gratings of 600 grooves mm^{-1} and 1200 grooves mm^{-1} which was used to cover a spectral range of 200 – 600 nm with a line resolution of 0.07 nm at 350 nm. The plasma assisted combustion reactor was mounted on a 3-D translation stage (0.01 mm resolution in all

axis). 1 –D spectrum acquisition was achieved with a resolution of 0.5 mm without the need for spatial filtering given the confocal lens setup, the high precision of the translation stage used (0.01 mm), and the small aperture size of the optical fiber of cross sectional area 0.5 mm^2. To obtain a better signal to noise ratio, each recorded emission spectrum was the average of 10 spectra obtained at the same fixed spatial location. The integration time was adjusted based on the emission intensity and ranged from 20 ms to 80 s. The optical emission system was operated by computer II as shown in figure 4.1.

The CRDS system was used to measure the absolute number density of the ground state hydroxyl, OH(X), radicals. The cavity was constructed from a pair of highly reflective (R=99.9% at 308 nm) plano-concave mirrors (radius of curvature r = 1 m) with a cavity length of 61 cm. The plasma assisted combustion flame was placed at the center of the ringdown cavity and the optical axis (y- axis) of the ringdown cavity was perpendicular to the flame axis (z-axis) as shown in figure 4.1. The UV laser beam used in the cavity ringdown study was obtained by frequency doubling (Inrad Autotracker III) the output of a tunable narrow line width, dual grating dye laser (Narrowscan, Radiant) being pumped by a 20 Hz Nd:YAG laser (Powerlite 8020, Continuum). The dye laser had a single pulse energy of a few μJ with a minimum scanning step of 0.0003 nm. The laser beam path lengths in the flame were estimated from the geometry of the flame images and the cross-section of the laser beam in the flame was ~ 0.5 mm^2. A detailed description of the ringdown system employed in this study can be seen elsewhere [15], [21]. The ringdown signal was detected by a photomultiplier tube (PMT, Hamamatsu) fitted with a 10 nm band pass interference filter. The signal was monitored by an oscilloscope (TDS 410A, Tektronix) interfaced with computer I running a home

developed ringdown software. The ringdown baseline noise averaged over 100 ringdown events was typically 0.5% without plasma-assisted combustion running and 0.8% with the plasma-assisted combustion flame on.

4.3 Results

4.3.1 Minimum ignition plasma power (MIPP) study

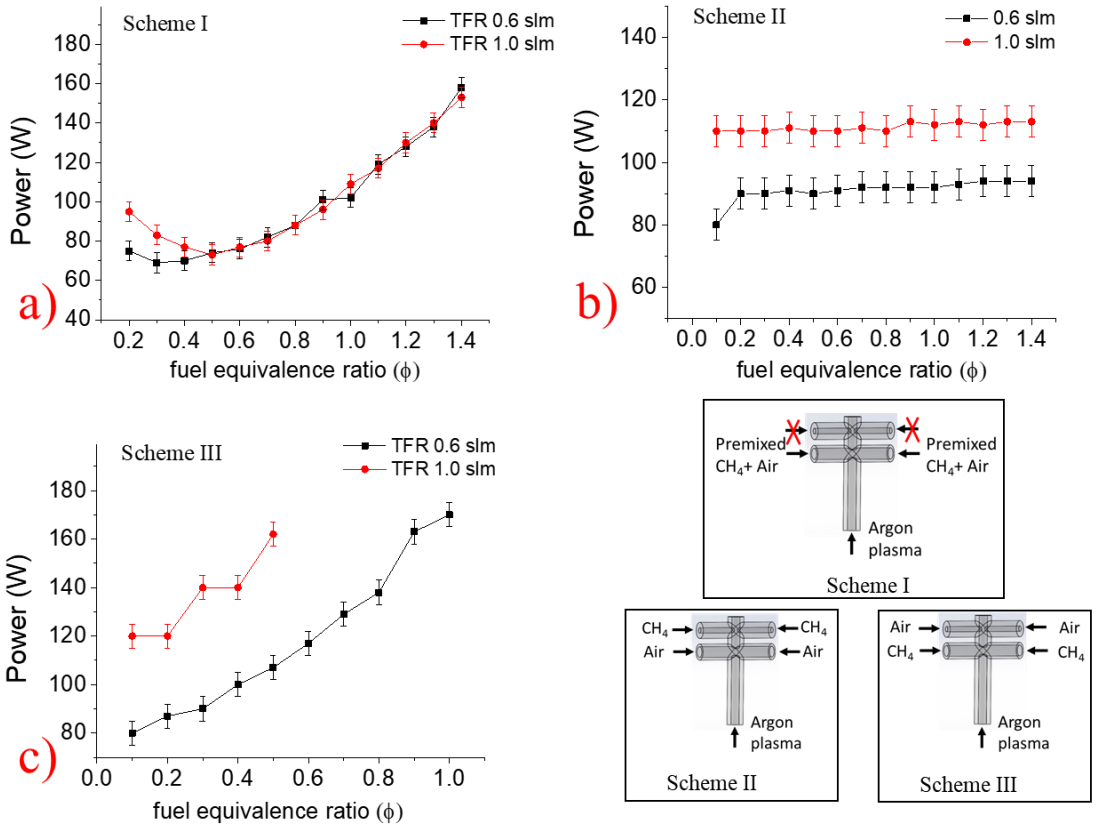

Figure 4.2 Minimum ignition energy vs fuel equivalence ratio curves for three operations schemes at different total fuel/air mixture flow rates

Minimum ignition energy vs fuel equivalence ratio curves for two different total methane/air mixture flow rates of 0.6 slm and 1.0 slm for the reactor operating in, a) Scheme I b) Scheme II c) Scheme III. In all three operation schemes, the plasma argon feed gas flow rate was fixed at 0.84 slm

Figure 4.3 shows plots for the minimum ignition plasma power at which a flame was observed outside the combustion reactor vs. fuel equivalence ratio obtained at total fuel/air mixture flow rates of 0.6 slm and 1.0 slm, when the combustion reactor was operated in Scheme I, Scheme II and Scheme III. The argon plasma feed gas flow rate was fixed constant at 0.84 slm throughout the entire study. These plots were obtained by increasing the plasma power from the minimum plasma power at which the surfatron can sustain a plasma of 5 W up until when a flame was observed outside the reactor orifice. The nonthermal argon microwave plasma supplies a variety of radicals, excited state species, energetic electrons and thermal energy to the combustion mixture to enhance ignition and flameholding [22]. The combination of plasma species supplied and thermal energy therefore enhances the plasma assisted ignition and combustion observed in this study. All attempts to externally ignite the mixture without the aid of the plasma for the three different operation schemes were unsuccessful.

When the reactor was operated in Scheme I, a U-shaped minimum plasma power required for ignition vs fuel equivalence ratio curve, shown in figure 4.3a was obtained similar to the one previously reported [23]–[25]. It was observed that for ultra-lean fuel equivalence ratios, the power required for ignition decreased with an increase in fuel equivalence ratio while for stoichiometric to rich fuel equivalence ratios, the plasma power required for ignition increased with an increase in fuel equivalence ratio. The decrease in plasma power observed with increase in fuel equivalence ratios for ultra-lean fuel equivalence ratios was due to the fact that thermal losses to the environment upon plasma assisted ignition of the lean fuel equivalence ratio far outweigh the heat released due to the lean nature of the fuel/air mixture. Hence a higher plasma power is needed to

offset the heat loss. Increasing the fuel equivalence ratio results in an increase in thermal energy released which counteracts the heat loss to the environment hence requiring less thermal input from the plasma. As a result, we observe a decrease in plasma power required to generate a flame outside the reactor with increase in fuel equivalence ratio for ultra-lean mixtures. A similar observation was also made by J. Han *et al.* [26] who concluded that leaner mixtures were more sensitive to heat loss to their surroundings. This conclusion was arrived at while studying numerically the spark ignition characteristic of a methane/air mixture using two different analytical model with and without electrodes. In this study, beyond a fuel equivalence ratio of 0.5, further increase in the fuel equivalence ratio resulted in an increase in plasma power required to initiate ignition.

The coupling of the plasma to the fuel/air mixture results in the creation of a radical pool composed primarily of reactive oxygen and nitrogen species along with fuel fragments from electron impact dissociation reactions. Reactive oxygen and nitrogen species have been credited with improved ignition and overall enhancement in previous studies. For example, Starik *et al.* [27] attributed the acceleration of flame propagation in a methane/air mixture to the intensification of chain reactions due to the addition of singlet delta oxygen molecules. Sun *et al.*[28] investigated the kinetic effects of non-equilibrium plasma-assisted methane oxidation on diffusion flame extinction limits. They concluded from a path flux analysis that oxygen generated by the plasma through electron impact dissociation reactions was critical for extending the extinction limits. For lean fuel equivalence ratios, due to the low percentage of fuel present, more reactive oxygen and nitrogen species are generated at a much lower plasma power resulting in

ignition. Hence for fuel equivalence ratios in the range 0.1 to 0.5, the competition from the fuel present in impeding the production of reactive species is lower resulting in the positive contribution of the heat released by the ignition with increase in fuel equivalence ratio to outweigh the negative effect of inhibiting the creation of reactive oxygen and nitrogen species. However, beyond a fuel equivalence ratio of 0.5, increasing the fuel equivalence ratio causes the balance to shift resulting in the negative effect of inhibition outweighing the positive effect of thermal heat released. Hence in order to counteract the production of less reactive oxygen and nitrogen species, a higher plasma power is needed to ensure that the required critical pool of the reactive oxygen and nitrogen species is generated for ignition to occur.

The observed increase in plasma power required for ignition for fuel equivalence ratios in the range 0.5 to 1.4 is due to the fact that increasing the fuel equivalence ratio results in more fuel dissociation than reactive oxygen and nitrogen species production requiring an increase in the plasma power to maintain the radical pool needed for ignition. Plasma quenching is henceforth used to describe the competition posed by fuel molecules to oxygen and nitrogen molecules from air in the generation of reactive species from the interaction with the plasma. From this and previous observations [23]–[26], it was inferred that ultra-lean fuel equivalence ratios are more susceptible to thermal energy losses to the environment and less susceptible to plasma quenching due to the low fuel content whereas for rich fuel equivalence ratios plasma quenching effects are more pronounced compared to thermal losses to the environment.

With the plasma assisted combustion reactor operating in Scheme II, it was observed that at a constant total flow rate, ignition occurred at a fixed plasma power

independent of the fuel equivalence ratio investigated. As shown in figure 4.3b, the minimum ignition plasma power remained constant even when the total mixture flow rates was varied from 0.6 slm to 1.0 slm. As discussed in Scheme I above, the microwave plasma supplies excited neutrals, radicals, electrons and thermal energy which when coupled with the premixed fuel/air mixture generates a radical pool which is responsible for enhancing ignition. Minimum ignition plasma power was observed to depend on the interplay between the ability of the plasma to establish a sufficient radical pool required for ignition and the quenching effect on the plasma with increase in fuel equivalence ratio. The quenching effect of the fuel refers to the competition between the fuel molecules and the oxygen and nitrogen present to generate fuel fragments or reactive oxygen and nitrogen species through mostly electron impact dissociation and recombination reactions as discussed above.

In Scheme II, it can be inferred from the independence of the ignition power on fuel equivalence ratio that at a particular plasma power, the plasma initially coupling with the air flow establishes the radical pool required for the ignition of the fuel subsequently. Since the radical pool is established before coupling with the fuel, the plasma quenching phenomena associated with higher equivalence ratios in Scheme I due to the presence of fuel is completely overridden. The increase in plasma power at which a flame occurs outside the combustor with increase in total flow rate for all fuel equivalence ratios is attributed to the flow dynamics in the reactor. Increasing the total flow rate results in a higher mixture flow speed and as a result, a larger radical pool is required to ignite and stabilize the flame.

Figure 4.3c shows the minimum ignition plasma power vs. fuel equivalence ratio curve obtained with the plasma operating in Scheme III. The plasma power required to ignite the fuel/air mixture is observed to increase with an increase in fuel equivalence ratio. This increase in ignition power with increase in fuel equivalence ratio is attributed to the plasma quenching effect of coupling the plasma to the fuel first. As a result of the plasma being quenched, the radical pool required for ignition is not achieved and hence a larger plasma power is required to ignite the mixture.

It is inferred from the above results that Scheme I is more efficient for ignition of ultra-lean fuel equivalence ratios whereas Scheme II is more efficient in the ignition of stoichiometric to rich fuel equivalence ratios. These results also buttress the fact that radicals generated in the plasma play a very significant role in enhancing ignition. This stems from the observation of a critical plasma power at which ignition is achieved for all fuel equivalence ratios investigated in Scheme II suggesting the existence of a critical radical pool size at which ignition occurs. The size of the radical pool is not determined in this study but by investigating the emission spectra, we are able to discuss the composition of the radical pool required for plasma assisted ignition to occur.

4.3.2 Flame structures

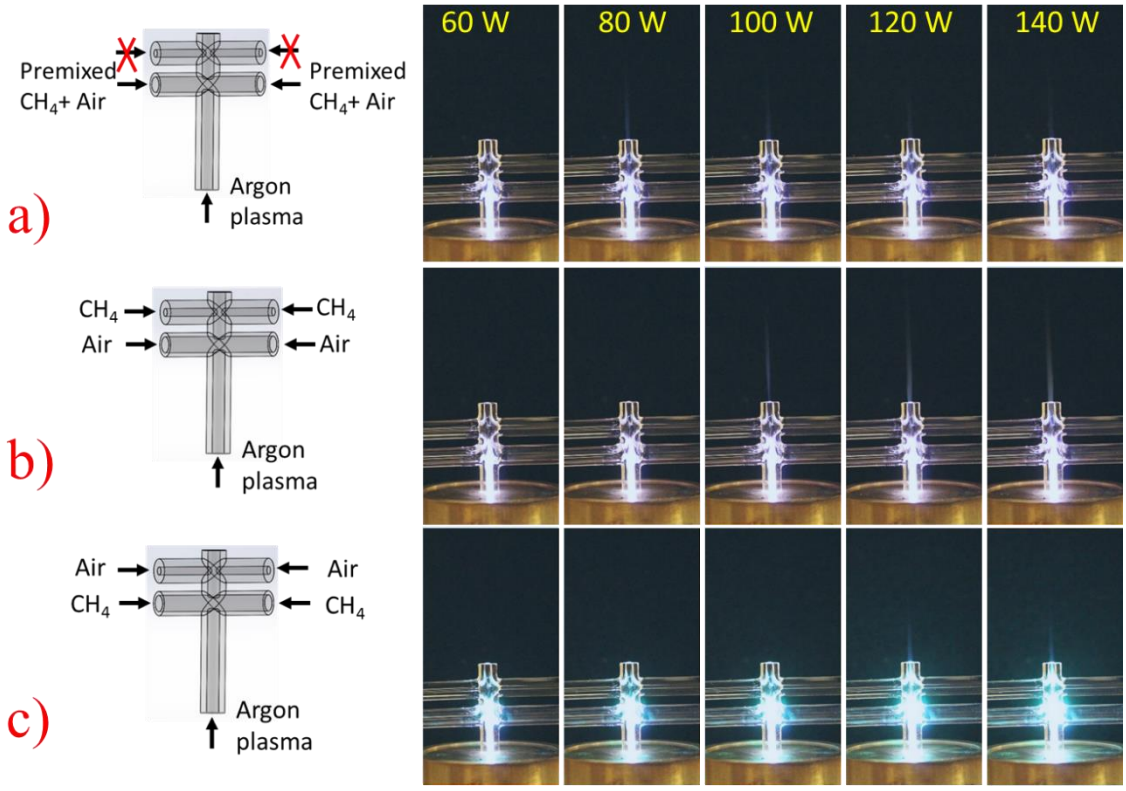

Figure 4.3 Flame images for different plasma powers in the three operation schemes

Flame images for fuel equivalence ratio, 0.4, total flow rate 0.6 slm and plasma feed gas flow rate of 0.84 slm at various powers for the reactor operating in a) Scheme I b) Scheme II, c) Scheme III. Exposure time was fixed at 1/15s

Images of the combustion reactor operating in Schemes I, II and III are shown in figures 4.3a, 4.3b, and 4.3c respectively at different plasma powers. The total fuel equivalence ratio was fixed at 0.4 slm while the argon plasma feed gas flow rate and total fuel/air mixture flow rate was fixed at 0.84 slm and 0.6 slm respectively.

In Scheme I, when the plasma power was increased from a minimum plasma power at which the surfatron can sustain a plasma of 5 W, ignition and successful

flameholding was achieved outside the combustion reactor at a plasma power of 80 W with a blue and comparatively longer flame emanating from the combustor orifice. Increasing the plasma power, resulted in an increase in flame tethering and a corresponding decrease in flame length. We propose that the improved tethering of the flame with increase in plasma power is due to the increase in the size of the reactive radical pool generated with increased plasma power. This increase in the radical pool generated allows for ignition of a larger amount of the fuel upstream of the flame resulting in improved flameholding. The decrease in flame length with increase in plasma power is a side effect of the improved flameholding in the combustion reactor due to the increase in radicals generated by the plasma. Due to the improved flameholding and the lean nature of the fuel/air mixture, a relatively larger percentage of the fuel is consumed upstream of the flow hence the shortening of the flame observed. The improvement in flameholding with radicals supplied was also reported by Dutta *et al.*[29] while studying the plasma assisted ignition and flameholding of ethylene/air and hydrogen/air flows. They attributed the improved flameholding in that study to the reduction in ignition delay time caused by the radicals generated by the nanosecond repetitively pulsed discharge used.

For the plasma reactor operating in Scheme II, as shown in figure 4.4b, a flame was not observed outside the tube for plasma powers of 60 W and 80 W. A thin blue flame was observed at a plasma power of 100 W outside the combustor orifice. Further increase in plasma power resulted in improved flameholding with a relatively thicker and more luminous flame profile observed. The improved flameholding observed with increase in plasma power is due to the increased production of radicals with increase in

plasma power as discussed above. The increase in luminosity of the flame compared to Scheme I is attributed to the more efficient generation of radicals in Scheme II since the plasma interacts initially with the air. Due to the absence of plasma quenching, all the available resources thus provided by the plasma are directed to the generation of reactive oxygen and nitrogen species resulting in the improved ignition and combustion.

Figure 4.4c shows the plasma reactor operating in Scheme III. Plasma assisted ignition was not achieved below a plasma power of 120 W. At a plasma power of 120 W, a greenish flame was observed emanating from the combustor orifice which became relatively more luminous when the plasma power was increased as observed in figure 4.3c. It should however be noted that the flame observed at the plasma power of 120 W was very unstable. A stable flame was only observed at a plasma power of 140 W. Upon prolonged operation at plasma powers 120 W and 140 W in Scheme III, soot was deposited on the walls of the combustor due to fuel pyrolysis. At a fuel equivalence ratio of 0.4, the soot deposition was observed upon prolonged use (time of operation > 4 hours) with soot deposition occurring much sooner when the fuel equivalence ratio was increased. Soot formation was not observed in any other operation schemes investigated upon prolonged use. Hence, an ultra-lean fuel equivalence ratio of 0.4 was chosen for this study due to the limitations of the soot formation in Scheme III.

Increasing the plasma power resulted in improved flame tethering in all configurations investigated with plasma assisted ignition occurring at much lower plasma powers in Scheme I compared to Scheme II and Scheme III respectively. As discussed in section I, lean fuel equivalence ratios are more susceptible to heat losses to the environment. In Schemes II and III, the plasma interacts with the air or fuel initially to

generate a radical pool containing reactive oxygen and nitrogen radicals or fuel fragments before subsequent ignition downstream. Whereas in Scheme I, the plasma interacts simultaneously with both the air and the fuel resulting in the radical pool facilitating the ignition of the fuel at the same spatial location. It is inferred that the spatial coincidence of radical pool and thermal energy from the fuel breakdown accounts for the lower plasma power at which ignition and flameholding occurs in Scheme I compared to the other schemes, where additional energy is required to ignite the mixture and hold the flame. It is further inferred from the improved luminosity of the flame with further increase in plasma power in Scheme II compared to Scheme I and III that reactive oxygen and nitrogen species generated when the plasma interacts with air play a more important role in plasma ignition and flameholding compared to fuel fragments generated due to plasma fuel interaction. Amongst the three operation schemes investigated, soot is only formed in Scheme III upon prolong operation.

4.3.3 Optical emission spectra

Optical emission spectroscopy was employed to obtain the composition of the species generated by the coupling of the plasma to the fuel/air mixture. Emissions were collected perpendicularly to and along the propagation axis at a spatial resolution of 2 mm. Four zones were defined along the propagation axis of the plasma and fuel/air mixture based on the mixing scheme employed in this study. The plasma zone was defined as referring to the region occupied by the plasma before interaction with the fuel or air or premixed fuel/air mixture (~ $z < -18$ mm). The hybrid zone referred to the region where the plasma met and was coupled with fuel/air mixture in Scheme I and the activation zone referred to the region in which the plasma was coupled to the air or fuel

in Scheme II or Scheme III (z = -18 ~ z = - 12 mm). The ignition zone was defined only for Scheme II or III and referred to the region where the activated air or fuel flow reached the fuel or air flow (z = - 12 mm ~ z = - 4 mm). While the flame zone referred to the regions downstream of the hybrid (z > -12 mm) and ignition zones (z > - 4 mm). It should be noted that there are not any clear cut boundaries between the zones described in this study with the zones mainly defined by their distinct emission features. Figure 4.5 shows the emission spectra obtained from the plasma and the hybrid/activation zones for Schemes I, II, and III. The plasma power and plasma feed gas flow rate was fixed at 140 W and 0.84 slm respectively. The fuel equivalence ratio and total flow rates were fixed at 0.4 and 0.6 slm respectively.

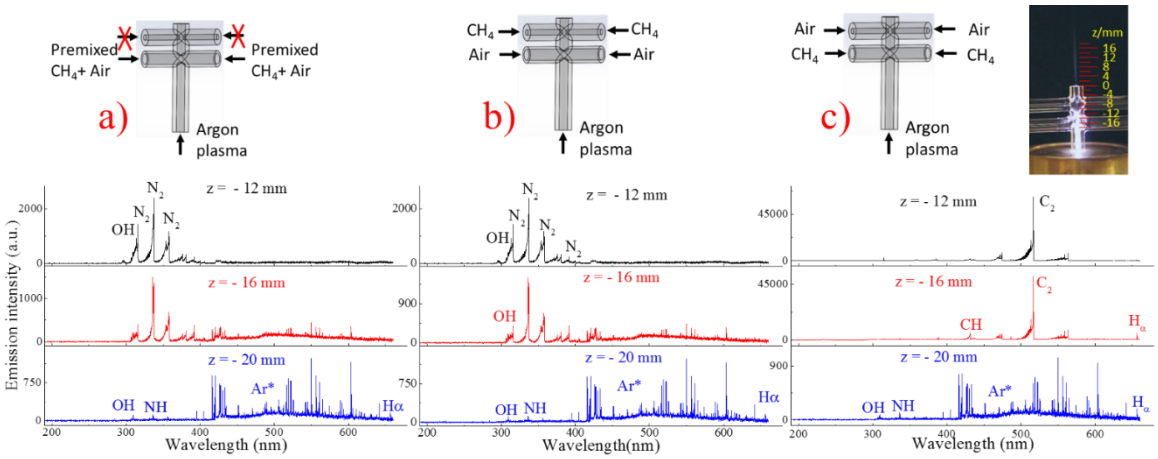

Figure 4.4 Optical emission spectra in the plasma and activation zones for all three operation schemes

Optical emission spectra at three spatial locations in the combustion reactor showing the species present at the plasma and hybrid/activation zones when the combustor is operating in the; a) Scheme I b) Scheme II c) Scheme III. The plasma power and feed gas flow rates were fixed at 140 W and 0.84 slm while the fuel equivalence ratio and total flow rates (fuel and air) were held constant at 0.4 and 0.6 slm respectively throughout the entire study.

Figure 4.4a shows the emission spectra obtained at three different spatial locations along the propagation axis for the combustion reactor operating in Scheme I. At z = -20 mm in the plasma zone, the spectrum obtained featured emissions from the electronic systems of OH($A^2\Sigma^+$–$X^2\Pi_{3/2}$)(0–0), NH($A^3\Pi$-$X^3\Sigma^-$)(0–0), and atomic lines from H_α, H_β, and Ar as the main species present supplied by the plasma. OH in the plasma zone is formed predominantly from electron impact dissociation of water molecules present as impurities in the argon plasma feed gas and electron recombination reactions [16], [30]. NH is generated in the plasma as a consequence of the recombination reaction N + H → NH [15] with N and H coming from the electronic impact dissociation of water and nitrogen impurities in the plasma feed gas. At z = - 16 mm the spectrum was dominated by emissions from OH($A^2\Sigma^+$–$X^2\Pi_{3/2}$)(0–0) and N_2($C^3\Pi_u$-$B^3\Pi_g$)(1 – 0)(0 – 0)(1 – 2)(0 – 1) generated from the coupling of the plasma to the ultra-lean premixed methane/air mixture. Due to the coupling of the plasma and the premixed fuel/air mixture, excited Ar is still observed at z = - 16 mm but the emission intensity is much lower due to the consumption of the excited argon in N_2 generation with N_2 coming from the energy transfer reaction when Ar($^3P_2$) from the plasma reacts with N_2 [31]. At x = -12 mm, the plasma is completely coupled with premixed methane air mixture and there are no emissions from excited argon observed.

The emission spectra obtained at three different locations for Scheme II and Scheme III are shown in figure 4.4b and 4.4c. The same species are observed throughout the plasma zones in all three operation schemes. This is to be expected since the plasma properties were maintained constant throughout the study. The principal species observed

are from the electronic systems of OH($A^2\Sigma^+$–$X^2\Pi_{3/2}$)(0–0), NH($A^3\Pi$-$X^3\Sigma^-$)(0–0), and atomic lines from H_α, H_β, and Ar as discussed. At z = - 16 mm in the activation zones, the spectrum obtained for Scheme II featured emissions from OH($A^2\Sigma^+$–$X^2\Pi_{3/2}$)(0–0) and N_2($C^3\Pi_u$-$B^3\Pi_g$)(1 – 0)(0 – 0)(1 – 2) (0 – 1) and very little excited Ar* whereas the spectrum for Scheme III was heavily dominated by the electronic systems of CH($A^2\Delta$-$X^2\Pi$)(0–0), and C_2($d^3\Pi_g$-$a^3\Pi_u$) Swan band. At z = - 12 mm further downstream, the spectrum for Scheme II in figure 4.5b featured emission from OH(A) and N_2(C-B) systems while the spectrum for Scheme III (figure 4.4c) featured emissions mainly from C_2(d). The similarities observed in the emission intensities of Scheme I and Scheme II can be attributed to the ultra-lean fuel equivalence ratio employed in this study. As discussed in section 3.1 the effects of plasma quenching are not significant for ultra-lean fuel equivalence ratios, the reason for the similar spectra obtained for Scheme I and Scheme II. However, plasma quenching is significant in Scheme III as observed in the emissions from the activation zone being dominated by CH(A) and C_2(d) obtained from the methane pyrolysis by the plasma. Consequently, the main species heading to the ignition zones in Scheme III are from the electron impact dissociation of methane, CH(A), C_2(d) observed along with CH_3, CH_2 as well as products of recombination reactions C_2H_2 and C_2H_4 [32] . The presence of emissions from metastable state Ar in the plasma zone (z = -20 mm) and absence in the activation zone (z = -12 mm) for all three operation schemes is proof that plasma generated radicals have little to no influence in the activation zone.

Due to the low emission intensities observed at the ignition zones, the integration time of the spectrometer was increased to 2000 ms with 10 spectra obtained and averaged

at each spatial location to improve on the signal-to-noise ratio. Figure 4.5 shows the emission spectra obtained in the hybrid/ignition zones (z = - 8 mm and – 4 mm) and the flame zones (z = 10 mm) of Scheme I, Scheme II and Scheme III respectively.

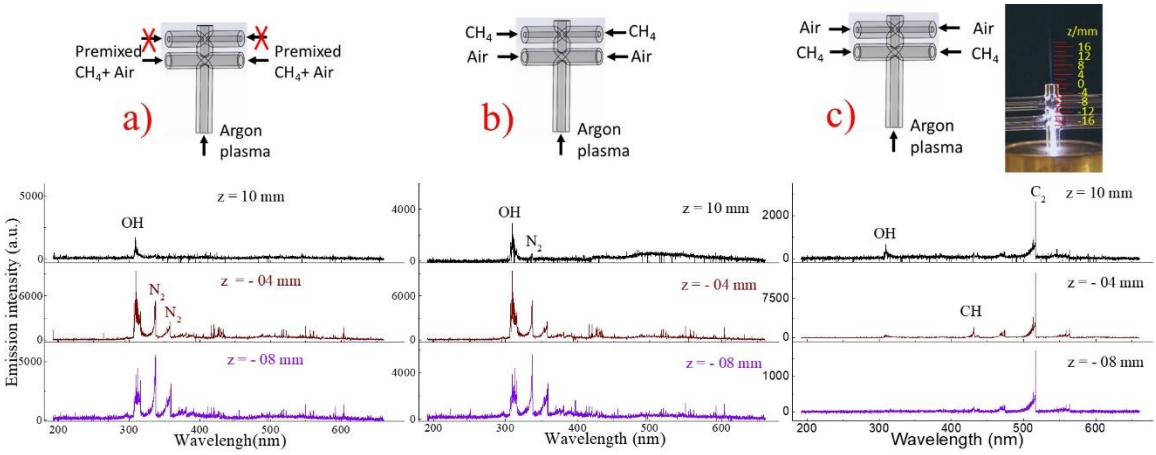

Figure 4.5 Optical emission spectra in the ignition and flame zones in all three operation schemes

Optical emission spectra at three spatial locations in the combustion reactor showing the species present at the hybrid/activation and flame zones when the combustor is operating in; a) Scheme I b) Scheme II c) Scheme III. The plasma power and feed gas flow rates were fixed at 140 W and 0.84 slm while the fuel equivalence ratio and total flow rates (fuel and air) were held constant at 0.4 and 0.6 slm respectively throughout the entire study

The emission spectra for Schemes I and II remain very similar due to the ultra-lean fuel equivalence ratio employed. Upon increasing the integration time to 2000 ms, the spectra at z = -8 mm and -4 mm in both Scheme I and II were dominated by emissions from the OH($A^2\Sigma^+$–$X^2\Pi_{3/2}$)(0–0) and N_2($C^3\Pi_u$-$B^3\Pi_g$)(1 – 0)(0 – 0)(1 – 2)(0 – 1) systems. Emissions from the excited state of Ar were again visible but very weak. Whereas for Scheme III, the spectra was dominated by emissions from the C_2(d) Swan

band and very little CH(A) observed at z = - 4 mm. Far downstream in the flame zone, due to the lower emission intensity, the integration time was further increased to 80 000 ms. At z = 10 mm, the spectra for Schemes I and II were typical of the emission spectra reported in the flame region as in previous studies dominated by OH(A) whereas for Scheme III, the emission spectra were predominantly dominated by C_2(d) with very little OH(A) was observed.

Thus by employing optical emission spectroscopy to characterize the species present at the various stages of plasma assisted ignition and combustion, for the three different mixing schemes, we are able to identify which plasma generated species are more responsible for the observed enhancement effects. From the emission spectra obtained at the activation zones, we observe that plasma generated reactive oxygen and nitrogen species (OH(A) and N_2) play a more important role as constituents of the radical pool required for ignition compared to the species resulting from fuel breakdown by the plasma (CH(A) and C_2(d)). This is inferred from the fact that plasma assisted ignition occurred at a much lower power for Scheme I and II compared to Scheme III. Also, the independence of the plasma ignition power on fuel equivalence ratio in Scheme II is evidence to further support the hypothesis that reactive oxygen and nitrogen species generated by the plasma are the main constituents of the radical pool that must attain a critical concentration for ignition to occur. W. Sun *et al.*[33] using a counter flow burner integrated with a nanosecond repetitively pulsed discharge investigated the effect of activating the oxidizer stream in the combustion of a methane/oxygen/argon mixture. They reported a significantly magnified reactivity of the diffusion flames, an increase in

the extinction strain rates and credited reactive atomic oxygen generated in the oxidizer stream for the observed enhancement effects above the critical crossover temperature.

4.3.4 Rotational temperature

The rotational temperature was obtained at a spatial resolution of 2 mm along the flame axis by fitting the experimentally obtained spectrum to a simulated spectrum and comparing the relative intensities of the P and R branches of the OH(A-X) spectra using Specair [34]. With the combustion reactor operating in Scheme I, the rotational temperature was observed to increase with an increase in the plasma power as shown in figure 4.6a. Coupling the plasma to the premixed fuel/air mixture resulted in an increase in the rotational temperature at z = - 18 mm. This dramatic increase in rotational temperature is attributed to two main processes, plasma heating from the fast relaxation of the electronic and vibrational energy of the excited species in the plasma in the presence of the heavy neutrals coming in from the premixed fuel/air mixture and the chemical fuel oxidations initiated by radicals generated by the plasma. A similar increase in temperature was observed by A. Bao *et al.* [35] during their investigation of the ignition of ethylene/air and methane/air flows using a low temperature repetitively pulsed nanosecond discharge. They observed that adding fuel to an air plasma resulted in a 350 ^{o}C increase in the rotational temperature while adding fuel to a nitrogen plasma resulted in just a 50 ^{o}C increase in the rotational temperature. It was concluded that the significant increase in temperature when fuel was added to the plasma was due to chemical fuel oxidation and the smaller temperature rise in the fuel/nitrogen case due to relaxation of the electronic and vibrational states of the excited N_2 molecules. In Scheme I, after the initial surge in temperature at z = - 18 mm for all powers investigated, continuous chain

initiation and branching reactions initiated by the plasma radicals causes the rotational temperature to attain a peak further downstream. The rotational temperature is observed to drop downstream in the flame zone due to losses to the environment through convection and radiation.

Increasing the plasma power resulted in a slight increase in the thermal input from the plasma as observed at z = 20 mm. The slight increase in the rotational temperature of the plasma at z = - 20 mm with increase in plasma power is however significantly amplified in the hybrid zone (z = - 18 mm to z = - 10 mm). This increase in rotational temperature with increase in plasma power is attributed to the size of the radical pools generated by the corresponding plasma powers. A higher plasma power results in the creation of a larger radical pool which in turns facilitates the oxidation of a larger percentage of the premixed methane/air mixture. Hence the higher temperatures attained by the higher plasma powers is attributed to a larger volume of fuel oxidized. The increase in radical pool size with increase in plasma power improves on the flameholding as observed in section 4.3.2. At a plasma power of 60 W, even though the rotational temperature from the plasma assisted oxidization of the premixed fuel/air mixture surpasses the auto ignition temperature of 873 K [36] of methane, no flame is observed outside the combustion reactor since the radical pool generated is too small to sustain the flame. Increasing the plasma power, increases the radical pool supplied which results in increased rotational temperatures and improved flameholding.

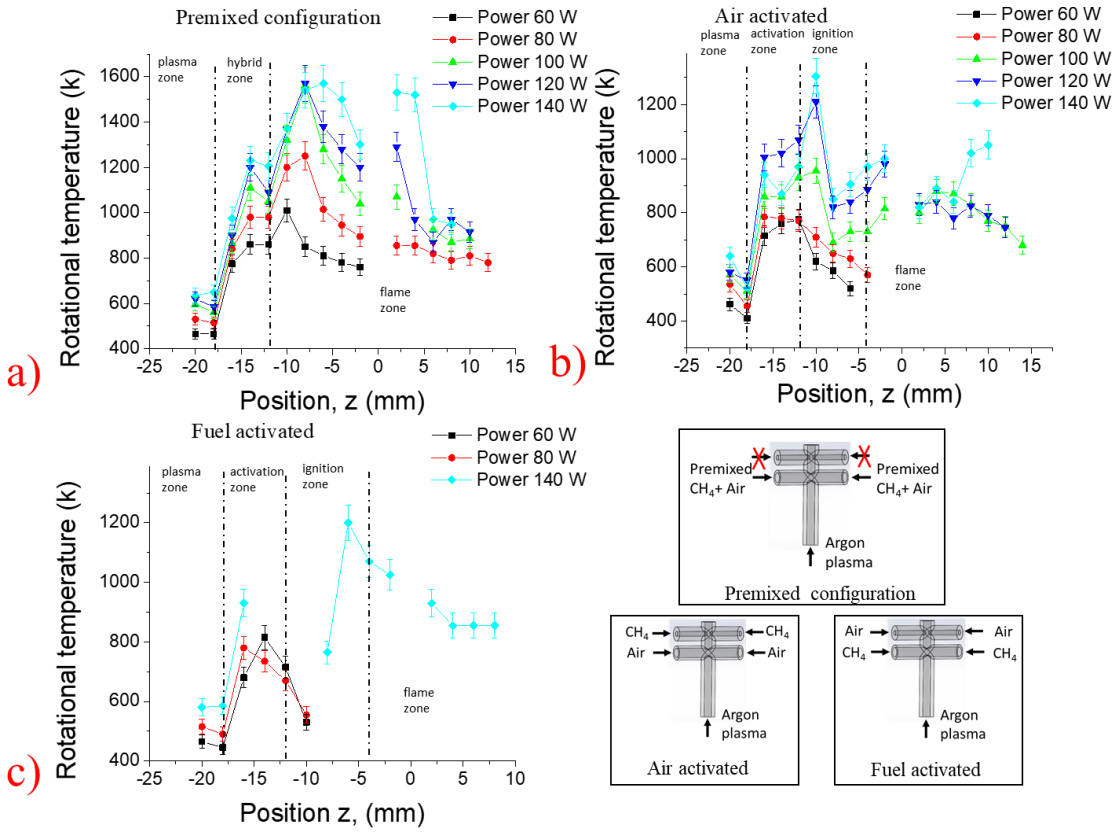

Figure 4.6 Rotational temperature profiles for different powers for the three operation schemes

Rotational temperature profiles obtained by simulation from the OH(A-X) spectra along the combustion axis of the plasma combustion reactor operating in; a) Scheme I b) Scheme II c) Scheme III. The plasma power and feed gas flow rates were fixed at 140 W and 0.84 slm while the fuel equivalence ratio and total flow rates (fuel and air) were held constant at 0.4 and 0.6 slm respectively throughout the entire study

Figure 4.6b shows the variation of the rotational temperature profile obtained along the propagation axis of the plasma assisted combustion reactor operating in Scheme III at different plasma powers. A similar increase in rotational temperature was observed at z = - 18 mm when the air was activated by the plasma. This increase in rotational temperature was mainly attributed to the plasma heating effect due to the relaxation of the electronic and vibrational excited species supplied by the plasma when coupled to the

neutral species present in the air. This is further supported by the observation that the rotational temperature increase observed in the activation zones in Scheme II or Scheme III is lower compared to the rotational temperature increase in the hybrid zone in Scheme I which was attributed to both plasma heating and exothermic fuel oxidation reactions. For plasma powers 60 W and 80 W in Scheme II, the temperature increase due to the plasma heating is lower than the autoignition temperature of methane and as a result, no flame is observed outside the combustion reactor. When the plasma power is increased to 100 W, the plasma heating effect also increases and despite the rotational temperature being below the auto ignition temperature, a flame is observed outside the combustor. The presence of the flame at a plasma power of 100 W alludes to the fact that the reactive species generated by the interaction of the plasma and air, improved flame ignition and flameholding. Increasing the plasma power results in an increase in rotational temperature observed in the activation zone implying an increase in both plasma heating and thermochemical energy released from the oxidation of a larger percentage of fuel due to the larger radical pool generated. For all powers, the flame temperature is observed to drop downstream of the flame due to conductive, convective and radiative losses to the surrounding environment.

Figure 4.6c shows the spatial variation in the rotational temperature profile obtained for Scheme III. The emission spectra and hence rotational temperature profiles at power 100 W and 120 W could not be obtained due to the flow and flame instabilities. From the powers investigated, it was observed that at z = - 18 mm, the increase in the rotational temperature when the methane was coupled to the plasma was attributed to the plasma heating effect similar to the increase in rotational temperatures in Scheme II.

Even though ignition is not achieved in both cases for the air activated and fuel activated at powers 60 W and 80 W, the temperature for the lower powers is observed to quickly decrease in Scheme III compared to Scheme II. This steeper drop in temperature is attributed to the endothermic methane pyrolysis reactions.

In all three operation schemes investigated, at a fixed power the peak rotational temperature attained was highest when the combustor was operated in Scheme I and least when operated in Scheme III. It is thus inferred from the higher temperatures observed in the ignition zones of Schemes I and II that, Schemes I and II, are more efficient than Scheme III. This also buttresses the conclusion that for ultra-lean fuel equivalent ratios Scheme I is more efficient in ignition and flameholding compared to Scheme II. Also the presence of a flame in Scheme II at a plasma power of 100 W when the rotational temperature is less than the auto ignition temperature for methane further supports the observation that efficient radical generation by the plasma enhances the ignition and flameholding process.

4.3.5 Measurements of the ground state OH(X)

Cavity ringdown spectroscopy was employed to measure the absolute number density of OH(X) in the flame zones when the combustor was operated in the three different operation schemes. The OH(X) number densities were measured along the direction of propagation of the flow with a spatial resolution of 2 mm. With the laser inside the plasma plume, a section of the OH(A-X)(0-0) absorption spectra was obtained by cavity ringdown spectroscopy near the 308 nm band with a low resolution of 0.005 nm. The absorption lines in the rotationally resolved spectra were assigned by comparison with a simulated spectra from LIFBASE [37].

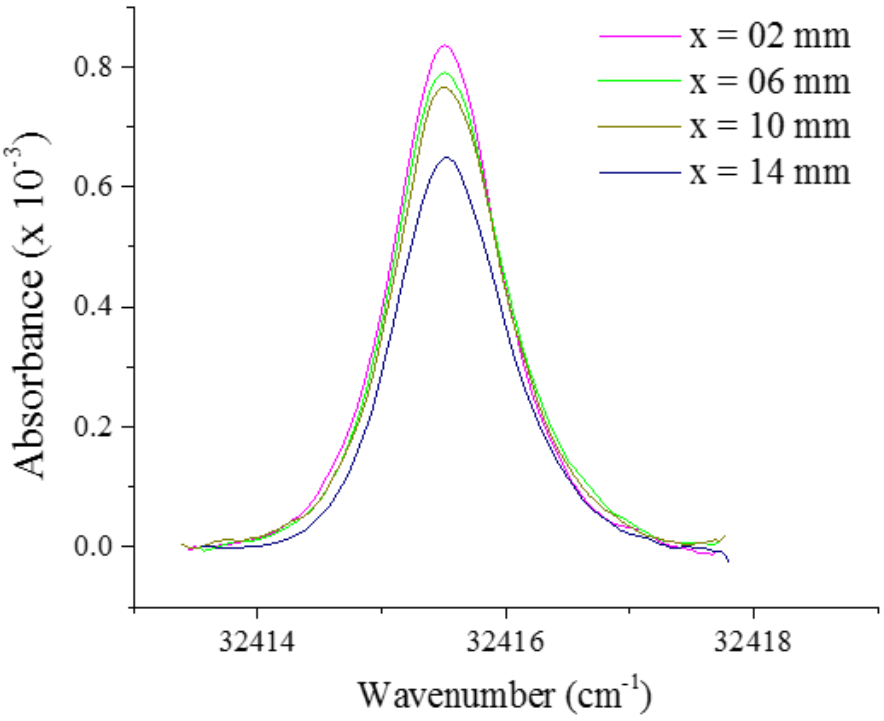

Figure 4.7 Measured ringdown spectral line shapes of the R2(1) rotational line in the OH A-X (0-0) band

Measured ringdown spectral line shapes of the $R_2(1)$ rotational line in the OH A-X (0-0) band obtained at four different spatial locations along the plasma assisted combustion flame in Scheme I. A ten-point adjacent-average was used with the plasma power and feed gas flow rates fixed at 140 W and 0.84 slm while the fuel equivalence ratio and total flow rates (fuel and air) were held constant at 0.4 and 0.6 slm respectively

The R2(1) rotational line was chosen and its integrated absorbance used to determine the absolute OH(X) number density since it has no spectral overlap with other rotational lines. The absolute number density of OH molecules were derived from the ringdown measurement using the formula,

$$\text{Absorbance} = Snl = \int_v \frac{L}{c}\left(\frac{1}{\tau^f(v)} - \frac{1}{\tau_0}\right) dv \qquad (3.5)$$

where n is the OH number density in the initial state of the $R_2(1)$ transition; and are the ringdown times obtained in the plasma-assisted combustion flames when the laser wavelength is tuned onto and off the absorption peak, respectively; c is the speed of light; L and l are the ringdown cavity length and the laser beam path-length respectively. S(T) is the temperature-dependent line intensity and can be calculated from Equation (2) [38]

$$S(T) = 3.721963 \times 10^{-20} \frac{T_{trans}}{273.16} \frac{1}{8\pi c \nu^2} \left(\frac{N}{P}\right) \left(\frac{e^{-1.4388E''/T_r}}{Q_{VR}}\right) A_{v''J''}^{v'J'} (2J' + 1)\left(1 - e^{-1.4388\nu/T_v}\right) \quad (3.6)$$

where T is the temperature in Kelvin, ν is the transition frequency of the OH $R_2(1)$ line of 32415.452 cm^{-1}, N is the total number density (molecule cm^{-3}) at pressure P (atm) and temperature T, is the Einstein coefficient in s^{-1}, E″ is the lower state energy, i.e. 126.449 cm^{-1}, and Q_{VR} is the vibrational rotational partition function with V and J vibrational and rotational quantum numbers, respectively. In this study, the temperatures used to calculate the temperature-dependent line intensities S(T) were determined by the spectra simulations using Specair as discussed in section 4.3.4.

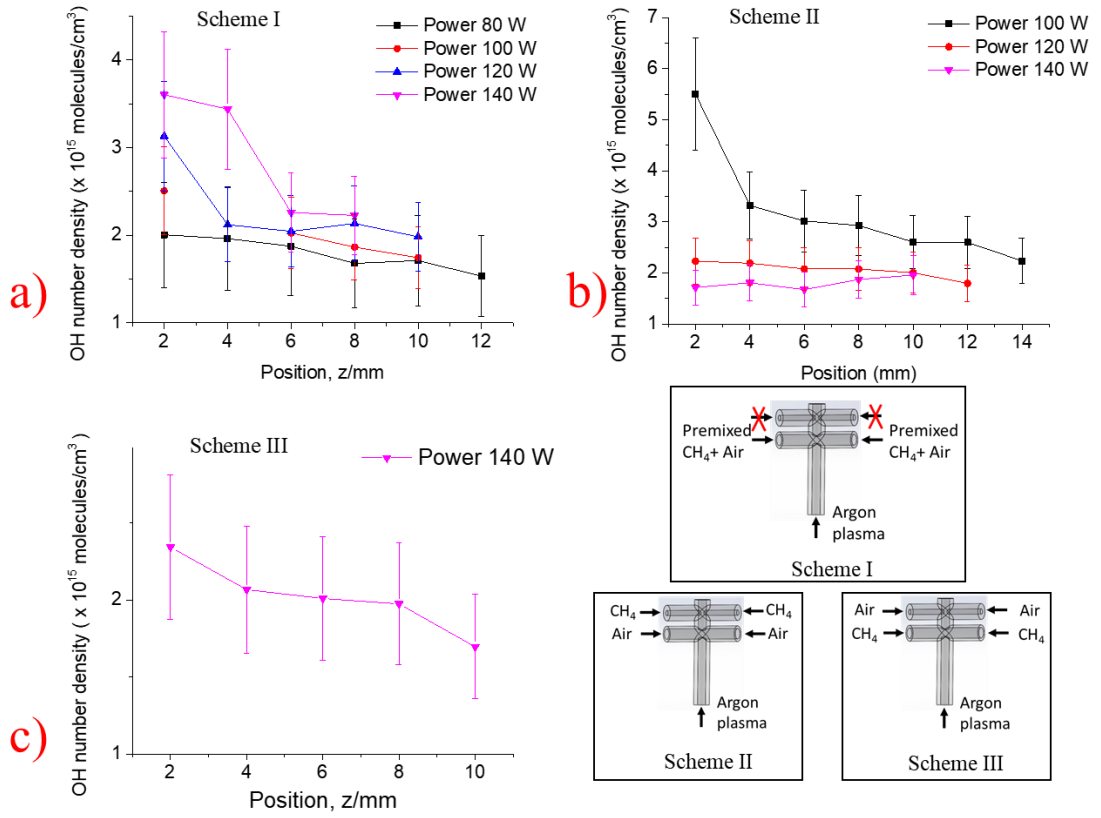

Figure 4.8 Absolute OH(X) number densities in the flame regions of the three operation schemes investigated

The measurement results of the absolute OH(X) number density in the flame regions of; a) Scheme I b) Scheme II c) Scheme III. The plasma power and feed gas flow rates were fixed at 140 W and 0.84 slm while the fuel equivalence ratio and total flow rates (fuel and air) were held constant at 0.4 and 0.6 slm respectively. The error bars indicate the maximum measurement uncertainty of ±30%

Figure 4.8 shows the spatially resolved OH(X) absolute number density profiles measured in the flame region outside the combustion reactor for Scheme I, Scheme II, and Scheme III respectively. The argon plasma feed gas flow rate and total fuel/air mixture flow rates were fixed constant at 0.84 slm and 0.6 slm while the fuel equivalence ratio and plasma power were fixed at 0.4 and 140 W for all the operation schemes

investigated. Considering the uncertainties in measuring the path lengths of the laser in the flame and obtaining the temperature by comparing the simulated and experimental spectra, the uncertainty in the measured OH(X) absolute number density was found to be ± 30%.

In the flame zone, the combustion process is largely dominated by species generated from the ignition process due to the short life time of the plasma species. OH(X) generation in the flame zone is as a result of chain initiation, chain branching and propagation reactions. OH(A) relaxation from the excited state also contributes to OH(X) generation. OH(X) is consumed through chain termination reactions and diffusion to the surrounding atmosphere.

In the flame zone, for all three operation schemes, the OH(X) number density is observed to decrease downstream along the propagation axis for all powers investigated. In Scheme I, the OH(X) number densities where observed to decrease spatially along the propagation axis of the flame as shown in figure 4.8a. For example, at a plasma power of 140 W, the OH(X) number densities drops from 3.6 x 10^{15} molecules/cm^3 at z = 2 mm to 2.2 x 10^{15} molecules/cm^3 at z = 8 mm. It is proposed that the spatial decrease in OH(X) number densities along the propagation axis of the flame for all plasma powers investigated is due to the OH(X) loss mechanism though diffusion and chain termination reactions far outweighing the OH(X) generation mechanisms as the flow progresses downstream. Increasing the plasma power resulted in an increase in the OH(X) number density at any given spatial location. For example at z = 8 mm, the OH(X) number density increases from 1.7 x 10^{15} molecules/cm^3 at a plasma power of 80 W to 2.2 x 10^{15} molecules/cm^3 at a plasma power of 140 W. This increase in OH(X) number density with

increase in plasma power is attributed to the improved odds of the generation of OH radicals when plasma power is increased in spite of competition from fuel dissociation processes. Due to the increase in OH(A) produced by the plasma, the contribution from the relaxation of OH(A) to OH(X) thus increases OH(X) number densities measured downstream in the flame region as shown in figure 4.8a. Nimisha *et al.*[19] measured the OH(X) radicals number densities downstream of a helium microwave plasma jet and also reported an increase in OH(X) radicals with increase in microwave plasma power.

In Scheme II, the OH(X) number densities were also observed to decrease spatially downstream along the propagation axis for all plasma powers as shown in figure 4.8b. The spatial decrease in OH(X) number densities downstream along the propagation axis is as a result of the loss mechanisms to diffusion and chain propagation reactions outweighing the OH(X) creation inside the flame zone. The OH(X) radical number density was observed to fall with an increase in plasma power in Scheme II. For example, at z = 8 mm downstream, the OH(X) number density was measured, dropped from 2.9 x 10^{15} molecules/cm^3 at a plasma power of 100 W to 1.9 x 10^{15} molecules/cm^3 at a plasma power of 140 W. This trend is opposite to the trend observed in Scheme I and it is hypothesized to be due to the improved radical pool generation in Scheme II. As discussed in section 4.3.1, due to the lack of competition during the activation phase from fuel molecules, there is efficient production of OH radicals in the activation zone which results in the ignition of a larger amount of fuel in the ignition zone. Hence downstream, there is very little OH observed since most the OH radicals have been used up in the ignition phase. This efficient creation of radicals in Scheme II, compared to Scheme I is further supported by the observation that, at z = 2 mm, the OH radical number density is

at 5.5 x 10^{15} molecules/cm^3 in Scheme II compared to 2.0 x 10^{15} molecules/cm^3 in Scheme I. The improved luminosity of the flame as seen in the figure 4.3 for Scheme II compared to Scheme I with increase in plasma power is further proof buttressing the improved radical formation and improved fuel consumption in Scheme II.

Due to the flame instability in the Scheme III, the OH(X) number density profile could only be obtained at a single plasma power of 140 W as shown in figure 4.8c. A similar spatial decrease in OH(X) from 2.3 x 10^{15} molecules/cm^3 at z = 2 mm to 1.6 x 10^{15} molecules/cm^3 at z = 10 mm was observed in Scheme III.

It is suggested that, increasing the plasma power mitigates the effect of plasma quenching in Scheme I resulting in larger radical pools being created by the higher plasma powers. Due to the larger radical pools generated, a larger percentage of the fuel is involved in the combustion process along the propagation axis resulting in the OH(X) measured outside the combustor. However, in Scheme II, the lack of plasma quenching results in the efficient creation of a larger pool in the activation zone thus allowing for a much greater percentage of the fuel to be ignited. Due to this efficient ignition process, a larger and more luminous flame is observed in Scheme II compared to Scheme I. Also it is proposed that, the efficient radical generation and consumption in the ignition zone accounts for the drop in OH(X) in the flame zone of Scheme II compared to Scheme I with increase in plasma power.

4.4 Summary

In this study, we investigated and compared the effects of coupling the plasma directly to a premixed fuel/air mixture (Scheme I), activating the oxidizer stream (Scheme II), or activating the fuel stream (Scheme III) in the plasma assisted ignition and

oxidation of methane by air. The different operation schemes explored provide significant information into the radical pool composition and mechanisms responsible for the observed enhancements in the plasma assisted combustion kinetics of fuel/air mixtures. The enhancement parameters investigated were the minimum ignition power and fuel efficiency. From the minimum ignition plasma power study, the previously reported U-shaped minimum ignition power curve was obtained when the system was operated in the control Scheme I. However, it was observed that in Scheme II, the plasma power required for ignition of the non-premixed methane/air mixture was independent of the fuel equivalence ratios studied whereas an increase in plasma power with fuel equivalence ratio was observed for the methane activated case providing further evidence to suggest the existence of a critical radical pool required for ignition to occur. From the analysis of the images from the three operation schemes, a green flame was observed in Scheme III whereas a blue flame was observed in both Schemes I and II. Based on results from the minimum ignition study, the observation that the optical emission spectra obtained from the Scheme III was heavily dominated by CH(A) and C_2(d) in the flame region, and the heavy sooting at lean fuel equivalence ratios observed in the combustion reactor upon prolonged operation of the system, we propose that Scheme III is the least fuel efficient scheme of all three operation schemes. Rotational temperature obtained from comparisons between the experimental spectra and simulated spectra for constant combustor conditions, showed higher peak temperatures observed in Scheme I, and least in Scheme III, lending further credence to the hypothesis that less energy is released from the fuel in Scheme III compared to the other operation schemes. OH(X) measurements in all three operation schemes were on the order of 10^{15} molecules/cm^3 and revealed an

increase in OH(X) number densities outside the combustor with increase in plasma power in Scheme I whereas in Scheme II, a decrease in OH(X) number densities was observed with increase in plasma power. By employing different operation schemes to decouple the interaction between the plasma and the methane/air mixture, we propose based on results obtained from the minimum ignition study, optical emission spectroscopy and cavity ringdown spectroscopy, that a critical radical pool size generated by the plasma is required for ignition to occur with reactive oxygen and nitrogen species playing a more important role in the observed plasma assisted ignition and enhancement effects.

4.5 References

1. Yu Y., Li X., An X., Yu X., Fan R., Chen D., and Sun R., 2017 "Optics & Laser Technology Stabilization of a premixed methane-air flame with a high repetition nanosecond laser-induced plasma," *Optics & Laser Technology*, **92**, 24–31

2. De Giorgi M. G., Sciolti A., Campilongo S., Pescini E., Ficarella A., Lovascio S., and Dilecce G., 2016 "Lean Blowout Sensing and Plasma Actuation of Non-Premixed Flames," *IEEE Sens. J.*, **16**, 3896–3903

3. Stockman E. S., Zaidi S. H., Miles R. B., Carter C. D., and Ryan M. D., 2009 "Measurements of combustion properties in a microwave enhanced flame," *Combust. Flame*, **156**, 1453–1461

4. Hammack S., Rao X., Lee T., and Carter C., 2011 "Direct-coupled plasma-assisted combustion using a microwave waveguide torch," *IEEE Trans. Plasma Sci.,* **39**, 3300–3306

5. Pancheshnyi S. V., Lacoste D. A., Bourdon A., and Laux C. O., 2006 "Ignition of Propane-Air Mixtures by a Repetitively Pulsed Nanosecond Discharge," *IEEE Trans. Plasma Sci.*, **34**, 2478–2487

6. Korolev Y. D., Frants O. B., Landl N. V., Geyman V. G., Shemyakin I. A., Enenko A. A., and Matveev I. B., 2009 "Plasma-assisted combustion system based on nonsteady-state gas-discharge plasma torch," *IEEE Trans. Plasma Sci.*, **37**, 2314–2320,

7. Aleksandrov N. L., Kindysheva S. V., Kosarev I. N., Starikovskaia S. M., and Starikovskii A. Y., 2009 "Mechanism of ignition by non-equilibrium plasma," *Proc. Combust. Inst.*, **32**, 205–212,

8. Ju Y. and Sun W., 2015 "Plasma assisted combustion: Dynamics and chemistry," *Prog. Energy Combust. Sci.,* **48**, 21–83

9. W. Sun, 2013 "Non-equilibrium Plasma-Assisted Combustion,"(Doctoral Dissertation) http://arks.princeton.edu/ark:/88435/dsp01pn89d663g

10. Chintala N., Bao A., Lou G., and Adamovich I. V. 2006 "Measurements of combustion efficiency in nonequilibrium RF plasma-ignited flows," Combust. Flame , **144**, 744–75

11. X. Li, Y. Yu, J. Peng, R. Fan, R. Sun, and D. Chen, 2016 "Laser ablation plasma-assisted stabilization of premixed methane/air flame," *Appl. Phys. B Lasers Opt.,* **122**, 1–7

12. Fuh C. A., Wu W., and Wang C., 2016 “Microwave plasma-assisted ignition and flameholding in premixed ethylene/air mixtures,” *J. Phys. D. Appl. Phys.,* **49** , 285202

13. Adamovich I. V and Lempert W. R. 2015, “Challenges in understanding and predictive model development of plasma-assisted combustion,” *Plasma Phys. Control. Fusion*, **57**, 14001.

14. Wu W., Fuh C. A., and Wang C., 2014 “Comparative study on microwave plasma-assisted combustion of premixed and nonpremixed methane/air mixtures,” *Combust. Sci. Technol.*, **187**, 999–1020

15. Wang C. and Wu W., 2013 “Simultaneous measurements of OH(A) and OH(X) radicals in microwave plasma jet-assisted combustion of methane/air mixtures around the lean-burn limit using optical emission spectroscopy and cavity ringdown spectroscopy,” *J. Phys. D. Appl. Phys.*, **46**, 464008

16. Wang C., Srivastava N., Scherrer S., Jang P. R., T. Dibble S., and Duan Y 2009 “Optical diagnostics of a low power—low gas flow rates atmospheric-pressure argon plasma created by a microwave plasma torch,” *Plasma Sources Sci. Technol.*, **18**, 25030

17. Srivastava N. and Wang C., 2011 “Effects of water addition on OH radical generation and plasma properties in an atmospheric argon microwave plasma jet,” *J. Appl. Phys.*, **110**, 53304,

18. Wang C., Srivastava N., and Dibble T. S., 2009 “Observation and quantification of OH radicals in the far downstream part of an atmospheric microwave plasma jet using cavity ringdown spectroscopy,” *Appl. Phys. Lett.*, **95**, 51501

19. Srivastava N. Srivastava and Wang C. Wang, 2011 “Determination of OH Radicals in an Atmospheric Pressure Helium Microwave Plasma Jet,” *Plasma Sci. IEEE Trans.,* **39**, 918–924

20. Wang C., Srivastava N., Scherrer S., Jang P.R., Dibble T. S., and Duan Y., 2009 “Optical diagnostics of a low power—low gas flow rates atmospheric-pressure argon plasma created by a microwave plasma torch,” *Plasma Sources Sci. Technol.,* **18**, 25030

21. Wang C. 2007 “Plasma-cavity ringdown spectroscopy (P-CRDS) for elemental and isotopic measurements,” *J. Anal. At. Spectro*., **22**, 1347–63

22. Sun W. and Yiguang J. Y. 2013 “Nonequilibrium Plasma-Assisted Combustion: A Review of Recent Progress,” Plasma Fusion Res, **89**, 208–219

23. Fuh C. A., Wu W., and Wang C., 2014 “Effects of a microwave induced argon plasma jet on premixed and nonpremixed methane/air mixtures,” 45th AIAA Plasma-dynamics and Lasers Conference, 2240

24. Wang C. and Wu W., 2014 “Roles of the state-resolved OH(A) and OH(X) radicals in microwave plasma assisted combustion of premixed methane/air: An exploratory study,” *Combust. Flame*, **161**, 2073–2084

25. Wu W., Fuh C. A., and Wang C., 2015 “Comparative study on microwave plasma-assisted combustion of premixed and nonpremixed methane/air mixtures,” *Combust. Sci. Technol.*, **187**, 999-1020

26. Han J., Yamashita H., and Yamamoto K., 2009 “Numerical Study on Spark Ignition Characteristics of a Methane-Air Mixture Using Detailed Chemical Kinetics,” *J. Therm. Sci. Technol.,* **4**, 305–313

27. Starik A. M., Kozlov V. E., and Titova N. S., 2010 “On the influence of singlet oxygen molecules on the speed of flame propagation in methane-air mixture,” *Combust. Flame*, 157, 313 – 327

28. Sun W., Uddi M., Won S. H., Ombrello T., Carter C., and Ju Y., 2012 “Kinetic effects of non-equilibrium plasma-assisted methane oxidation on diffusion flame extinction limits,” *Combust. Flame*, **159**, 221–229

29. Dutta A., Yin Z., and Adamovich I. V., 2011 “Cavity ignition and flameholding of ethylene–air and hydrogen–air flows by a repetitively pulsed nanosecond discharge,” *Combust. Flame*, **158**, 1564–1576

30. Liu X. Y., Pei X. K., Ostrikov K., Lu X. P., and Liu D. W., 2014 “The production mechanisms of OH radicals in a pulsed direct current plasma jet,” *Phys. Plasmas*, **21**, 093513

31. Jauberteau J. L., Cinelli M. J., and Aubreton J., 2002 “Reactivity of methane in a nitrogen discharge afterglow,” *New J. Phys.,* **4**, 2002. 39.1–39.13

32. Chen H. H., Der Liao J., Weng C., Hsieh J. F., Chang C. W., Lin C. H., and Cho T. P., 2011 “The influence of methane/argon plasma composition on the formation of the hydrogenated amorphous carbon films,” Thin Solid Films, **519**, 2049–2053

33. Sun W., Uddi M., Ombrello T., Won S. H., Carter C., and Ju Y., 2011 “Effects of non-equilibrium plasma discharge on counter flow diffusion flame extinction,” *Proc. Combust. Inst.*, **33**, 3211–3218

34. Laux C O, Spence T, GKruger C H and Zare R N 2003 Optical diagnostics of atmospheric pressure air plasmas *Plasma Sources Sci. Technol.* **12** 125–38

35. Bao A., Utkin Y. G., Keshav S., Lou G., and Adamovich I. V., 2007 "Ignition of ethylene-air and methane-air flows by low-temperature repetitively pulsed nanosecond discharge plasma," *IEEE Trans. Plasma Sci.* , **35** , 1628–1638

36. Robinson C. and Smith D. B., 1984 "The auto-ignition temperature of methane," J. Hazard. Mater., **8**, 199–203

37. Luque J. and Crosley D. R., 1999 "'LIFBASE: Database and spectral simulation (version 1.5)', SRI International Report MP 99-009."

38. Goldman A. Goldman and Gillis J. R. Gillis, 1981 "Spectral line parameters for the $A^2\sum$-$X^2\Pi(0,0)$ band of OH for atmospheric and high temperatures," ournal Quant. Spectrosc. *Radiat. Transf.,* **25**, 111–135, Feb. 1981.

CHAPTER V

MEASUREMENT OF OH(X) IN THE MICROWAVE PLASMA ASSISTED IGNITION OF METHANE/AIR MIXTURE BY CAVITY RINGDOWN SPECTROSCOPY

5.1 Introduction

The introduction of plasmas to conventional fuel/air combustion systems have been reported to bring about improvements in reduced ignition delay time[1], fuel efficiency [2], [3], flame holding[4][5], flow control [6] etc. Even though this enhancement effects are being reported, the mechanism through which they are brought about is still not well understood. There are several roadblocks hindering the scientific community's progress in understanding the plasmas assisted combustion process with the lack of accurate experimental data to validate theoretical studies being one of the most pertinent of them [7]. In order to address the need for accurate experimental data to validate theoretical mechanisms, efforts have been made by the scientific community to accurately measure the absolute number density of several important species generated in plasma assisted combustion. OH is an important transient specie produced in plasma assisted ignition and combustion and is responsible for key chain initiation and chain branching reactions. Knowing the absolute number densities of this specie in plasma assisted combustion systems is important in determining reaction rate constants which can be used to fine tune current reaction mechanisms. Several studies have been done with the aim of measuring the absolute number densities of this important specie with the

main techniques widely employed being absorption spectroscopy and laser induced fluorescence spectroscopy (LIFS). For example, researchers such as Kosarev *et al.* [8] used a single pass UV absorption technique to measure the ground state concentrations of OH radical in the afterglow of a pulsed nanosecond high voltage plasma assisted ignition of hydrogen/oxygen/argon mixture. Yin *et al.* [9] employed LIFS to measure the time resolved OH concentrations in a mildly preheated hydrogen/air mixture excited by a repetitively pulsed discharge plasma in a plasma flow reactor. They reported a 20 – 50 fold increase in OH number density during ignition. Ombrello *et al.* [10] employed planar laser induced fluorescence spectroscopy to measure the OH radical number density in a piecewise nonequilibrium gliding arc discharge integrated with a couterflow flame burner where they measured a 2.20 % increase in extinction rates at low power inputs. Nagaraja *et al.* [11] also measured the time resolved absolute OH concentration and temperature using laser induced fluorescence in the ignition of a preheated hydrogen/air mixture excited by a pulsed nanosecond dielectric barrier discharge.

However, these techniques are plagued by several drawbacks including the need for calibration and collisional quenching of the excited states in the case of LIF and low sensitivity for absorption spectroscopy due to its single pass nature. Hence in this study, we employ cavity ringdown spectroscopy (CRDS) to measure and report the absolute OH(X) number density in the hybrid plasma flame zone in the plasma assisted combustion of a methane/air mixture. Cavity ringdown is a very versatile, ultra-sensitive, self-calibrated absorption technique with the sensitivity arising from the increase in the absorption path length in the sample due to its multi-pass nature. CRDS has been previously employed in plasma diagnostics and plasma assisted combustion studies to

measure the absolute ground state number density of the OH radicals in several plasma devices [12]–[15] and in the flame zone of several plasma assisted combustion flames [4], [16]–[19]. The use of CRDS to measure the absolute number density of OH(X) has thus far been constrained to the flame zone due to the complexity of the experimental setup used. Hence in this study, we employ a novel plasma assisted combustion reactor made up of a double armed, cross-shaped, triple layered quartz combustor to measure the absolute OH(X) number density for the first time in the hybrid plasma-flame zone of a plasma assisted combustion flame. Methane and air are used as the fuel and oxidizer in this study with a premixed mixture of the fuel and air, flowing coaxially along the second layer of the combustor, surrounding an argon plasma emanating from the innermost layer. The experimental setup is described in section 5.2 while the results are discussed in section 5.3 and a summary of the chapter follows subsequently in section 5.4.

5.2 Experimental setup

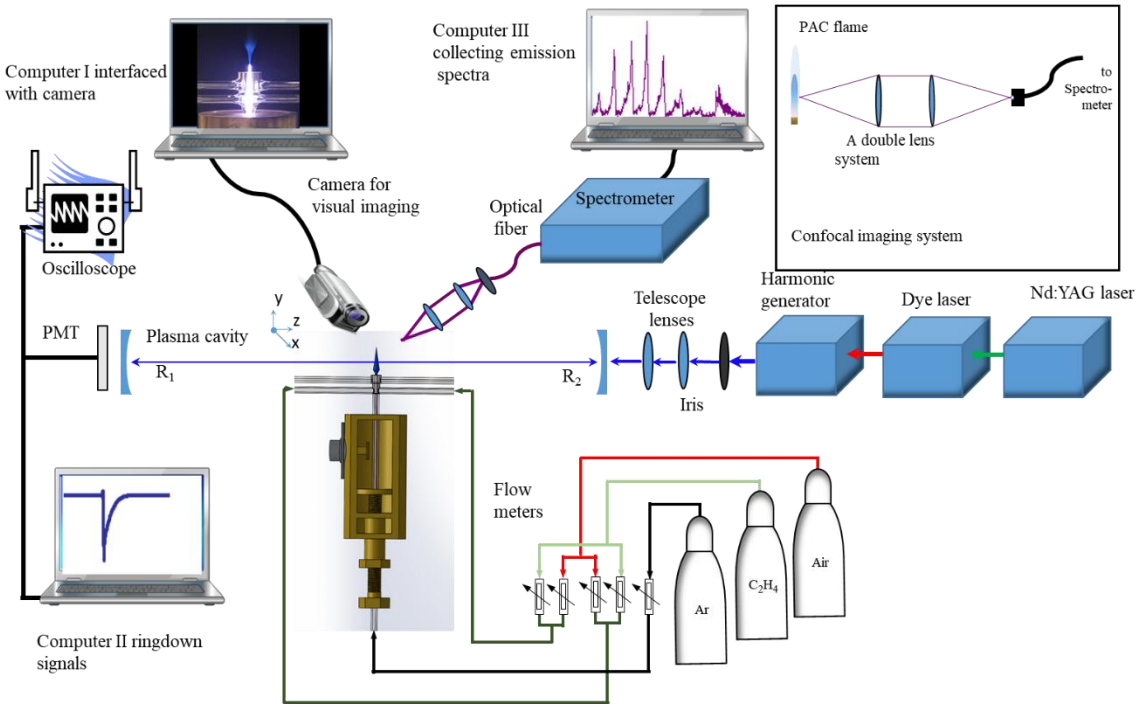

Figure 5.1 Schematic of experimental setup

Figure 5.1 shows a schematic of the experimental setup employed in this study. The setup used was made up of a plasma assisted combustion reactor, the gas flow control manifold and an optical diagnostic system. The plasma assisted combustion reactor consists of a quartz combustor and a microwave plasma cavity (surfatron). The quartz combustor is a double cross shaped quartz tube with the inner and outer diameters of all five of the arms being 2 mm and 6 mm respectively. The sixth arm which served as the combustor orifice was made up of 3 coaxial cylindrical orifices with inner diameters of, 2 mm, 5 mm and 7 mm respectively. Inner and outer diameters of the other five combustor arms were fixed by the microwave surfatron and were chosen so as to obtain a stable plasma flame. The inner diameters of the cylindrical orifice were chosen so as to

obtain concentric circular coflows outside the combustor orifice. A 2.45 GHz microwave power source (AJA international) was employed to power the surfatron via a 0.6 m low-loss coaxial cable (LMR-400, Times Microwave Systems). The forward and reflected powers were given as readouts from the microwave source and the coupling was optimized so that the reflected power was typically between 2 – 8 W for forward powers in the range 60 – 160 W. The coupling efficiency was not measured in this study and microwave plasma power as used in this text refers to the forward power readout from the microwave power source. The vertical arm of the double-cross shaped quartz tube was connected to the central coaxial cylinder and was inserted vertically into the surfatron. The vertical arm conveyed argon which was excited in the surfatron to generate an argon plasma emanating from the central coaxial tube. The lower horizontal arms were used to convey a premixed methane/air mixture which exited in the innermost coaxial orifice close to the center. The third/top most pair of horizontal tubes were shut off. In depth diagnostics of the diffused argon plasma generated in this study including emission spectra, plasma power effects, plasma temperature, plume shapes etc. can be found in [13], [20]–[22]. The plasma assisted combustion reactor was set up on a high precision (0.01 mm translation in all axis) 3D translation stage.

The gas flow control manifold consisted of five flow meters, along with three gas cylinders containing Argon (99.9% purity, Airgas), Methane (99.9 % purity, Airgas) and Air (ultra zero, Airgas), with each component connected to the plasma assisted combustion reactor as depicted in figure 5.1. One of the flow meters was used to vary the argon plasma feed gas flow rate with a range of 0 – 1.78 standard liter per minute (slm). An identical pair of rotameters was used to vary the methane flow rate and had a range of

0 – 434 standard cubic centimeter per minute (sccm, 1 slm = 1000 sccm). The last pair of identical flow meters were used to regulate the flow rate of the air mixture and had a range of 0 – 1.38 standard liters per minute. The outputs of each methane and air rotameter were joined to make a premixed flow with the resultant connected to the quartz reactor as shown in figure 5.1. The argon plasma feed gas was fixed constant at a flow rate of 0.84 slm throughout the entirety of the study.

The optical diagnostics system was made up of a digital camera, a fiber guided optical emission system and a cavity ringdown spectroscopy system. The digital camera used was a Sony camera (FCB-EX78BB) connected to computer I which had a time resolution of 100 µs – 1 s and was optimized for visual observation of the plasma and flame behavior. The optical emission spectroscopy system was used to characterize emissions spatially in the plasma assisted combustion reactor. A confocal imaging setup was employed using two identical lenses (f = 15 cm) eliminating the need for spatial filtering to transmit the emissions to a dual grating spectrometer (Avantes) via an optical fiber (aperture size 400 µm). The spectrometer housed two gratings of 600 grooves mm^{-1} and 1200 grooves mm^{-1} which were used to cover a spectral range of 200 – 600 nm with a resolution of 0.07 nm at 350 nm. The high precision translation stage, coupled with the small aperture of the optical fiber and confocal lens setup, allowed for a spatial resolution of 0.5 mm. The optical emission spectroscopy was operated by computer III as shown in figure 5.1.

The cavity ringdown spectroscopy system was constructed from a pair of highly reflective(R = 99.85 % at 308 nm) plano-concave mirrors with the length of the cavity being 74 cm. The plasma assisted combustion reactor was placed at the center of the

cavity with the optical axis (x axis) perpendicular to the plasma assisted combustion flame as shown in figure 5.1. A 20 Hz Nd:YAG laser (Powerlite 8020, Continuum) was used to pump a tunable line width dual grating dye laser (Narrowscan, Radiant) whose output was frequency doubled (Inrad Autotracker III) to produce the UV laser beam utilized in the system. The cross section of the laser in flame was 0.5 mm^2 while the minimum scanning step of the dye laser was 0.0003 nm with a pulse energy of a few μJ. The ringdown signal monitored with an oscilloscope (TDS 410A Tektronix) interfaced with computer II, was detected using a photo multiplier tube (PMT, R928, Hamamatsu) fitted with a 10 nm band pass interference filter. The baseline noise averaged over 100 ringdown events was typically 0.5 % without plasma assisted combustion and 0.8% with the plasma assisted combustion flame on. A detailed description of the experimental setup used can be found in [23] [24].

5.3 Results and discussion

5.3.1 Flame structure

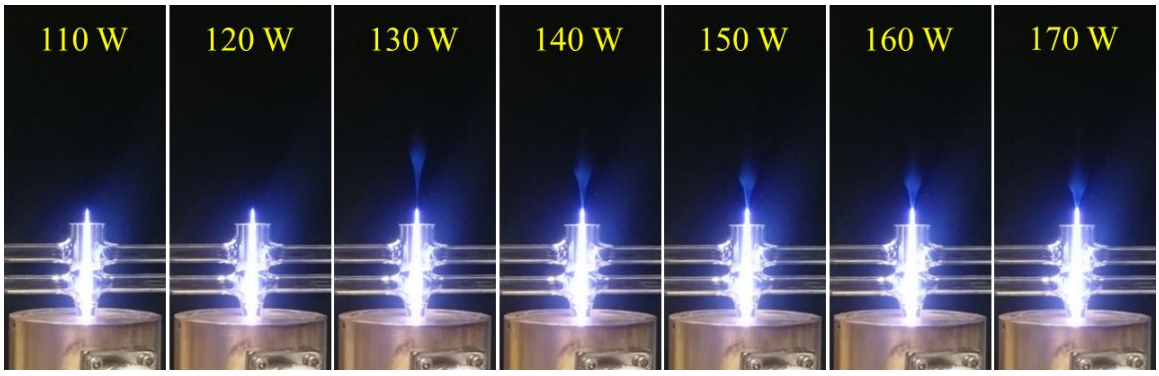

Figure 5.2 Images showing effect of plasma power on flame structure

The plasma feed gas flow rate was kept constant at 0.84 slm, the fuel equivalence ratio at 0.8 and total methane/air mixture flow rate was kept constant at 2.0 slm

Figure 5.3 above shows the effect of varying the plasma power and fuel equivalence ratio on the flame geometry. The argon plasma feed gas flow rate was fixed at 0.84 slm to ensure the generation of a stable plasma while the fuel equivalence ratio was fixed at 0.8 and the total methane/air flow rate fixed at 2.0 slm. Increasing the plasma power resulted in ignition at a plasma power of 130 W and improved tethering of flame produced. A blue inverted conical flame anchored to the plasma column was observed outside the flame when the plasma was turned on. Increasing the plasma power resulted a shortening of the flame waist and increased stabilization of the flame. It is suggested that the increased stability with increase in plasma power is due to the increase in the radical pool generated by the plasma. The presence of the larger radical pool and thermal energy due to the increase in plasma power enhances the flame speed which improves on flame holding. This is supported by the reports of Zaidi *et al.* [25] who measured the enhancement of flame speeds in hydrocarbon flames and observed an increase in flame speeds with the coupling of a microwave plasma into the reaction zone. It was inferred from the observations made that an increase in the coupling efficiency, or higher microwave powers resulted in a higher degree of enhancement. Rao *et al.* [26] also reported an increase in flame speed with increase in plasma power. A similar increase in flame speed and flame tethering with increase in plasma power was reported for the microwave plasma assisted ignition and flameholding of ethylene/air mixtures [4].

5.3.2 Emission spectra

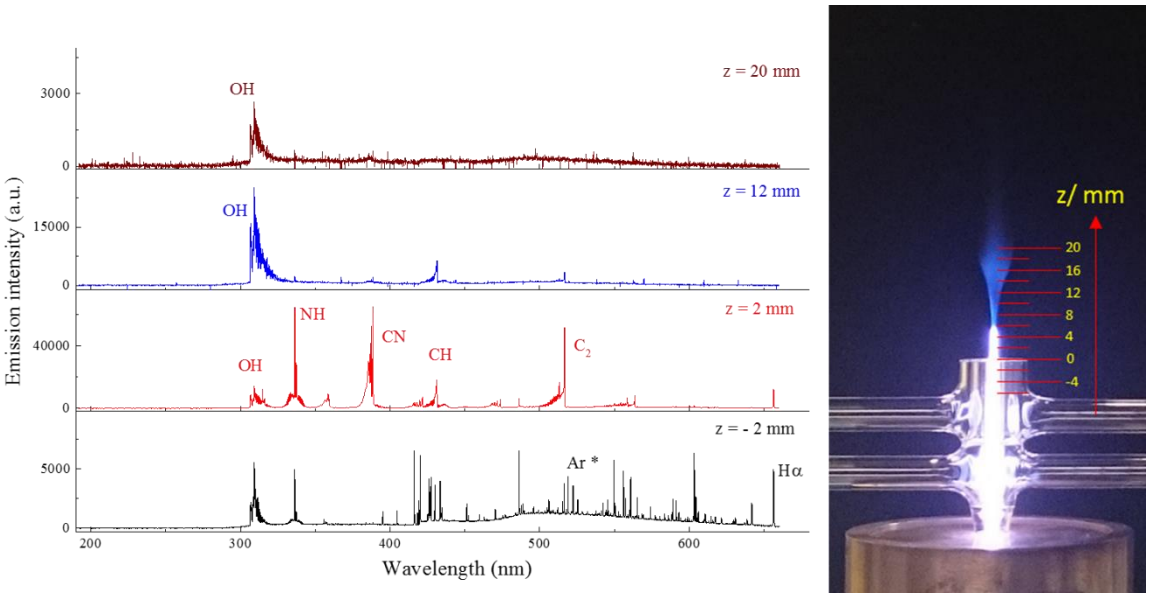

Figure 5.3 Emission spectra obtained spatially at four different locations in PAC flame

Emission spectra obtained spatially at 4 different locations in the plasma assisted combustion reactor. The plasma power was fixed at 150 W, the plasma feed gas flow rate at 0.84 slm, the fuel equivalence ratio at 0.8 and the total methane/air flow rate at 2.0 slm

Optical emissions were obtained spatially along the propagation axis of the plasma assisted combustion reactor. Ten spectra were obtained and averaged at each spatial location to improve on the signal to noise ratio. The spectrometer integration time used was varied spatially along the propagation axis of the combustion reactor due to the change in emission intensity along the propagation axis during the plasma assisted oxidation of the methane. The integration time used in the plasma zone ($z < 0$ mm) was 400 ms, while 20 ms was used in the hybrid/ignition region ($0 \text{ mm} < z < 6$ mm) where the plasma interacted with the premixed methane/air mixture and 40 s was used in the flame zone ($z > 6$ mm) downstream of the flow. It was observed that in the plasma zone as shown at position z = - 2 mm in figure 5.3, the emission spectrum featured emissions

from the electronic systems of OH($A^2\Sigma^+$–$X^2\Pi_{3/2}$)(0–0), NH($A^3\Pi$-$X^3\Sigma^-$)(0–0) along with atomic H_α and excited Ar* atoms. The OH(A) and NH(A) observed at this location are from the collisional dissociation, electronic impact dissociation and recombination reactions of H_2O and N_2 impurities present in the argon plasma feed gas [15], [18], [22]. Outside the combustor orifice, in the hybrid plasma flame zone where the plasma is coupled with the surrounding premixed methane/air coflow, the emission spectra in this region featured emissions from the electronic systems of CN($B^2\Sigma^+$-$X^2\Sigma^+$)(0–0), CH($A^2\Delta$-$X^2\Pi$)(0–0), and C_2($d^3\Pi_g$-$a^3\Pi_u$)(0–0) in addition to the OH($A^2\Sigma^+$–$X^2\Pi_{3/2}$)(0–0), NH($A^3\Pi$-$X^3\Sigma^-$)(0–0),, and H_α observed in the plasma zone. This species were the byproducts generated from further chain branching and recombination reactions as a result of the ignition of the incoming premixed methane/air mixture by the plasma. This species observed are short-lived and are quickly consumed by the ongoing fuel oxidation downstream of the flow with only emissions from OH($A^2\Sigma^+$–$X^2\Pi_{3/2}$)(0–0) observed at z = 20 mm.

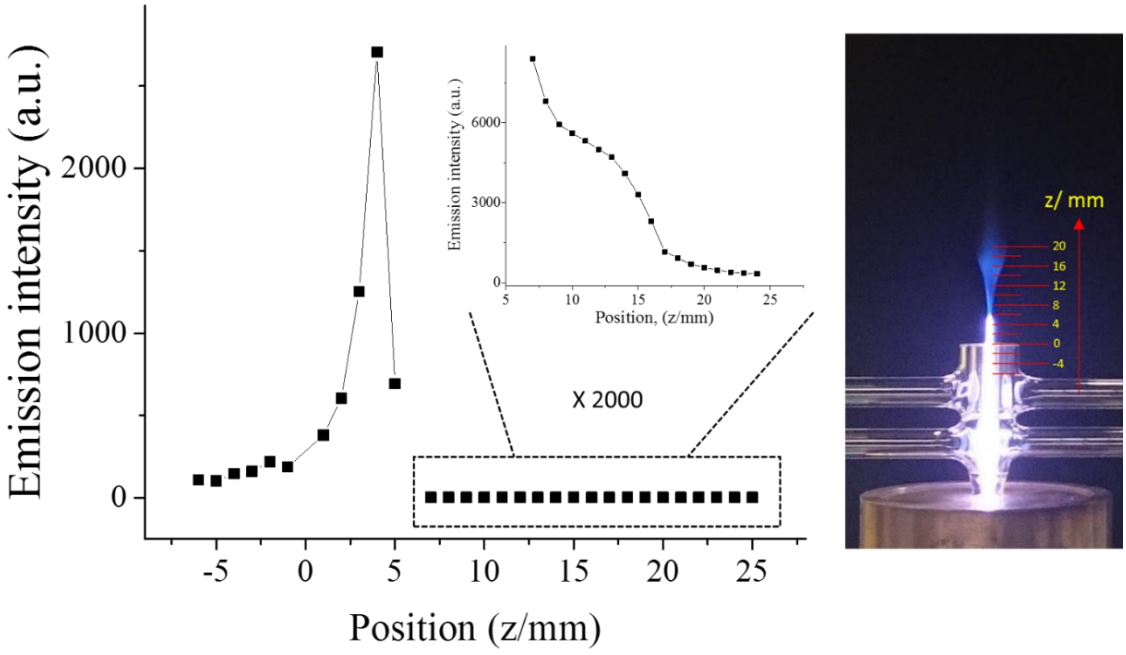

Figure 5.4 Emission intensity profile for OH(A) obtained along flame axis

Emission intensity profile for OH(A) obtained along flame axis for integration times of 20 ms and 40s. Experimental parameters were fixed with a plasma power of 150 W, fuel equivalence ratio of 0.8, total flow rate of 2.0 slm and argon flow rate of 0.84 slm

By obtaining the spatially resolved emission spectra along the propagation axis of the flame, we obtained the emission profile of OH(A) as shown in figure 5.4. Due to the weak emission intensity in the flame zone, the integration time was increased from 20 ms to 40 s. OH(A) was observed to be almost constant in the plasma zone but upon transitioning to the hybrid plasma-flame zone, the OH(A) emission intensity increased exponentially reaching a maximum at z = 4 mm. Beyond this point, the OH(A) emission intensity steadily decreased downstream of the flame region.

The spatially resolved emission intensity profile obtained for OH is attributed to the flow dynamics outside the combustor with the peak in OH(A) employed as the

criteria for ignition as defined by Nagaraja *et al.*[11] during their investigation of the ignition of hydrogen air mixtures using a pulsed nanosecond dielectric barrier plasma discharge in plane-to-plane geometry. Outside the combustor, the plasma channel is initially laminar spreading out downstream of the flow as the argon gas mixes with the surrounding methane/air coflow. The mixing results in the entrainment of the premixed methane/air coflow improving coupling of the plasma to the methane/air coflow. This entrainment of the methane/air coflow results in the creation of an inner radically rich flame thus the observed peak in OH(A) intensity in this region. This inner radically rich flame preheats, ignites and stabilizes the coflow as seen by the spreading out of the flame into the conicnal shape observed in section 3.1. The ignition of the secondary coflow results in the creation of the secondary weaker peak in the emission intensity profile of the OH(A) profile as shown in figure 5.4. The subsequent drop in OH(A) emission intensity downstream of the flame is due to the loss mechanisms from chain termination reactions, convection and diffusion losses to the environment outweighing the creation mechanisms for OH(A). The creation of the radically rich inner flame which ignites and stabilizes the coflow was also reported by Kim *et al.*[27] while using an ultra-short repetitively pulsed discharge to stabilize a premixed methane air flame. They observed a cold inner flame with an abundance of OH radicals which had an unusually high vibrational temperature and low rotational temperature when compared with OH found in conventional lean premixed flames. From that study, they concluded that the OH may be important in igniting the surrounding combustible mixture. Also in our previous study [4] investigating the effects of a microwave plasma in the flameholding of a premixed

ethylene/air mixture, it was observed that flameholding was achieved by the creation of an inner radically rich flame which ignites and stabilizes the surrounding coflow.

5.3.3 Rotational temperature

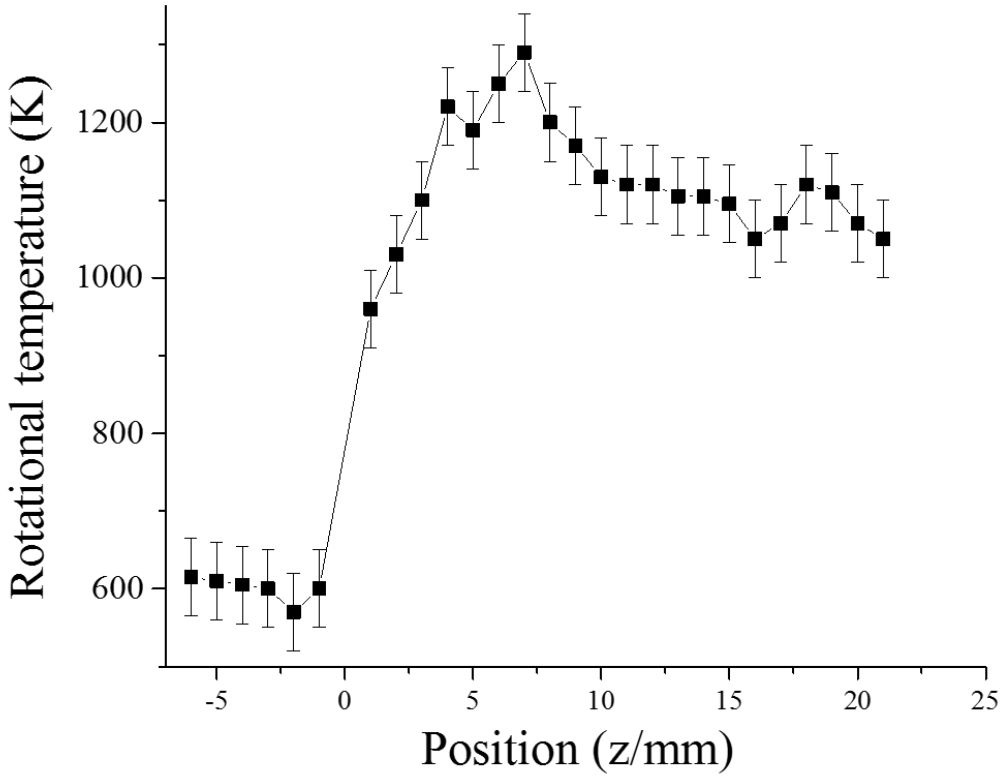

Figure 5.5 Rotational temperature profile obtained along propagation axis of PAC flame

Figure 5.5 shows the rotational temperature which was obtained by matching the relative intensities of the R and P branches from the experimentally obtained emission spectra of OH(A) to a simulated spectra from Specair [28]. The experimental parameters were fixed with a plasma power of 150 W, a plasma argon feed gas flow rate of 0.84 slm, a total flow rate of the fuel/air mixture of 2.0 slm and a fuel equivalence ratio of 0.8 during the study. The rotational temperature was observed to be constant around 600 K in

the plasma zone z < 0 mm. Outside the combustor orifice, the rotational temperature increase significantly to 960 K at x = 1 mm before peaking at 1290 K downstream of the flow at x = 7 mm from whence it is observed to fall downstream. The rotational temperature profile shown in figure 5.5 is attributed to the fluid dynamics in the combustor, whereby the gradual increase in turbulence in the plasma channel results in progressive entrainment of the premixed fuel/air mixture resulting in its ignition. The temperature hike observed outside the combustor orifice at z = 01 mm is due to exothermic reactions stemming from the pre-ignition and oxidation of the premixed methane/air coflow. The continuous increase in the rotational temperature outside the combustor is attributed to the improved degree of mixing between the plasma gas and the surrounding premixed fuel/air coflow. This improved mixing allows for preheating of the surrounding coflow and its interaction with the plasma generated radicals resulting in the ignition of a larger percentage of the coflow. Complete mixing between the argon plasma and surrounding coflow occurs at the tip of the plasma plume at which point ignition of the coflow is achieved and the flame is observed to be anchored. Beyond this ignition point, the rotational temperature is observed to drop as the loss processes from convection and radiation outweigh the heat generation processes.

5.3.4 Ground State OH(X) measurements

Absolute OH(X) number density profile along the propagation axis of the premixed methane/air flame was obtained via cavity ringdown spectroscopy. This is the first time cavity ringdown spectroscopy has been employed to measure the ground state OH(X) number densities in the ignition zone of an argon plasma assisted methane/air mixture. The OH(X) number densities were obtained at a spatial resolution of 1 mm

along the flame axis. Initially, a section of the OH(A-X)(0-0) absorption spectrum was obtained by CRDS at a low resolution of 0.003 nm near the 308 nm band with the rotationally resoled spectra obtained assigned through comparisons with a simulated spectra from LIFBASE [29].

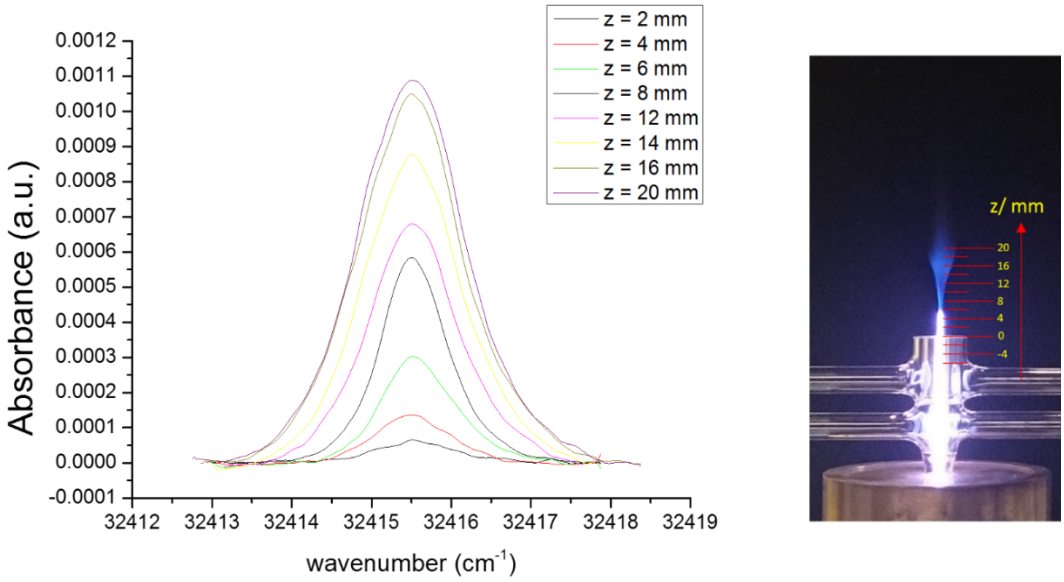

Figure 5.6 Spatially resolved CRDS measured line shapes of the $R_2(1)$ line of the OH(A-X)(0-0) band. Ten point averaging was used

The OH(X) number density was determined from $R_2(1)$ line. The $R_2(1)$ line was chosen since it has no spectra overlap with other rotational lines. The OH(X) number densities were calculated from the absorption spectra obtained using the formula,

$$\text{Absorbance} = Snl = \int_{\nu} \frac{d}{c}\left(\frac{1}{\tau^{f}(\nu)} - \frac{1}{\tau_0^{f}}\right) d\nu \qquad (4.1)$$

where n is the OH(X) number density in the initial state of the $R_2(1)$ transition; and are the ringdown times measured in the plasma-assisted combustion flames with the laser wavelength tuned onto and off the absorption peak, respectively; c is the speed of

light; l and d are the laser beam path-length and the ringdown cavity length respectively. S(T) is the temperature-dependent line intensity and is calculated from Equation (2) [30]

$$S(T) = 3.721963 \times 10^{-20} \frac{T_{trans}}{273.16} \frac{1}{8\pi c v^2} \left(\frac{N}{P}\right) \left(\frac{e^{-1.4388E''/T_r}}{Q_{VR}}\right) A_{v''J''}^{v'J'} (2J' + 1)\left(1 - e^{-1.4388v/T_v}\right) \quad (4.2)$$

where ν is the transition frequency of the OH $R_2(1)$ line of 32415.452 cm^{-1}, T is the temperature in Kelvin, N is the total number density (molecule cm^{-3}) at pressure P (atm) and temperature T, E″ is the lower state energy, i.e. 126.449 cm^{-1}, is the Einstein coefficient in s^{-1}, and Q_{VR} is the vibrational rotational partition function with V and J vibrational and rotational quantum numbers, respectively. The temperature-dependent line intensities S(T) was calculated from temperatures determined by the spectra simulations using Specair [31].

Table 5.1 Cavity ringdown spectroscopy of OH(X) number densities in the PAC reactor

Position (z /mm)	*Flame temperature obtained from simulation (K)*	*Line intensity (S) of the $R_2(1)$ line (x 10^{-18} cm/ molecule)*	*Path length (mm)*	*Integrated Absorbance (x 10^{-4} cm^{-1})*	*OH number density (V" = 0, J" = 0.5) (x 10^{15} molecule cm^{-3})*
1	960	3.63	1.60	0.78	0.14
2	1030	3.41	1.60	0.66	0.12
3	1100	3.21	1.53	0.81	0.16
4	1220	2.92	1.47	1.40	0.33
5	1190	2.99	1.20	2.56	0.71
6	1250	2.85	0.93	3.05	1.15
7	1290	2.77	1.00	4.55	1.64
8	1200	2.96	1.07	5.87	1.86
9	1170	3.04	1.40	6.29	1.48
10	1130	3.14	1.73	6.03	1.11
11	1120	3.16	2.00	6.28	0.99
12	1120	3.16	2.27	6.86	0.96
13	1105	3.20	2.73	7.87	0.90
14	1105	3.20	3.20	8.83	0.86
15	1095	3.23	3.87	9.61	0.77
16	1050	3.35	4.53	10.60	0.70
17	1070	3.30	5.00	10.80	0.66
18	1120	3.16	5.47	11.00	0.64
19	1110	3.19	5.40	11.20	0.65
20	1070	3.30	5.33	11.00	0.63

Table 1 shows the spatially resolved OH(X) number densities calculated from the absorbance measured at a spatial resolution of 1 mm outside the combustor orifice. The uncertainty in the OH(X) number densities reported can be estimated by from the measurements errors in the gas temperature and from the estimation of the laser beam path length. The temperature sensitivity was 5% per 100 K at 2000 K of the OH A-X (0-0) $R_2(1)$ line. The laser path length in the PAC flame was determined from images and had an error of 0.5 mm accounting for a maximum error of 53 % at z = 6 mm and a minimum error of 9 % at z = 18 mm. Therefore the total uncertainty in the OH(X) number densities ranged from 14% to 58%.

The OH(X) number densities were of the order of 10^{15} molecules/cm^3. The OH(X) number densities were observed to increase downstream of the plasma assisted combustion flame, reaching a peak of 1.86 x 10^{15} molecules/cm^3 at z = 8mm downstream before falling downstream of the flame.

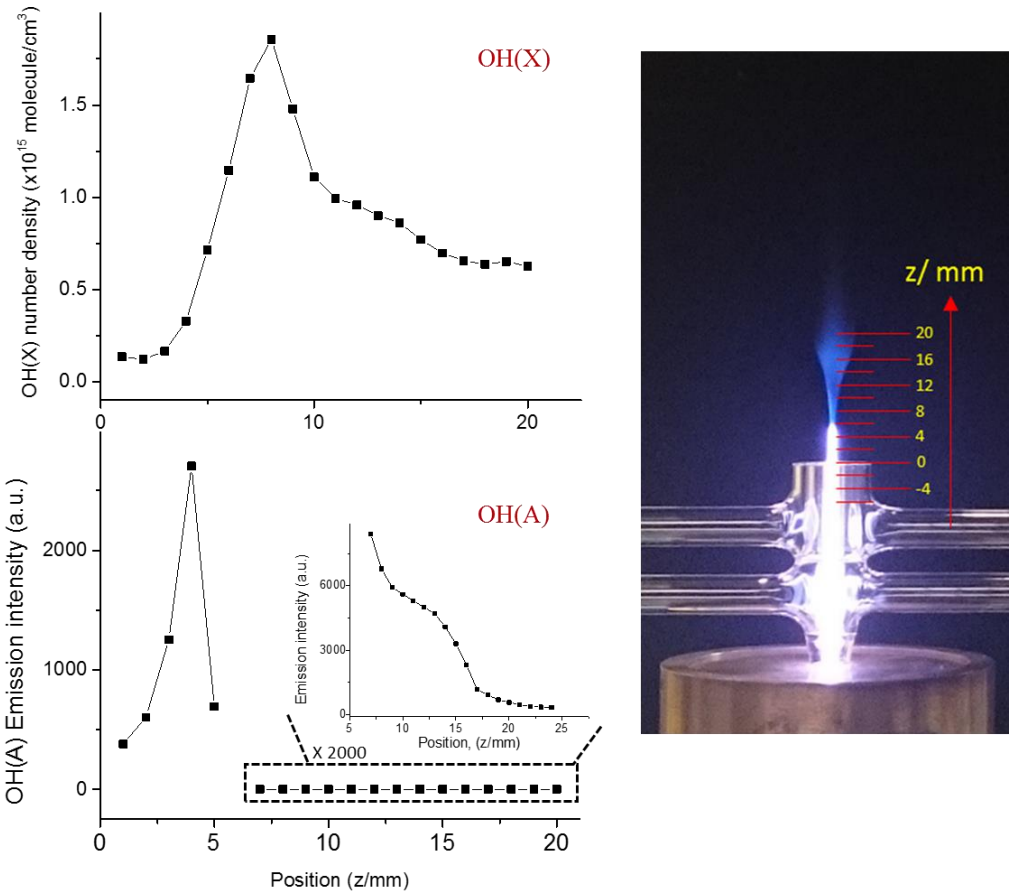

Figure 5.7 OH(X) number density profile measured from the ignition zone to downstream of the flame zone. The experimental conditions were fixed with the plasma

Figure 5.7 shows the spatially resolved emission intensity profiles of excited state OH(A) and the ground state OH(X) number density profile obtained in the flame zone. The coupling of the plasma to the premixed methane/air mixture results in a peak and

secondary bump in both the OH(A) emission intensity profile and OH(X) number density profile. However, the primary peak in OH(A) emission intensity occurs at z = 4 mm along the propagation axis whereas OH(X) number densities were observed to peak further downstream at a spatial location of z = 8 mm. The secondary bumps in the emission intensity profile of OH(A) and number density profile for OH(X) both match up in the range 10 mm < z < 17 mm. It is thus suggested that the initial peak in OH(A) emission intensities before subsequent peak in OH(X) emission intensities is due to OH(A) playing a more active role during the ignition of the methane/air mixture whereas OH(X) plays a more active role in the flameholding. Leonov *et al.* [32] while studying the mechanism of flameholding in a plasma assisted supersonic combustor observed a two zone mechanism of flame holding. In that study, fuel conversion occurs in zone one and combustion is completed in zone two. Hence it is inferred in this study that the initial peak in OH(A) and subsequent peak in OH(X) is due to the fact that OH(A) plays a more important role in the ignition of the methane/air mixture while OH(X) peaking downstream is more involved with flameholding. A similar observation was made by Wang *et al.*[33] when they developed a microwave plasma assisted combustion platform to study the role of the plasma on the combustion process. They proposed in that study based on the rate of consumption of the OH(A) and OH(X) states that excited state OH played a more important role in ignition while ground state species played a more important role in flameholding. Both emission intensity profiles for OH(A) and number density profile for OH(X) are observed to drop downstream thus indicating the loss mechanism through chain termination and diffusion outweigh OH(A,X) creation mechanisms downstream of the flame.

5.4 Summary

In this study, the effect of a microwave argon plasma on the plasma assisted combustion of a premixed methane/air mixture is performed in a novel coaxial flow combustor. A blue inverted cone shaped PAC flame was obtained and it was observed that increasing the plasma power resulted in improved flameholding of the flame. The spatially resolved emission spectra were obtained with three main reaction zones identified. The spatially resolved rotational temperature was also obtained from comparing an experimentally obtained emission spectrum of OH(A) to a simulated spectrum using Specair. The temperature profile exhibited a peak of 1290 K at z = 7 mm. Cavity ringdown spectroscopy which is a very sensitive multi-pass absorption spectroscopic technique was employed to measure the OH(X) number densities for the first time in the hybrid zone of the argon microwave generated plasma of a premixed methane/air mixture due to the novel coaxial combustor employed. The OH(X) number density reported was of the order of 10^{15} molecules cm^{-3} and exhibited a dual peak nature with a pronounced primary peak of 1.8 x 10^{15} molecules/cm^3 at z = 8 mm and a less pronounced secondary peak downstream. Comparison between the OH(A) emission intensity profile and the OH(X) number densities profile showed that OH(A) emission intensity peaking earlier at z = 4 mm while the ground state number density peaks much later at z = 8 mm. This representation of both ground state and excited states provides a complete picture of the evolution of this specie in the ignition zone and further sheds light into the interaction mechanisms influencing the plasma enhancements of a premixed methane/air combustion. Inferring from the images obtained, the relative peaks in the emission intensities of OH(A), number densities of OH(X) and the rotational temperature

profile, the results further buttress the hypothesis that OH(A) is more involved in the ignition process while OH(X) plays a more important role in the flameholding.

5.5 References

1. J. B. Liu, J. Sinibaldi, C. Brophy, A. Kuthi, C. Jiang, P. Ronney, and M. A. Gundersen, 2005 "Transient plasma ignition of quiescent and flowing air/fuel mixtures," *IEEE Trans. Plasma Sci*., **33**, 844–849

2. N. Chintala, A. Bao, G. Lou, and I. V. Adamovich, 2006 "Measurements of combustion efficiency in nonequilibrium RF plasma-ignited flows," Combust. Flame, **144**, 744–756

3. C. U. Bang, Y. C. Hong, S. C. Cho, H. S. Uhm, S. Member, and W. J. Yi, 2006 "Methane-Augmented Microwave Plasma Burner," **34**, 1751–1756

4. C. A. Fuh, W. Wu, and C. Wang, 2016 "Microwave plasma-assisted ignition and flameholding in premixed ethylene/air mixtures," *J. Phys. D. Appl. Phys.*, **49**, 285202

5. K. V Savelkin, D. A Yarantsev, I. V Adamovich, and S. B. Leonov, 2015 "Ignition and flameholding in a supersonic combustor by an electrical discharge combined with a fuel injector," *Combust. Flame*, **162**, 825–835

6. I. V Adamovich, I. Choi, N. Jiang, J.-H. Kim, S. Keshav, W. R. Lempert, E. Mintusov, M. Nishihara, M. Samimy, and M. Uddi, 2009 "Plasma assisted ignition and high-speed flow control: non-thermal and thermal effects," *Plasma Sources Sci. Technol.,* **18**, 34018

7. N. Aleksandrov, 2014 "Kinetics of low-temperature plasmas for plasma-assisted combustion and aerodynamics," *Sources Sci.*, **23**, 15017

8. I N Kosarev, G V Ivanov, S V Kindysheva, P V Sagulenko, N L Aleksandrov, S M Starikovskaia, A Yu Starikovskii., 2008 "Measurement of intermediates in the process of plasma assisted ignition," *17th International Conference on Gas Discharges and Their Applications*, Cardiff, 2008, pp. 621-624.

9. Z. Yin, I. V. Adamovich, and W. R. Lempert, 2013 "OH radical and temperature measurements during ignition of H2-air mixtures excited by a repetitively pulsed nanosecond discharge," *Proc. Combust. Inst.,* 34, 3249–3258

10. T. Ombrello, X. Qin, Y. Ju, A. Gutsol, A. Fridman, and C. Carter, 2006 "Combustion Enhancement via Stabilized Piecewise Nonequilibrium Gliding Arc Plasma Discharge," *AIAA J*., **44**, 142–150

11. S. Nagaraja, V. Yang, Z. Yin, and I. Adamovich, "Ignition of hydrogen-air mixtures using pulsed nanosecond dielectric barrier plasma discharges in plane-to-plane geometry," Combust. Flame, **161**, 1026–1037, 2014

12. C. Wang, N. Srivastava, and T. S. Dibble, 2009 "Observation and quantification of OH radicals in the far downstream part of an atmospheric microwave plasma jet using cavity ringdown spectroscopy," *Appl. Phys. Lett.*, 95, 51501

13. N. Srivastava and C. Wang, 2011 "Determination of OH Radicals in an Atmospheric Pressure Helium Microwave Plasma Jet," *Plasma Sci. IEEE Trans.*, **39**, 918–924

14. N. Srivastava and C. Wang, 2011 "Effects of water addition on OH radical generation and plasma properties in an atmospheric argon microwave plasma jet," *J. Appl. Phys.,* **110**, 53304

15. C. A. Fuh, S. M. Clark, W. Wu, and C. Wang, 2016 "Electronic ground state OH(X) radical in a low-temperature atmospheric pressure plasma jet," *J. Appl. Phys.,* **120**, 163303

16. C. Wang, W. Wu, and P. Sahay, "Simultaneous measurements of OH (A) and OH (X) radicals toward understanding of plasma-assisted combustion (PAC)," 2012.

17. C. A. Fuh, W. Wu, and C. Wang, 2014 "Effects of a microwave induced argon plasma jet on premixed and nonpremixed methane/air mixtures," in *45th AIAA Plasmadynamics and Lasers Conference*, , 2240

18. W. Wu, C. A. Fuh, and C. Wang, 2015 "Plasma-Enhanced Ignition and Flame Stabilization in Microwave Plasma-Assisted Combustion of Premixed Methane/Oxygen/Argon Mixtures," *IEEE Trans. Plasma Sci*., **43**, 3986–3994

19. W. Wu, C. A. Fuh, and C. Wang, "Two dimensional OH radical measurements in argon plasma-assisted combustion flame of premixed and nonpremixed methane/air mixtures using cavity ringdown spectroscopy," in *45th AIAA Plasmadynamics and Lasers Conference*, 2014,.

20. N. Srivastava and C. Wang, 2011 "Effects of water addition on OH radical generation and plasma properties in an atmospheric argon microwave plasma jet," *J. Appl. Phys.*, **110**, 53304

21. C. Wang, N. Srivastava, and T. S. Dibble, 2009 “Observation and quantification of OH radicals in the far downstream part of an atmospheric microwave plasma jet using cavity ringdown spectroscopy,” *Appl. Phys. Lett*., **95**, 51501

22. C. Wang, N. Srivastava, S. Scherrer, P.R. Jang, T. S. Dibble, and Y. Duan, 2009 “Optical diagnostics of a low power—low gas flow rates atmospheric-pressure argon plasma created by a microwave plasma torch,” *Plasma Sources Sci. Technol.*, 18, 25030

23. C. Wang 2007 “Plasma-cavity ringdown spectroscopy (P-CRDS) for elemental and isotopic measurements,” *J. Anal. At. Spectro*, **22**, 1347–63

24. C. Wang and W. Wu, 2014 “Roles of the state-resolved OH(A) and OH(X) radicals in microwave plasma assisted combustion of premixed methane/air: An exploratory study,” *Combust. Flame*, **161**, 2073–2084,

25. S. H. Zaidi, E. Stockman, X. Qin, Z. Zhao, S. Macheret, Y. Ju, R. B. Miles, D. J. Sullivan, and J. F. Kline, “Measurements of Hydrocarbon Flame Speed Enhancement in High-Q Microwave Cavity,” *44th AIAA Aerospace Sciences Meeting and Exhibit,* 2006, p. 1217.

26. X. Rao, K. Hemawan, I. Wichman, C. Carter, T. Grotjohn, J. Asmussen, and T. Lee, 2011 “Combustion dynamics for energetically enhanced flames using direct microwave energy coupling,” *Proc. Combust. Inst*., **33**, 3233–3240

27. W. Kim, H. Do, M. G. Mungal, and M. A. Cappelli, 2006 “Flame Stabilization Enhancement and NOx Production using Ultra Short Repetitively Pulsed Plasma Discharges,” 1–13.

28. C. O. Laux, T. G. Spence, C. H. Kruger, and R. N. Zare, 2003 “Optical diagnostics of atmospheric pressure air plasmas,” *Plasma Sources Sci. Technol.*, **12**, 125–138

29. J. Luque and D. R. Crosley, “‘LIFBASE: Database and spectral simulation (version 1.5)’, SRI International Report MP 99-009 (1999).”

30. A. Goldman and J. R. Gillis, “Spectral line parameters for the $A^2\sum$-$X^2\Pi(0,0)$ band of OH for atmospheric and high temperatures,” *Journal Quant. Spectrosc. Radiat. Transf*., 25, 2, 111–135, 1981.

31. T. G. S. C. H. K. C O Laux and R. N. Zare, 2003 “Optical diagnostics of atmospheric pressure air plasmas,” Plasma Sources Sci. Technol., **12**, 125-138,.

32. S. Leonov, V. Sabelnikov, A. Vincent-randonnier, and A. Firsov, "Mechanism of flameholding in plasma- assisted supersonic combustor," pp. 1–10.

33. C. Wang and W. Wu, 2014 "Roles of the state-resolved OH (A) and OH (X) radicals in microwave plasma assisted combustion of premixed methane/air: An exploratory study," *Combust. Flame*, 1–12

34. A. Dutta, Z. Yin, and I. V. Adamovich, "Cavity ignition and flameholding of ethylene-air and hydrogen-air flows by a repetitively pulsed nanosecond discharge," *Combust. Flame*, 158, 1564–1576

CHAPTER VI

SUMMARY AND RECOMMENDATION OF FUTURE WORK

In this chapter, a summary for the experiments performed, in a bid to elucidate the role played by a microwave argon plasma on the combustion of several fuel/air mixtures was investigated and reported. Recommendations for future studies to continue reducing the knowledge gap in our current understanding of plasma assisted combustion are presented.

6.1 Research summary

Plasma assisted combustion refers to the coupling of a plasma to a fuel/air mixture in a bid to enhance the combustion process. Several researchers have reported on the positive effects the addition of a plasma can have on oxidation of fuels such as improved flameholding and stabilization [1]–[5], reduction in ignition delay time [6]–[8], reduced pollutant emissions [9]–[11]etc. Despite all of these positive enhancement effects being reported, the mechanism through which plasma assisted combustion is brought about is still poorly understood. Hence in this study, a number of experiments are performed in order to narrow the knowledge gap existing in our current understanding of plasma assisted combustion. Initially, the effect of a microwave argon plasma on the ignition and flameholding of ethylene/air mixtures was investigated. The vertical arm of a cross shaped quartz combustor is inserted into a microwave resonant cavity. Argon flowing in this vertical arm was ionized into a plasma and was coupled to a premixed

ethylene/air mixture flowing in the horizontal arms. A minimum ignition plasma power vs. fuel equivalence ratio study was performed and a suite of optical diagnostic techniques were employed to probe the ensuing PAC flame. It was concluded from that study that ultra-lean fuel equivalence ratios were more susceptible to heat losses from the environment while lean to rich fuel equivalence ratios were more susceptible to the mixing scheme. Improved ignition and flameholding were also reported with an increase in plasma power. From the data collected from the imaging systems, optical emissions spectroscopy and cavity ringdown spectroscopy it was suggested in that study that the plasma enhanced ignition and combustion of ethylene/air mixtures was achieved in two stages with the creation of a radically rich inner flame which ignites and stabilizes the surrounding coflow. From that study, and armed with data reported in the literature pertaining to the investigation of the effect of plasmas on combustion enhancement [12], [13], it was observed that plasma enhancement of the combustion process is brought about by interwoven complex processes arising from the physical and kinetic processes occurring during the coupling of the plasma to the fuel/air mixture. Decoupling these interwoven processes and studying them separately is the key to understanding plasma assisted combustion. Hence, a new combustor platform was designed aimed at discriminating between the various enhancement pathways through which the plasma enhances the combustion process. This was done by initially physically separating the plasma, the oxidant and the fuel and systematically coupling them to each other. The combustor was made from a double crossed quartz tube with the vertical arm of the quartz tube inserted in to a microwave resonant cavity and conveyed the argon plasma. The two horizontal arms were used to conduct either the oxidizer, fuel or a mixture of

both. In order to test the versatility of the newly developed platform to discriminate between the various enhancement pathways, the platform was run in three different operation schemes with the same experimental parameters. In Scheme I, the argon plasma flowing in the vertical arm was coupled to the premixed methane/air mixture flowing in the lower two horizontal arms while the top horizontal arms were closed. In Scheme II, the argon plasma flowing in the vertical arm was first coupled to the air stream in the lower horizontal arms. The activated air flow was subsequently coupled to the fuel stream in the uppermost horizontal arms. In Scheme III, the argon plasma was initially coupled to the fuel flow in the lower horizontal arms before being subsequently coupled to the oxidizer stream. Different flame structures, emissions features and different rotational temperature profiles were obtained in all three operational schemes even though the experimental parameters (argon flow rate, fuel equivalence ratio, plasma power and total fuel/air mixture flow rate) were kept constant in all three schemes. These results thus demonstrated the versatility of the newly developed PAC platform to discriminate between the various enhancement mechanisms. Using the newly developed PAC platform, a comparative study on the effects of a microwave plasma activated methane vs. plasma activated air in the PAC of a non-premixed methane/air mixture was carried out. The relationship between the minimum ignition plasma power required for ignition and fuel equivalence ratio was investigated where it was observed that the plasma power required for ignition was independent of the fuel equivalence ratio when the oxidizer was activated. Whereas, the reported U shaped minimum ignition plasma power vs fuel equivalence ratio curve was obtained when a premixed fuel/air mixture was coupled to the plasma. Activating the fuel, first resulted in an increase in minimum required plasma

power for ignition with increase in fuel/equivalence ratio. Based on the results from the minimum ignition plasma power required for ignition investigation, images of the PAC flame structures, optical emission spectra, and rotational temperature profiles, it was inferred that there exists a critical radical pool size that must be established by the plasma for ignition to occur. Reactive oxygen and nitrogen species were identified to be the most important species in the radical pool and played a more important role in the observed plasma assisted ignition and enhancement effects.

The lack of accurate experimental data to validate theoretical mechanisms is one of the major roadblocks hindering the understanding of PAC [14]. Current techniques for measuring the absolute number density of ground state species are laser induced fluorescence(LIF) and single pass absorption spectroscopy. However, this techniques are plagued by several drawbacks for example, LIF requires calibration and is often plagued by collisional quenching whereas single pass absorption spectroscopy, is not very sensitive due to its single pass nature. Seeing this shortfall, a new combustor design was proposed which will allow for the probing of the hybrid zone, (region where the plasma is coupled to the fuel/air mixture) for the first time with a cavity ringdown laser permitting the measurement of absolute concentrations of ground state number densities of important transient species during the plasma enhancement process by cavity ringdown spectroscopy. The combustor employed was made up of a double cross shaped quartz tube whose nozzle was made up of three concentric cylinders. Argon was conveyed through the vertical arm, which was inserted into a microwave resonant cavity to generate a plasma plume flowing in the inner most cylinder. The lower and upper horizontal arms were used to convey a premixed mixture of the methane and air which flowed coaxially

to the plasma plume. The third coaxial cylinder was shut off. Cavity ringdown spectroscopy (CRDS) is a very sensitive multi-pass absorption technique requiring no calibration. Cavity ringdown spectroscopy is an absorption spectroscopic technique whereby a beam of light is trapped between two highly reflective mirrors, causing the laser beam to undergo more than a hundred thousand reflections before decaying. A plot of the intensity of the laser beam with time results in an exponential decay time with a characteristic time constant or ringdown time which is related to the losses at the mirror surface and the inherent losses in the cavity. Introducing an absorbing sample in the ringdown cavity results in a new ringdown time and the concentrations of the absorbing sample can be obtained by comparing the two ringdown times (with and without a sample present). Due to its multi-pass nature, the effective path length of the laser in the sample is increased by almost ten thousand fold resulting in a very sensitive absorption technique. Ringdown spectroscopy was first proposed by A. O'keefe et al. [15] in 1988 inspired by an earlier idea of J. M. Herbelin et al. [16] in 1981. The information obtained from being able to accurately quantify the presence of ground state species in the hybrid zone will allow for fine tuning of current reaction mechanisms thus furthering the understanding of PAC. The ground state number density of OH(X) radical was measured in the microwave plasma assisted combustion of a premixed methane/air mixture. In this study, the effect of the plasma power on flame geometry was reported and the spatially resolved emission spectra and rotational temperatures were also reported along with the spatially resolved OH(X) number densities. The OH(X) number densities reported were of the order 10^{15} molecules/cm^3. The OH(A) and OH(X) number densities were compared in the plasma assisted combustion of the methane/air mixture thus giving the

complete picture of the behavior of the excited and ground state radicals of OH in the plasma assisted combustion process. The OH(X) number densities reported is the first step in providing more accurate experimental data indispensable in the fine tuning of current kinetic mechanisms.

6.2 Recommendation for future work

Much still remains to be done in order to further narrow and eventually close the knowledge gaps in the current understanding of plasma assisted combustion. Using the newly designed combustor to measure the number densities of other reactive species will provide much needed accurate experimental data to fine tune and propose new kinetic mechanisms. The design of kinetic mechanisms to account for the experimentally reported enhancement effects and data collected is still an ongoing task.

Furthermore, detailed kinetics taking into consideration the role of the different modes of internal excitation (rotational, vibrational, and electronic excitation) of atoms and molecules in plasma assisted ignition and combustion still have to be addressed. Other challenges still plaguing the field of plasma assisted combustion are further enumerated in Refs [11].

6.3 References

1. K. V. Savelkin, D. A. Yarantsev, I. V. Adamovich, and S. B. Leonov, 2014 “Ignition and flameholding in a supersonic combustor by an electrical discharge combined with a fuel injector,” *Combust. Flame*, 1–24

2. A Dutta, I. Choi, M. Uddi, E. Mintusov, A. Erofeev, and Z. Yin, 2009 “Cavity Flow Ignition and Flameholding in Ethylene-Air by a Repetitively Pulsed Nanosecond Discharge 1,” 1–19

3. S. Leonov, V. Sabelnikov, A. Vincent-Randonnier, A. Firsov, and D. Yarantsev, 2014 “Mechanism of flameholding in plasmaassisted supersonic combustor,” *29th Congr. Int. Counc. Aeronaut. Sci.* ICAS 2014,

4. J. Votano, M. Parham, and L. Hall, 2004 “Plasma Assisted Combustion and Flameholding in High Speed Cavity Flows,” Chem, 621–624

5. M. G. De Giorgi, A. Sciolti, S. Campilongo, E. Pescini, A. Ficarella, S. Lovascio, and G. Dilecce, 2016 “Lean Blowout Sensing and Plasma Actuation of Non-Premixed Flames,” *IEEE Sens. J.*, **16**, 3896–3903

6. S. A. Bozhenkov, S. M. Starikovskaia, and A. Y. Starikovskii, 2003 “Nanosecond gas discharge ignition of H_2 and CH_4 containing mixtures,” *Combust. Flame*, **133**, 133–146

7. I. V Adamovich, I. Choi, N. Jiang, J.-H. Kim, S. Keshav, W. R. Lempert, E. Mintusov, M. Nishihara, M. Samimy, and M. Uddi, 2009 “Plasma assisted ignition and high-speed flow control: non-thermal and thermal effects,” *Plasma Sources Sci. Technol.*, **18**, 34018

8. A. Y. Starikovskii, 2005 “Plasma supported combustion,” *Proc. Combust. Inst.*, **30**, 2405–2417

9. S. M. Starikovskaia, 2006 “Plasma assisted ignition and combustion,” *J. Phys. D. Appl. Phys.*, 39, R265–R299

10. S. Samukawa, M. Hori, S. Rauf, K. Tachibana, P. Bruggeman, G. Kroesen, J. C. Whitehead, A. B. Murphy, A. F. Gutsol, S. Starikovskaia, U. Kortshagen, J. P. Boeuf, T. J. Sommerer, M. J. Kushner, U. Czarnetzki, and N. Mason, 2012 “The 2012 Plasma Roadmap,” *J. Phys. D Appl. Phys.* **45**, 253001–253001

11. P. J. Bruggeman, U. Czarnetzki, S. Samukawa, M. Hori, and M. Armelle, 2017 “The 2017 Plasma Roadmap : Low temperature The 2017 Plasma Roadmap : Low temperature plasma science and technology,”

12. Starikovskii, A. Yu, N. B. Anikin, I. N. Kosarev, E. I. Mintoussov, S. M. Starikovskaia, and V. P. Zhukov, 2006 “Plasma-assisted combustion,” *Pure Appl. Chem.,* **78**, 1265–1298

13. W. and J. Y. Sun, 2013 “Nonequilibrium Plasma-Assisted Combustion: A Review of Recent Progress,” *Plasma Fusion Res*, **89**, 208–219

14. N. Aleksandrov, 2014 “Kinetics of low-temperature plasmas for plasma-assisted combustion and aerodynamics,” *Sources Sci.,* **23**, 15017

15. A. O’Keefe and D. A. G. Deacon, 1988 “Cavity ring-down optical spectrometer for absorption measurements using pulsed laser sources,” *Rev. Sci. Instrum.*, 59, 2544–2551

16. J. M. Herbelin and J. A McKay, 1981 “Development of laser mirrors of very high reflectivity using the cavity-attenuated phase-shift method.” *Appl. Opt.,* **20**, 3341–3344.